Open Access
ChemistryOPEN

Supporting Information

Host-Guest Chemistry of Truncated Tetrahedral Imine Cages with Ammonium Ions

Jochen C. Lauer, Ziwei Pang, Paul Janßen, Frank Rominger, Tobias Kirschbaum, Marcus Elstner, and Michael Mastalerz*An invited contribution to a Special Collection dedicated to Functional Supramolecular Systems

-Supporting Information-

Table of Content

1 General Remarks

Analytical Thin Layer Chromatography was performed with POLYGRAM® SIL G/UV_{254} gel plates sold by Macherey-Nagel. Detection was accomplished using UV-light (254 nm). Flash column chromatography was accomplished using Silica gel 60 (40 – 63 µm / 230 – 400 mesh ASTM) purchased from Macherey-Nagel. Melting points (not corrected) were measured with a Büchi Melting Point B-545. IR-Spectra were recorded on a Bruker Tensor 27 spectrometer on a ZnSe ATR crystal. NMR spectra were taken on a Bruker Avance III 300 (300 MHz), Bruker Avance DRX 300 (300 MHz), Bruker Avance III 400 (400 MHz), Bruker Avance III 500 (500 MHz) and Bruker Avance III 600 (600 MHz) spectrometer. Chemical shifts (δ) are reported in parts per million (ppm) relative to traces of the non-deuterated solvent in the corresponding deuterated solvent. HRMS experiments were carried out on a Fourier Transform Ion Cyclotron Resonance (FTICR) mass spectrometer solariX (Bruker Daltonik GmbH, Bremen, Germany) equipped with a 7.0 T superconducting magnet and interfaced to an Apollo II Dual ESI/MALDI source. MALDI-TOF MS experiments were carried out on a Bruker Daltonik Reflex III, on a Bruker ApexQe or on a Bruker AutoFlex Speed TOF with DCTB (*trans*-2-[3-(4-*tert*-butylphenyl)-2-methyl-2-propenylidene]malononitrile) as matrix. Elemental analysis was performed by the Microanalytical Laboratory of the University of Heidelberg using an Elementar Vario EL machine. Crystal structure analysis was accomplished on a STOE Stadivari diffractometer with a copper source (Cu Kα = 1.54178 Å). All crystallographic information files (1970309 (**3-Me**) and 1970310 (**(NPr_4^+⊂3-H)BF_4**) have been deposited in the Cambridge Crystallographic Data Centre and can be downloaded free of charge via www.ccdc.camac.uk/data_request/cif.

2 Synthesis and Characterization

Synthesis of Cage Compound 3-Me:

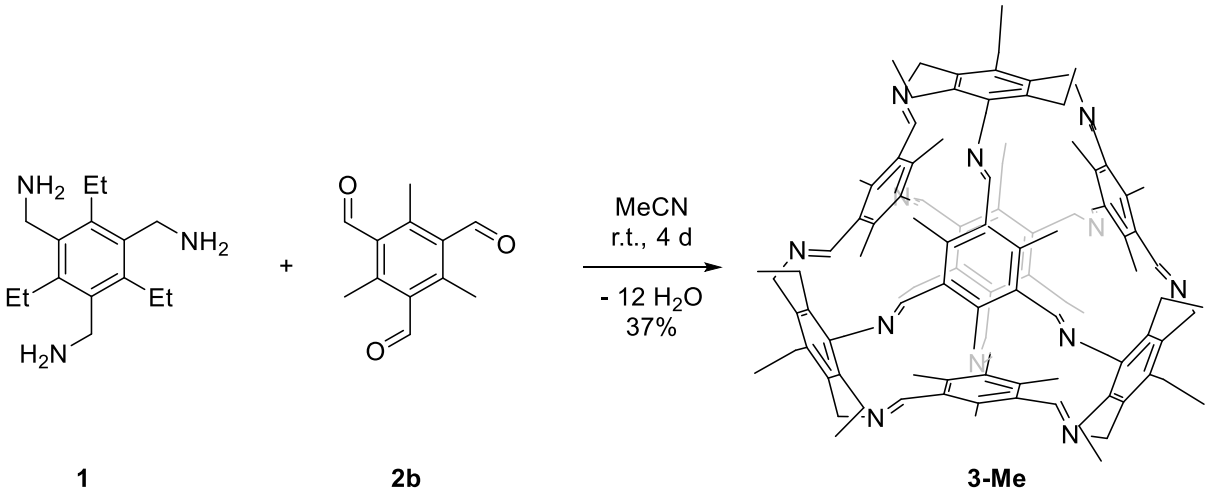

1 **2b** **3-Me**

To a solution of **2b**[S1] (408 mg, 2 mmol) in MeCN (50 mL) a solution of **1**[S2] (498 mg, 2 mmol) in MeCN (150 mL) was added dropwise under vigorous stirring at room temperature within 3 hours. The suspension was stirred for 3 days and the precipitate was filtered and washed with MeCN (2 x 50 mL). The solid residue was extracted with MeOH (250 mL) and solvent removed in vacuo. The solid residue was treated with MeCN (50 mL) in the supersonic bath for 15 minutes, collected by filtration, washed with MeCN (50 mL) and dried in vacuo to give 290 mg (37%) of cage compound **3-Me** as a colourless solid. M.p.: 233 °C (decomp.).^{1}H NMR (400 MHz, C_6D_6): δ = 7.97 (s, 12H, -C*H*N-), 5.03 (s, 24H, CH_2N-), 2.77 (q, J = 7.4 Hz, 24H, -CH_2CH$_3$), 2.23 (s, 36H, -CH_3), 1.15 (t, J = 7.4 Hz, 36H, -CH$_2$CH_3) ppm. ^{13}C NMR (150 MHz, C_6D_6): (ppm) = 160.8 (-*C*HN-), 143.6 (-*C*CH$_2$CH$_3$), 135.7 (-*C*CH$_2$N-), 133.6 (-*C*CH$_3$), 132.1 (-*C*CH$_2$N-) , 56.7 (-*C*H$_2$N-), 23.8 (-*C*H$_2$CH$_3$), 17.4 (-*C*H$_3$), 16.4 (-CH$_2$*C*H$_3$) ppm. FT-IR (ATR): (cm^{-1}) = 770 (m), 942 (m), 965 (m), 1030 (w), 1044 (m), 1076 (w), 1233 (w), 1317 (m), 1490 (s), 1559 (w), 1641 (s), 1689 (m), 2871 (m), 2902 (m), 2930 (m), 2963 (m). HRMS (MALDI, DCTB): *m/z* = 1599.0816 [M+H]$^+$ (*m/z* calc. for $C_{120}H_{156}N_{12}$+H$^+$: 1599.0849). Anal. calc. for $C_{96}H_{108}N_{12}$·5 H_2O: C 76.83, H 8.48, N 9.96; found: C 76.91, H 8.60, N 9.80.

3 Analytics of 3-Me

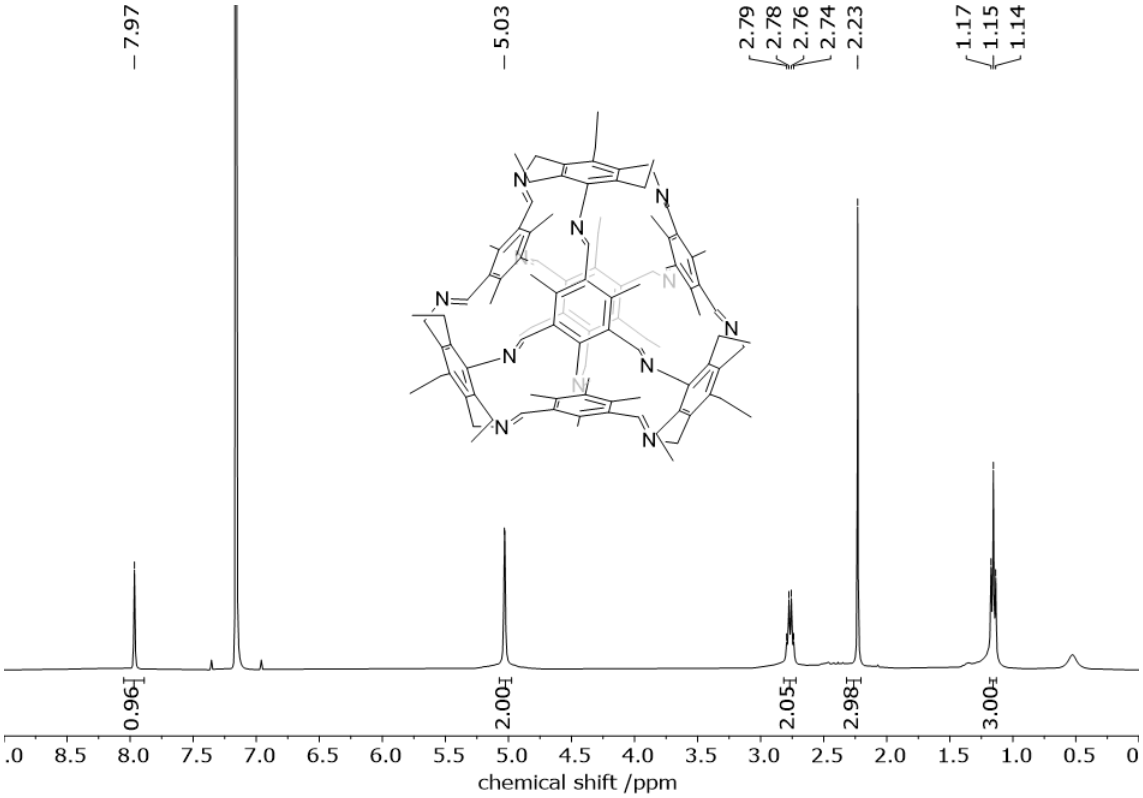

Figure S1: ^{1}H NMR spectrum (400 MHz, C_6D_6) of cage compound **3-Me**.

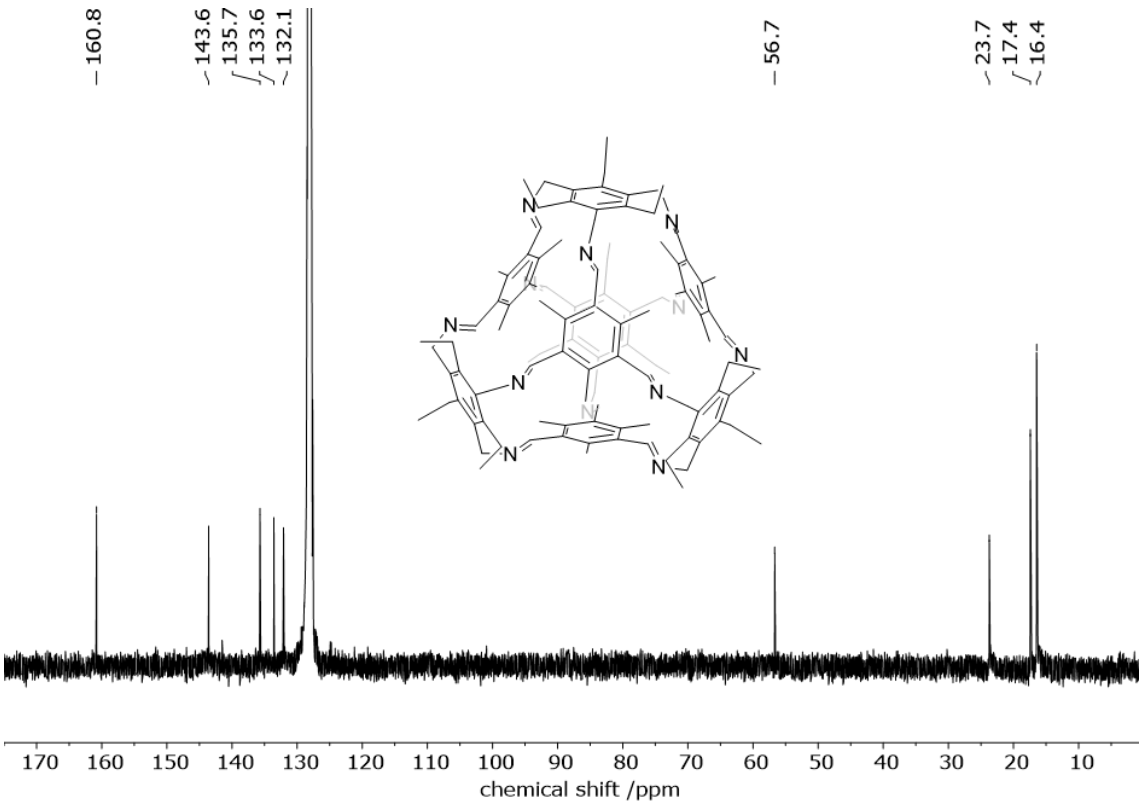

Figure S2: ^{13}C NMR spectrum (150 MHz, C_6D_6) of cage compound **3-Me**.

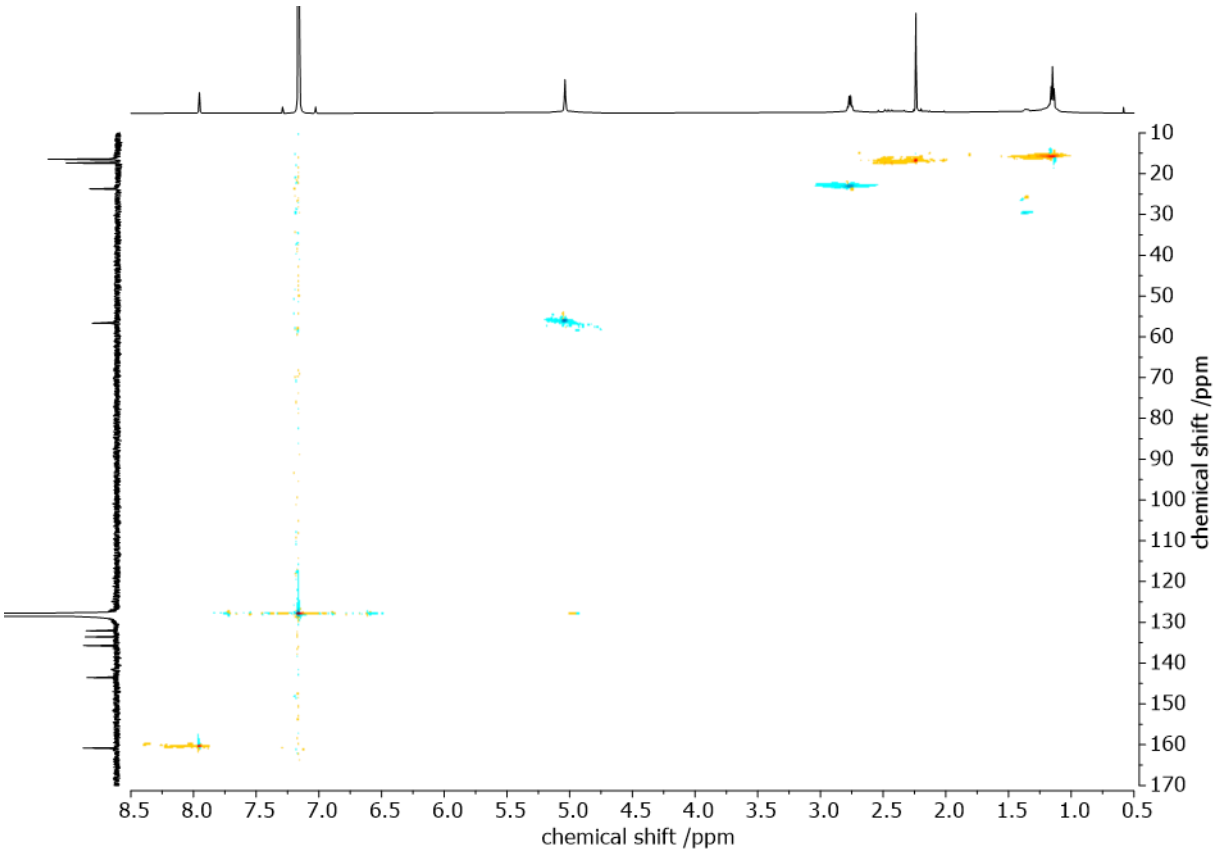

Figure 3: ^{1}H-^{13}C HSQC NMR spectrum (600/150MHz, C_6D_6) of cage compound **3-Me**.

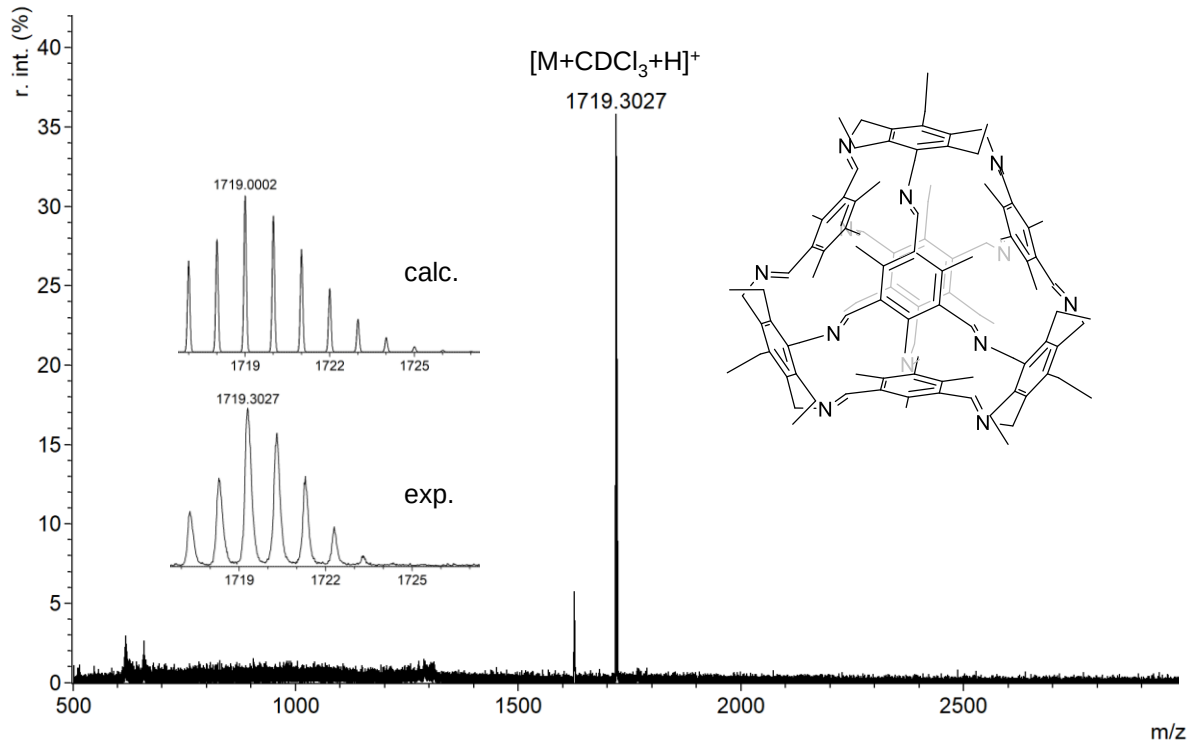

Figure S4: MALDI-TOF-MS (DCTB) of compound **3-Me**.

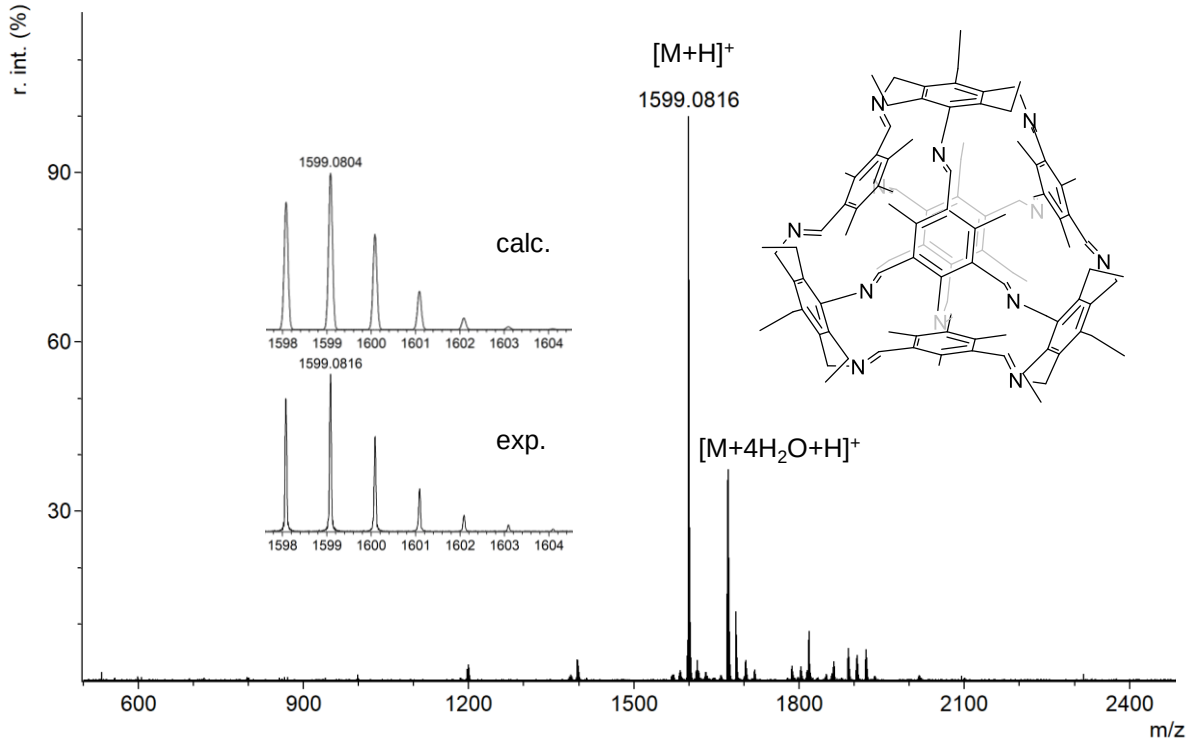

Figure S5: HR-MALDI-MS (DCTB) of compound **3-Me**.

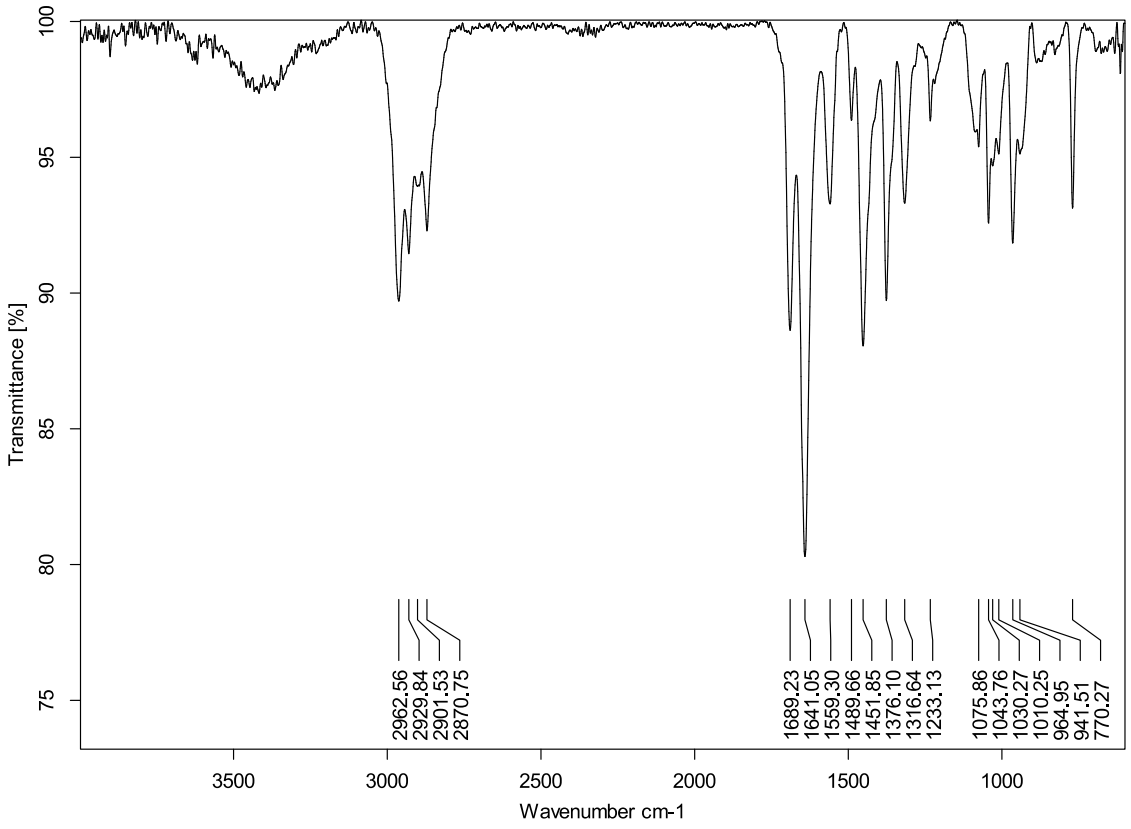

Figure S6: IR spectrum (ATR) of compund **3-Me**.

4 DOSY Experiments

DOSY NMR experiments were recorded at 298 K and calibrated using known self-diffusion values for the solvents used (D_{solv}).[S3] The solvodynamic radii were estimated using the Stokes-Einstein equation. This equation was solved for r_s using values of η from the literature.[S4]

$$D = \frac{k_B T}{6\pi\eta r_s}$$

D is the measured diffusion coefficient ($m^2 \cdot s^{-1}$); k_B is Boltzmann constant (1.3806485 $\cdot 10$ $m^2 \cdot kg \cdot s^{-2} \cdot K^{-1}$), ***T*** is the temperature (K), r_s is the hydrodynamic radius of the analyte (m); η is the viscosity of the solvent at temperature *T* ($kg \cdot m^{-1} \cdot s^{-1}$).

Table S1: Estimation of the solvodynamic radii (r_h) in CD_2Cl_2 or THF-d_8 as solvent using parameters from the literature and diffusion coefficients measured by DOSY NMR.

Compound	Solvent	T [K]	$D_{solv} \cdot 10^{-9}$ [$m^2 \cdot s^{-1}$]	$\eta \cdot 10^{-3}$ [$kg \cdot m^{-1} \cdot s^{-1}$]	$D \cdot 10^{-10}$ [$m^2 \cdot s^{-1}$]	r_s [nm]
3-H	DCM-d_2	298	3.53	0.413	6.92	0.76
3-Me	DCM-d_2	298	3.53	0.413	6.61	0.80
3-Et	DCM-d_2	298	3.53	0.413	4.47	1.18
$(NMe_4 \subset 3\text{-}H)BF_4$	DCM-d_2	298	3.53	0.413	7.59	0.82
$(NEt_4 \subset 3\text{-}H)BF_4$	DCM-d_2	298	3.53	0.413	7.08	0.73
$(NPr_4 \subset 3\text{-}H)BF_4$	DCM-d_2	298	3.53	0.413	6.31	0.84
(Acc⊂3-H)Cl	DCM-d_2	298	3.53	0.413	7.94	0.67
(Mus⊂3-H)Cl	DCM-d_2	298	3.53	0.413	6.61	0.80
$(NMe_4 \subset 3\text{-}Me)BF_4$	DCM-d_2	298	3.53	0.413	7.24	0.73
$(NEt_4 \subset 3\text{-}Me)BF_4$	DCM-d_2	298	3.53	0.413	6.74	0.78
(Acc⊂3-Me)Cl	DCM-d_2	298	3.53	0.413	6.61	0.80
(Mus⊂3-Me)Cl	DCM-d_2	298	3.53	0.413	5.62	0.94
$(NEt_4 \subset 3\text{-}Et)BF_4$	DCM-d_2	298	3.53	0.413	6.31	0.84
$(NMe_4 \subset 3\text{-}H)BF_4$	THF-d_8	298	2.33	0.47	9.12	0.51
$(NEt_4 \subset 3\text{-}H)BF_4$	THF-d_8	298	2.33	0.47	6.49	0.70
$(NPr_4 \subset 3\text{-}H)BF_4$	THF-d_8	298	2.33	0.47	6.76	0.69
$(NBu_4 \subset 3\text{-}H)BF_4$	THF-d_8	298	2.33	0.47	6.46	0.72

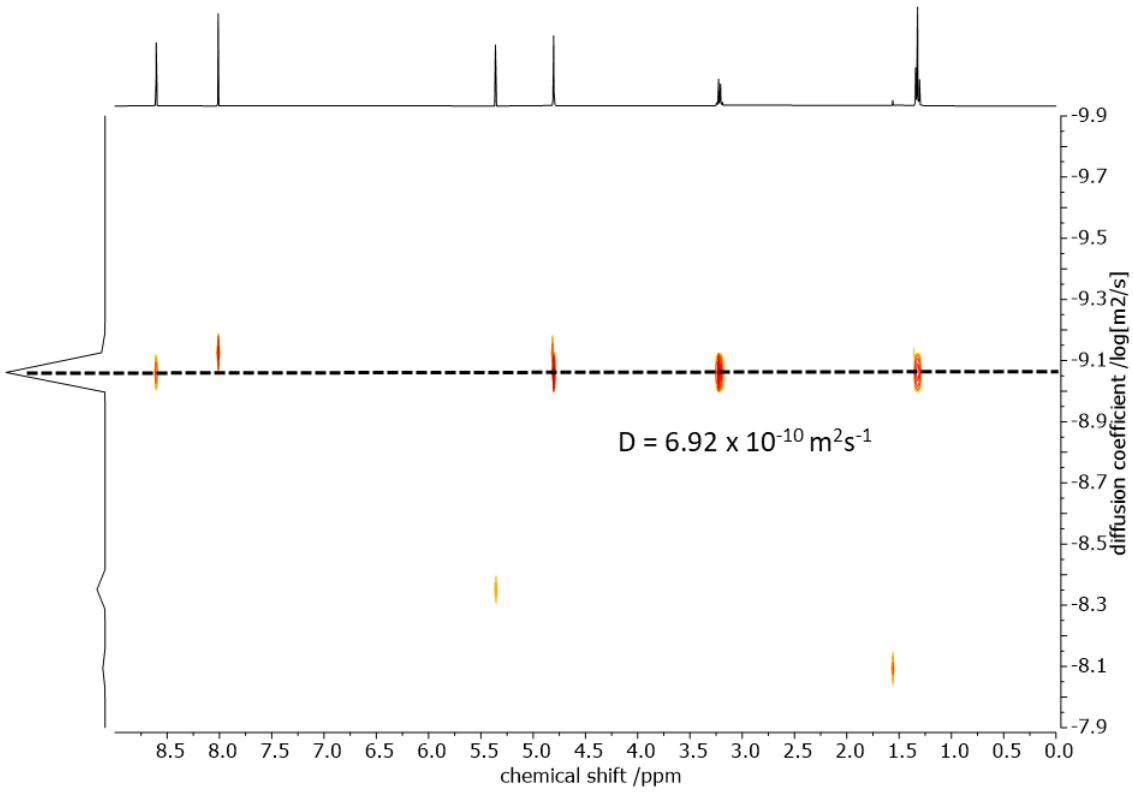

Figure S7: ^{1}H-DOSY NMR spectrum (400 MHz, CD_2Cl_2) of cage compound **3-H**.

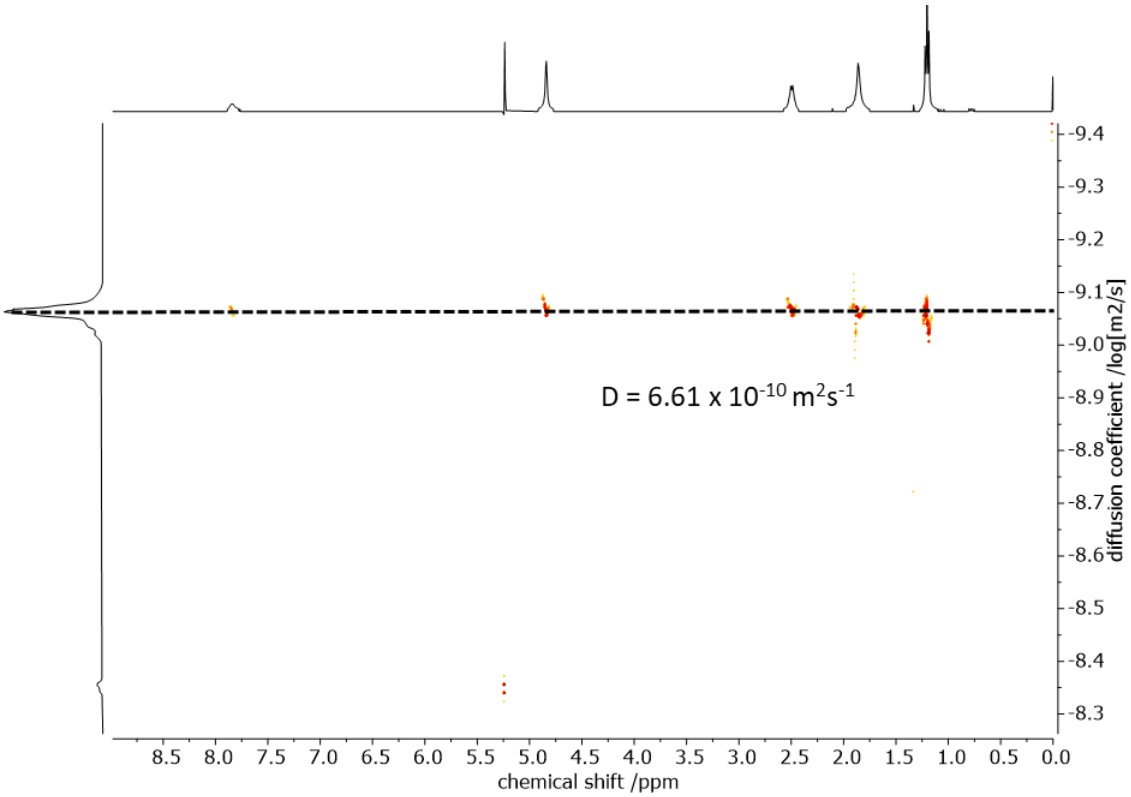

Figure S8: ^{1}H-DOSY NMR spectrum (400 MHz, CD_2Cl_2) of cage compound **3-Me**.

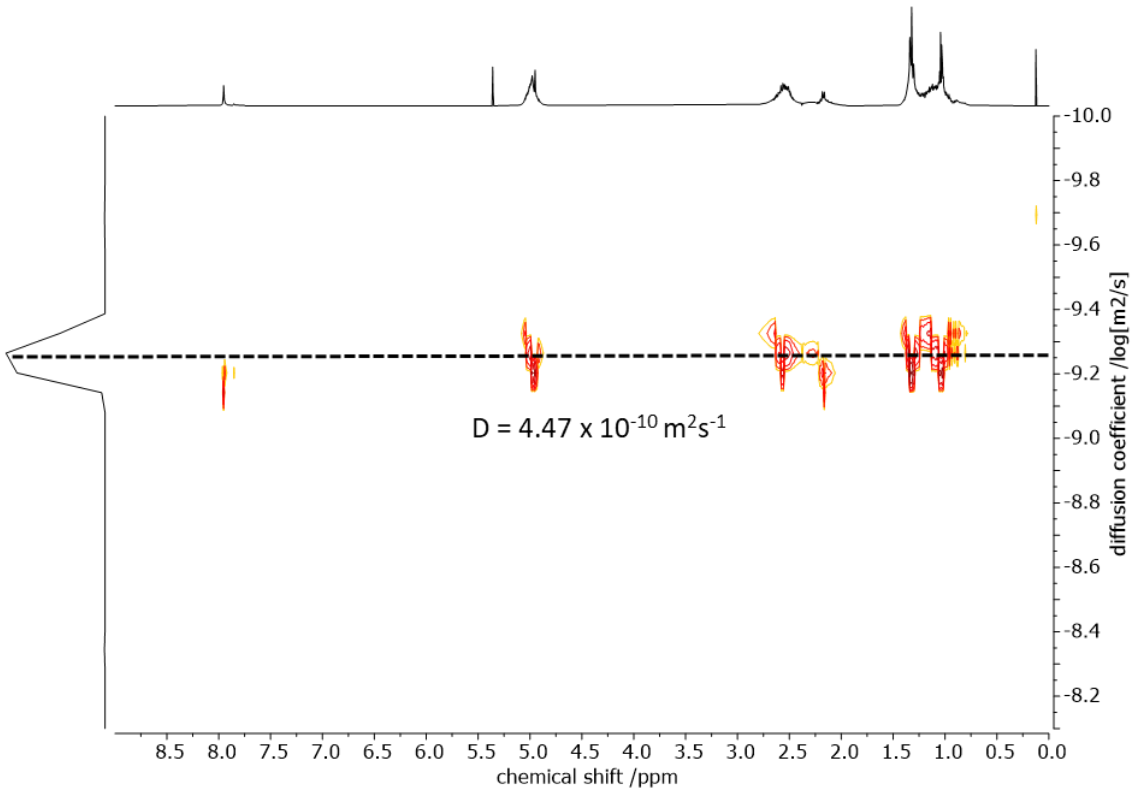

Figure S9: ^{1}H-DOSY NMR spectrum (400 MHz, CD_2Cl_2) of cage compound **3-Et**.

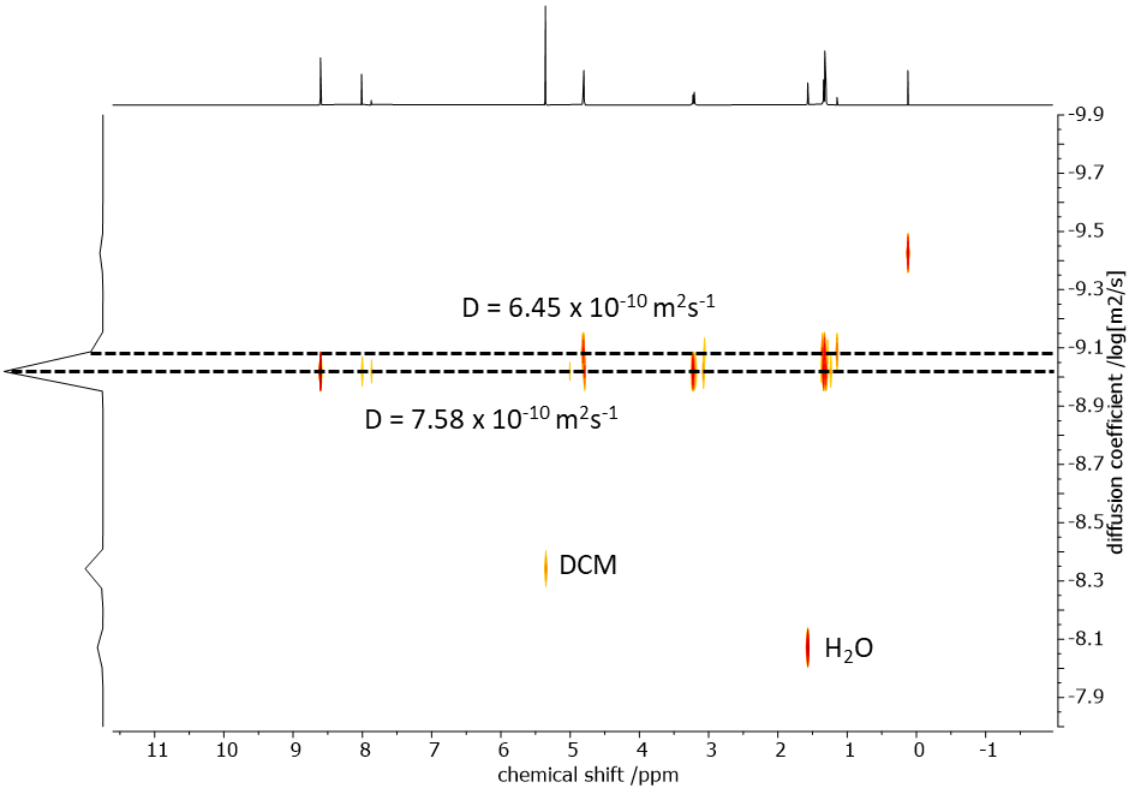

Figure S10: ^{1}H-DOSY NMR spectrum (400 MHz, CD_2Cl_2) of cage compound **(NMe_4⊂3-H)BF_4** + free **3-H**-Cage.

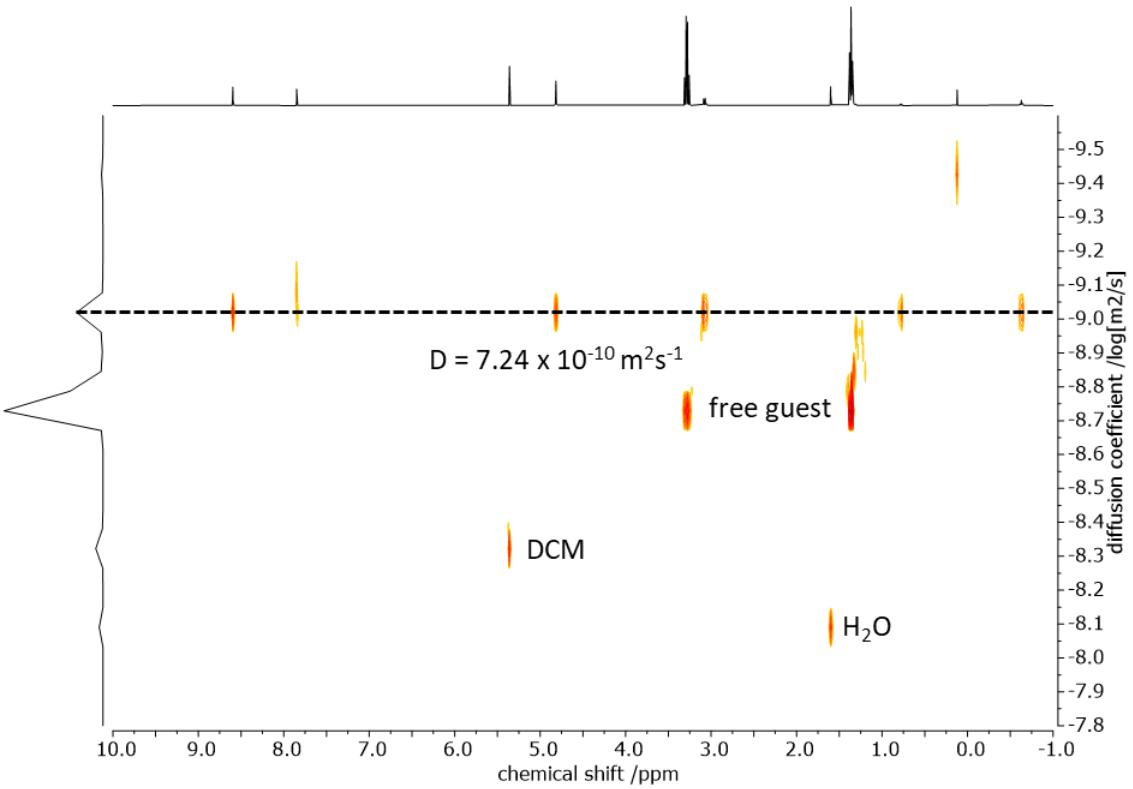

Figure S11: ^{1}H-DOSY NMR spectrum (400 MHz, CD_2Cl_2) of cage compound **(NEt$_4$⊂3-H)BF$_4$**.

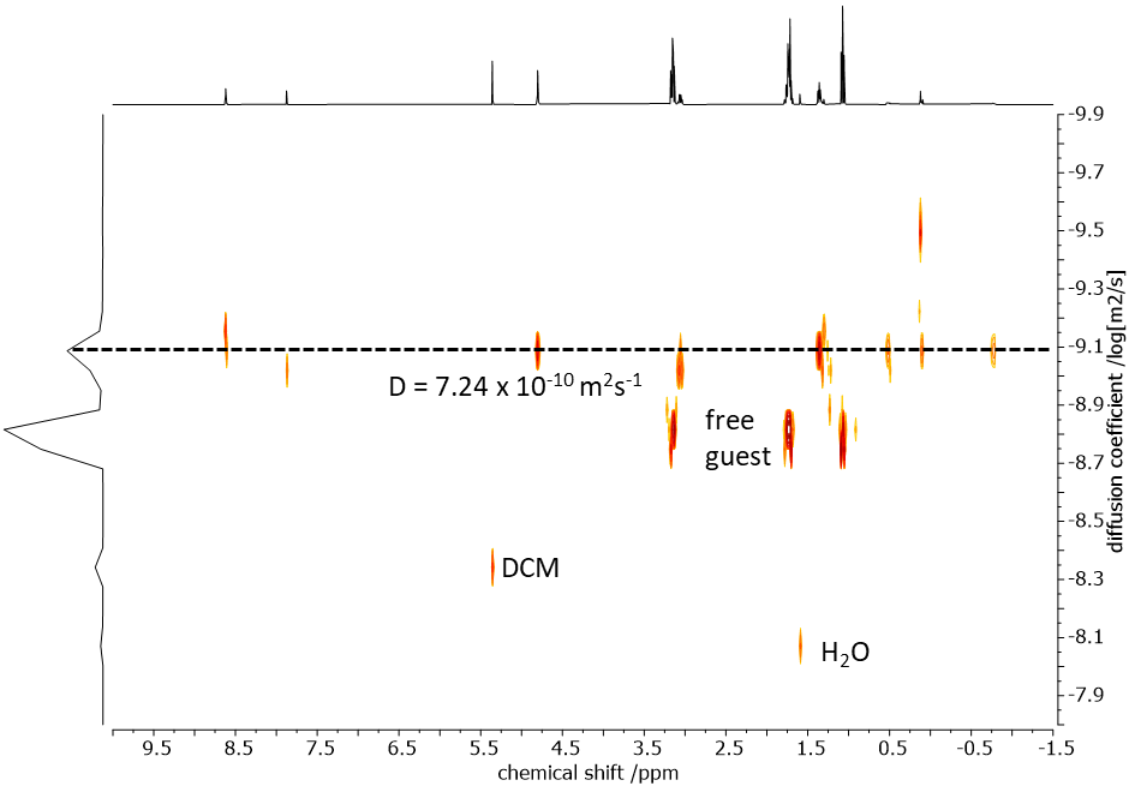

Figure S12: ^{1}H-DOSY NMR spectrum (400 MHz, CD_2Cl_2) of cage compound **(NPr$_4$⊂3-H)BF$_4$**.

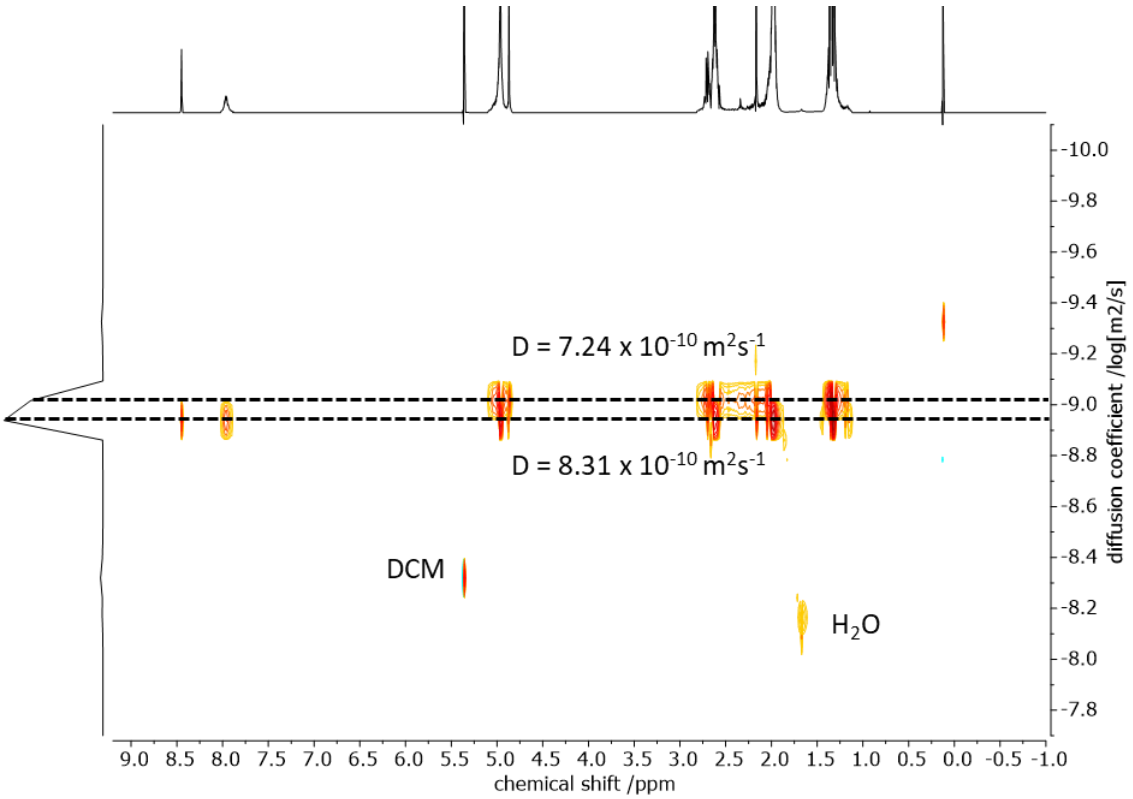

Figure S13: ^{1}H-DOSY NMR spectrum (400 MHz, CD_2Cl_2) of cage compound **(NMe$_4$⊂3-Me)BF$_4$** + free **3-Me**-Cage.

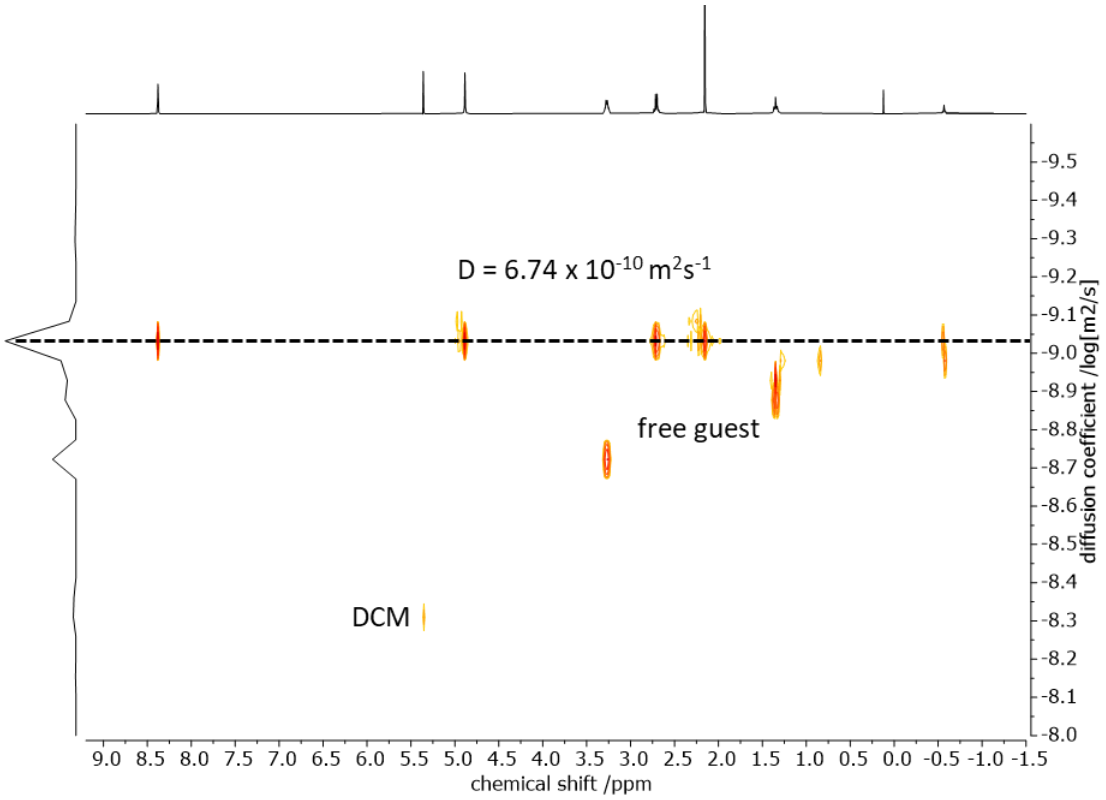

Figure S14: ^{1}H-DOSY NMR spectrum (400 MHz, CD_2Cl_2) of cage compound **(NEt$_4$⊂3-Me)BF$_4$**.

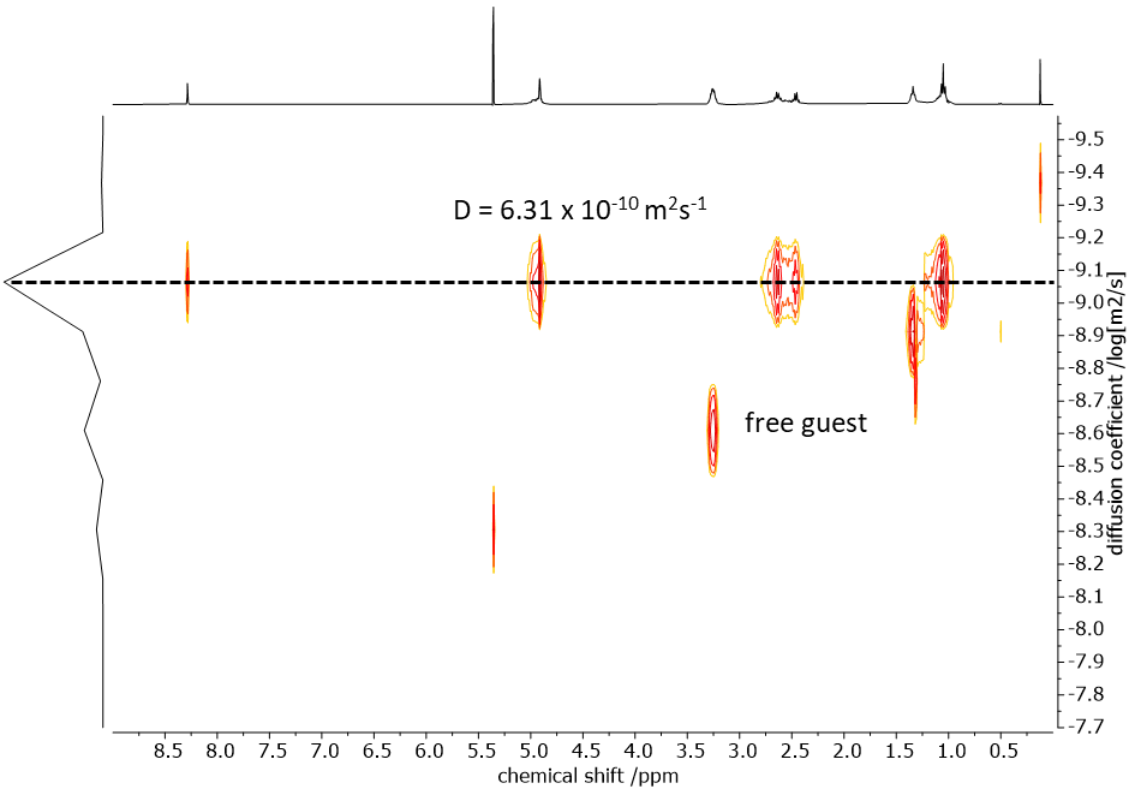

Figure S15: ^{1}H-DOSY NMR spectrum (400 MHz, CD_2Cl_2) of cage compound **(NEt$_4$⊂3-Et)BF$_4$**.

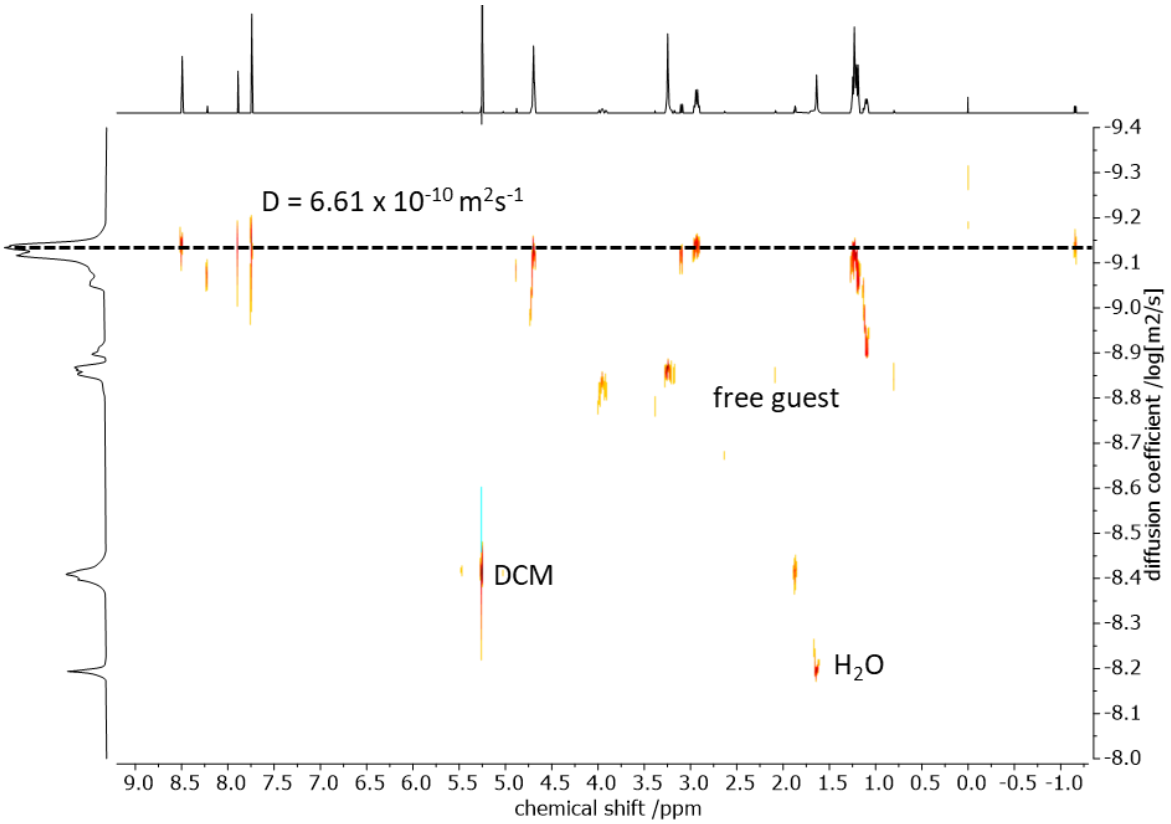

Figure S16: ^{1}H-DOSY NMR spectrum (400 MHz, CD_2Cl_2) of cage compound **(acetylcholine⊂3-H)Cl**.

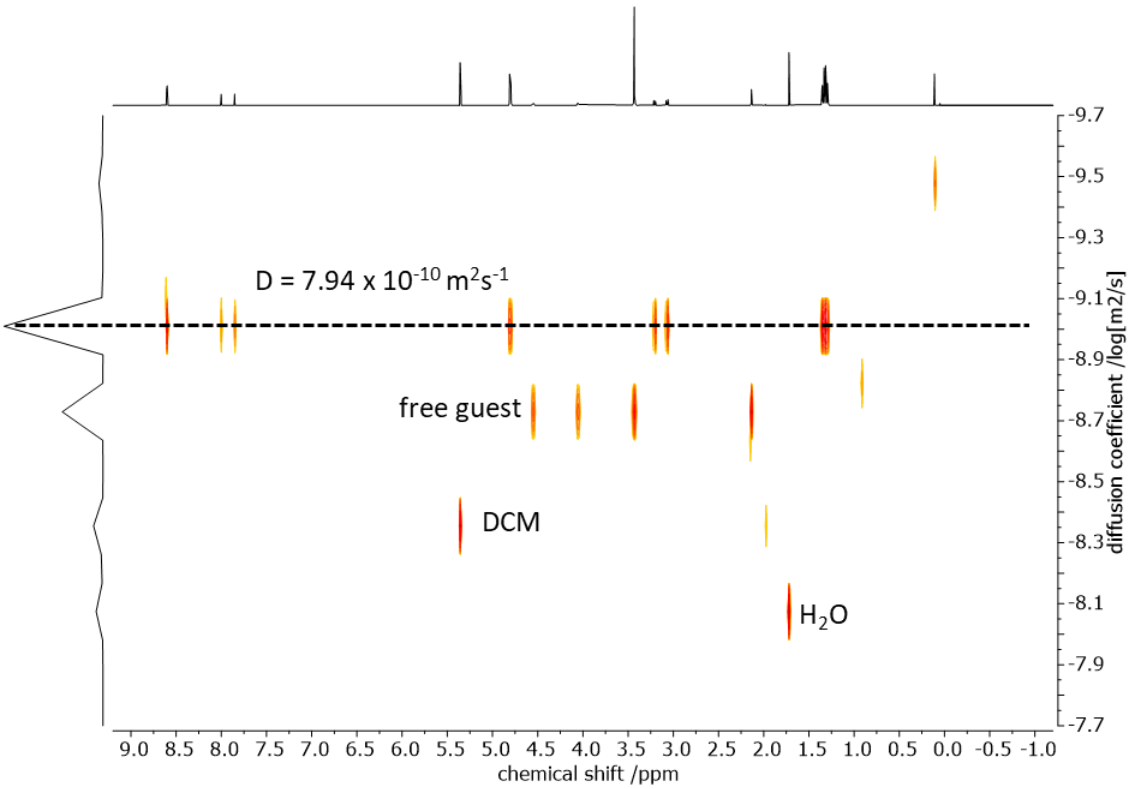

Figure S17: ^{1}H-DOSY NMR spectrum (400 MHz, CD_2Cl_2) of cage compound **(muscarine⊂3-H)Cl**.

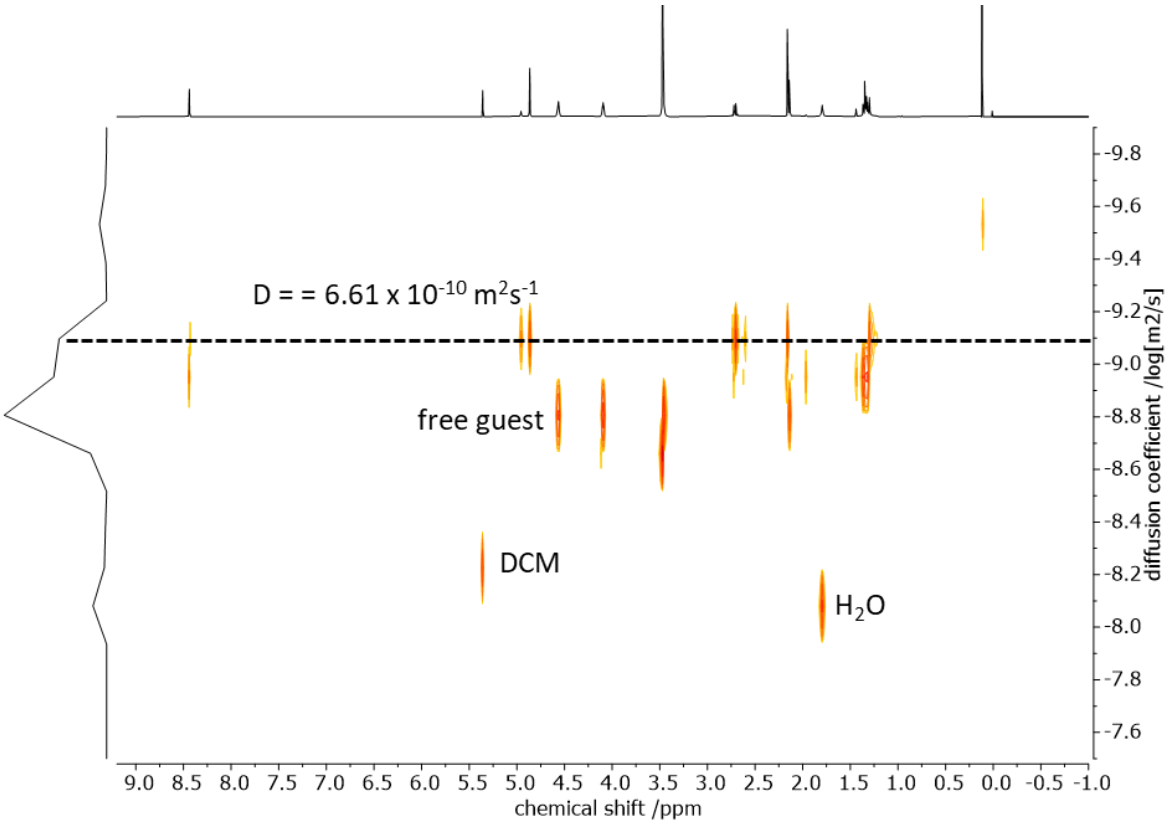

Figure S18: ^{1}H-DOSY NMR spectrum (400 MHz, CD_2Cl_2) of cage compound **(acetylcholine⊂3-Me)Cl**.

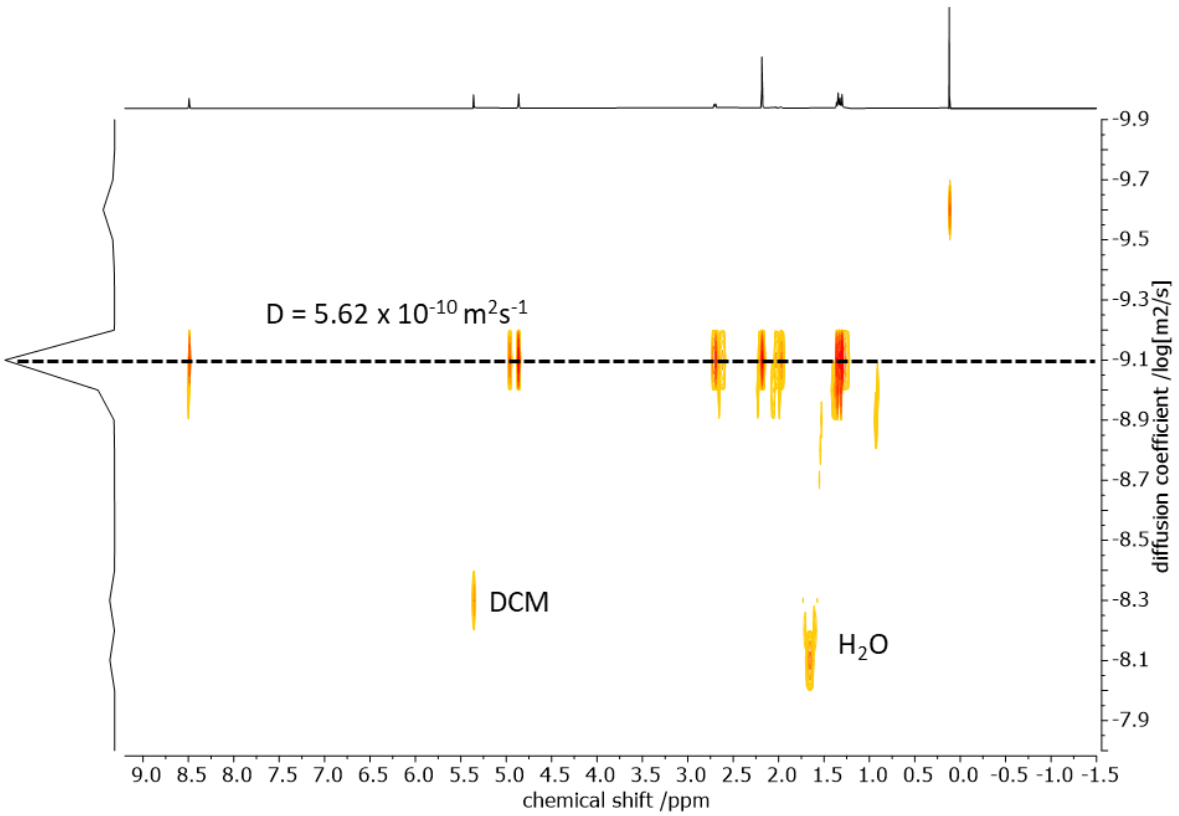

Figure S19: ^{1}H-DOSY NMR spectrum (400 MHz, CD_2Cl_2) of cage compound **(muscarine⊂3-Me)Cl**.

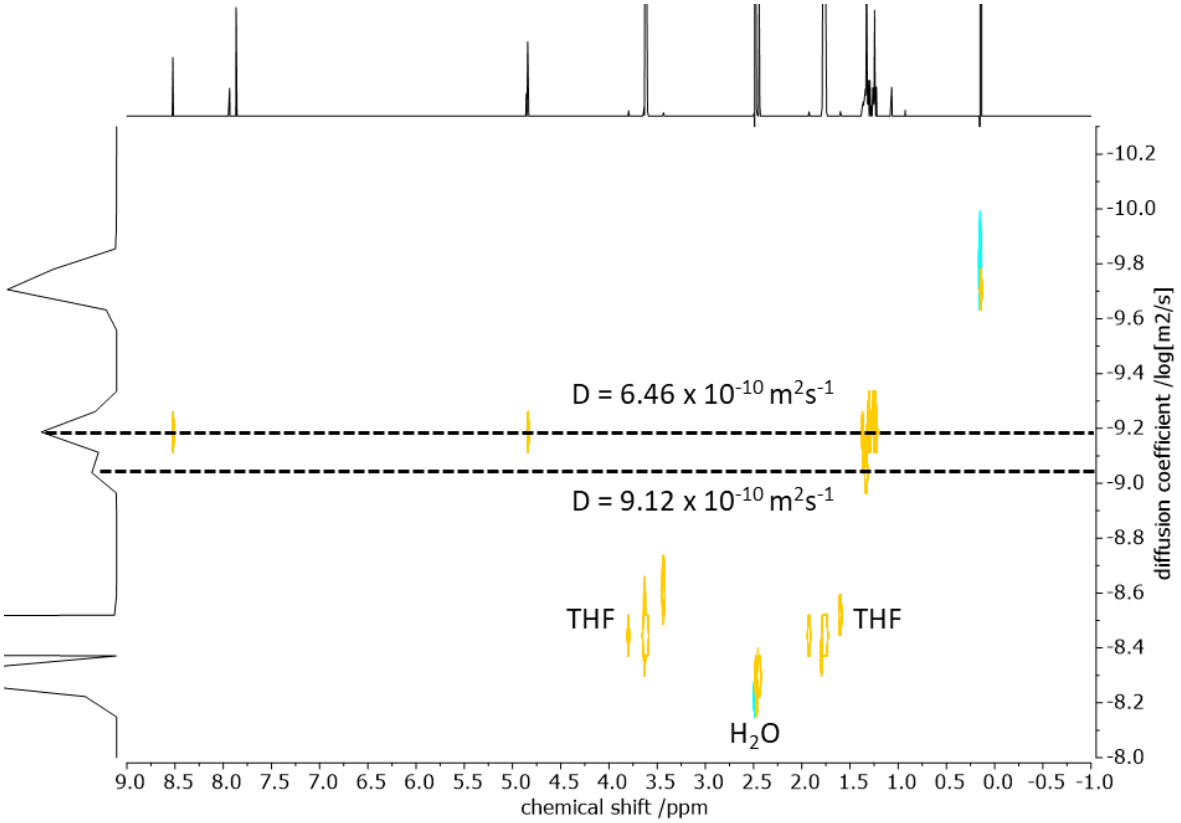

Figure S20: ^{1}H-DOSY NMR spectrum (400 MHz, THF-d_8) of cage compound **(NMe_4⊂3-H)BF_4** free **3-H**-Cage.

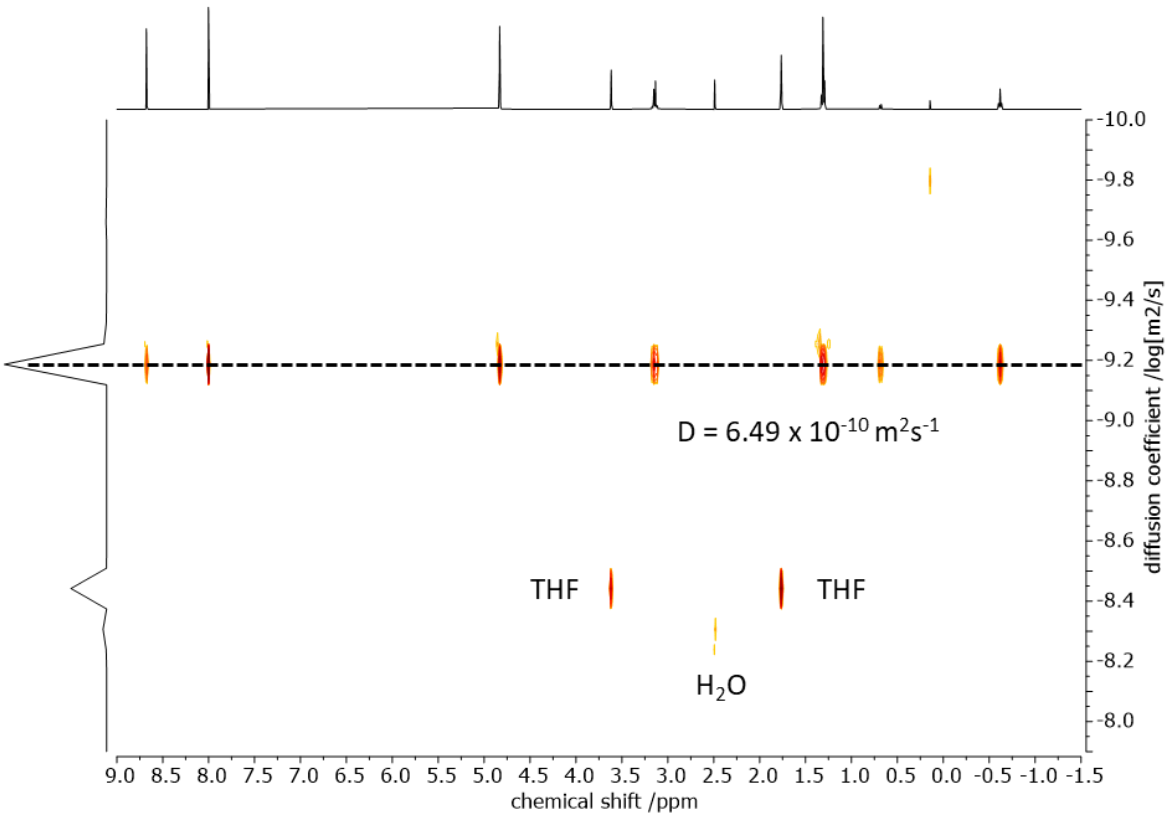

Figure S21: ^{1}H-DOSY NMR spectrum (400 MHz, THF-d_8) of cage compound **(NEt$_4$⊂3-H)BF$_4$**.

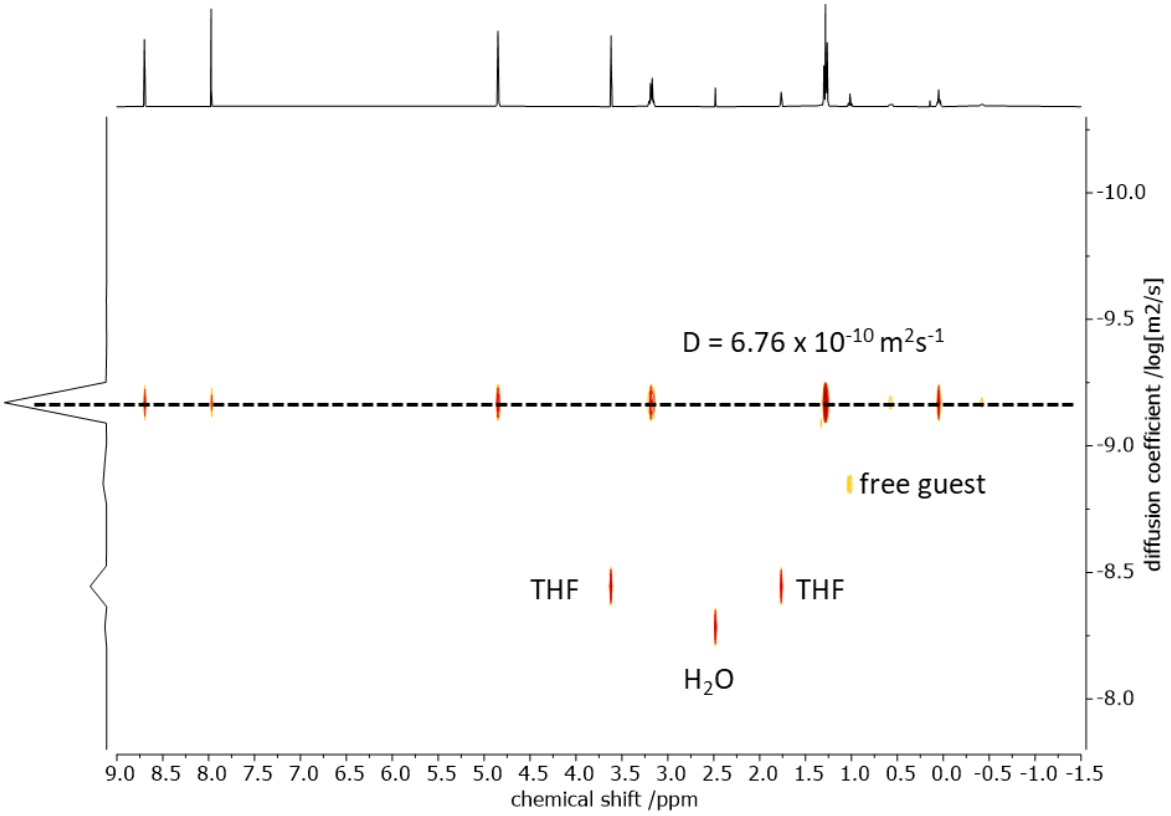

Figure S22: ^{1}H-DOSY NMR spectrum (400 MHz, THF-d_8) of cage compound **(NPr$_4$⊂3-H)BF$_4$**.

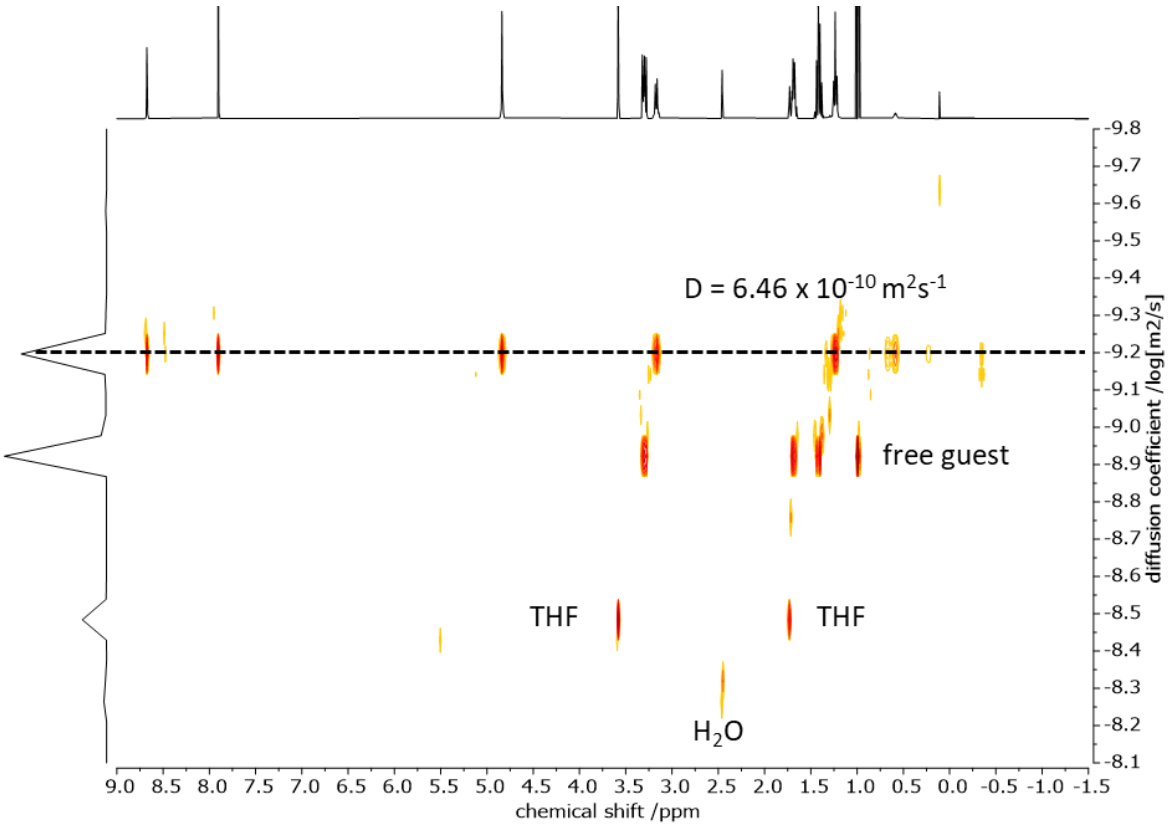

Figure S23: ^{1}H-DOSY NMR spectrum (400 MHz, THF-d_8) of cage compound **(NBu$_4$⊂3-H)BF$_4$**.

5 Host Guest Experiments

5.1 ^{1}H NMR Spectra of Free Cages

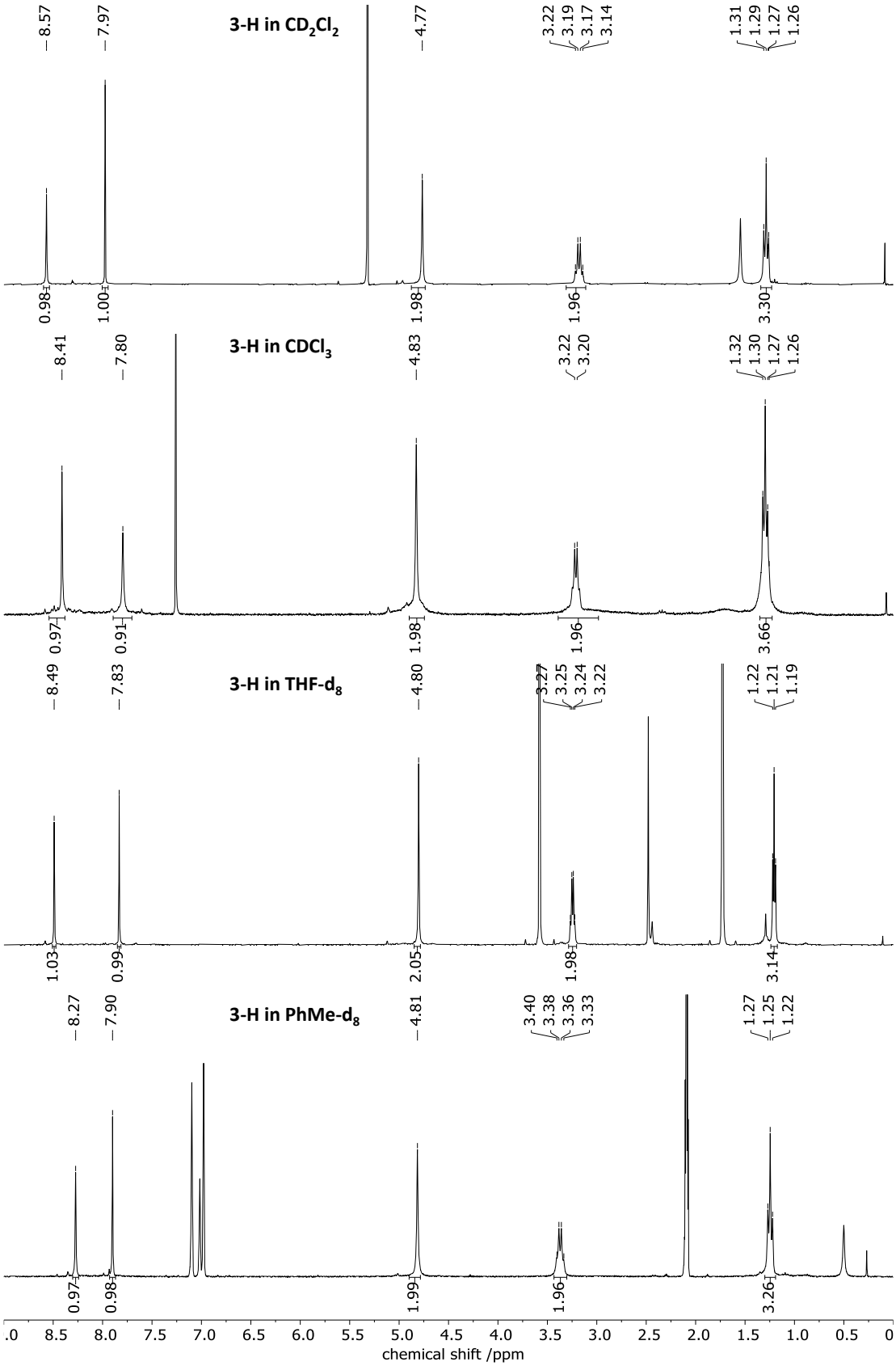

Figure S24: ^{1}H NMR spectra (300 MHz) of **3-H** in CD_2Cl_2, $CDCl_3$, THF-d_8 and PhMe-d_8.

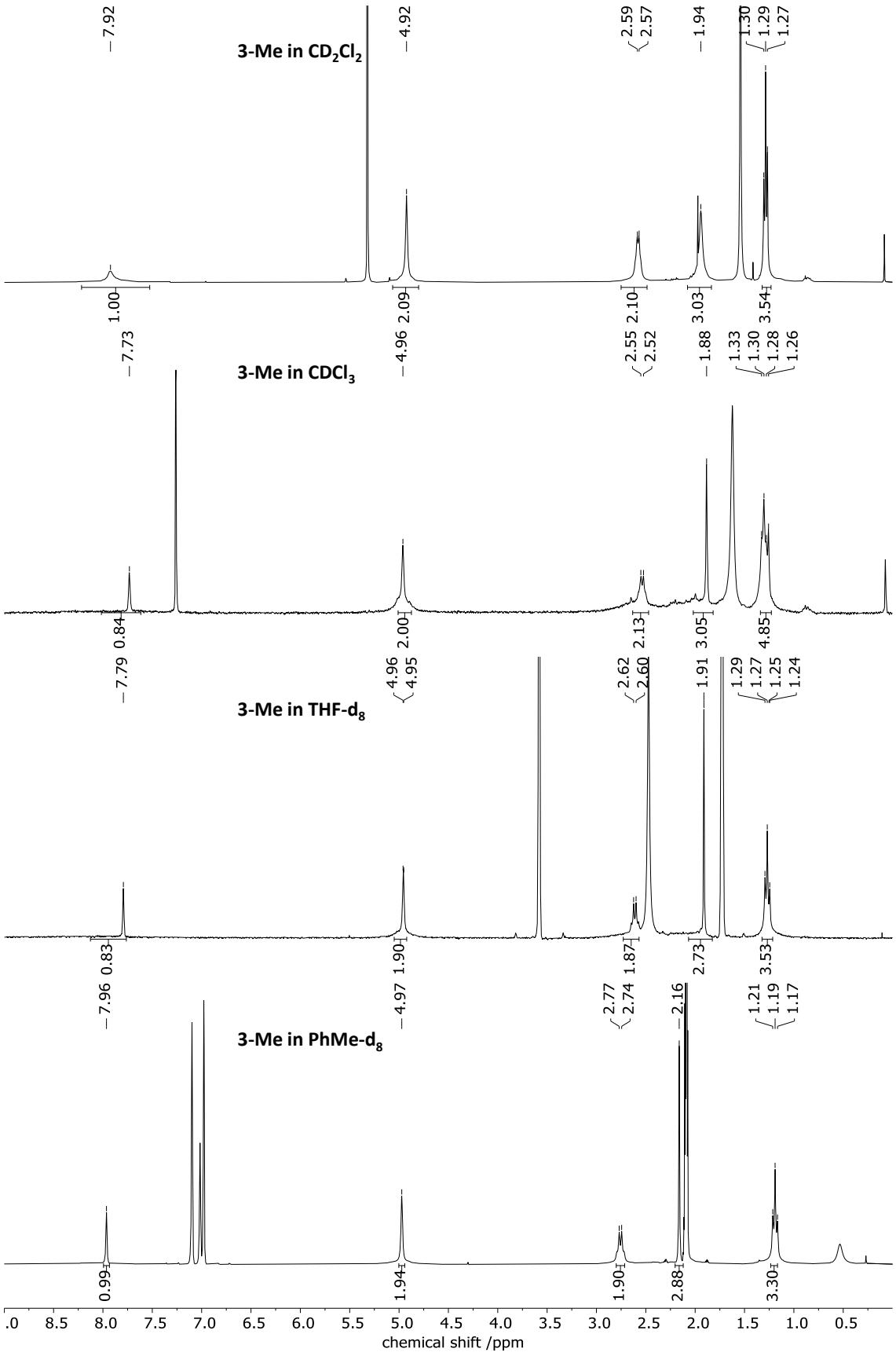

Figure S25: ^{1}H NMR spectra (300 MHz) of **3-Me** in CD_2Cl_2, $CDCl_3$, THF-d_8 and PhMe-d_8.

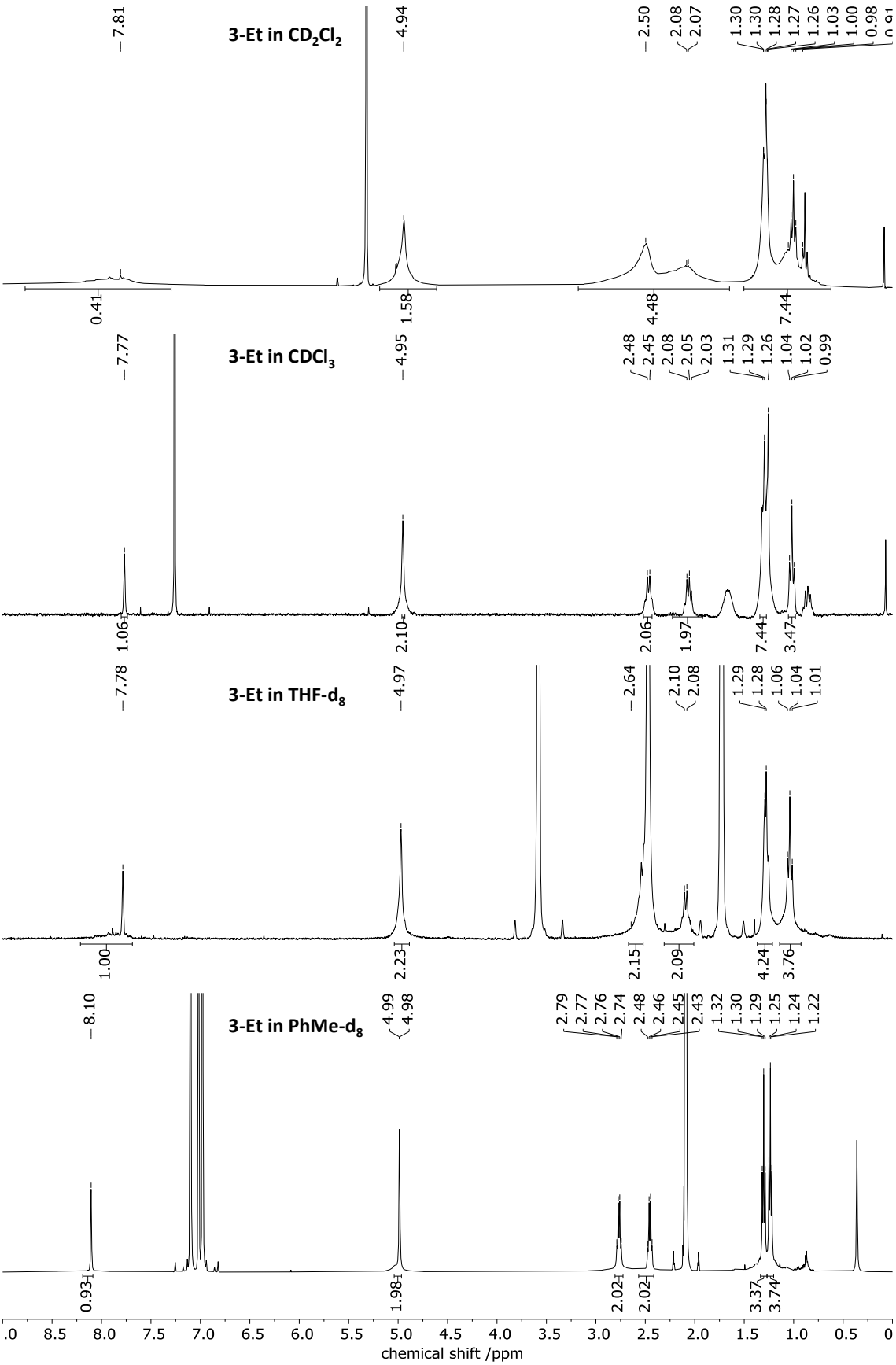

Figure S26: ^{1}H NMR spectra (300 MHz) of **3-Et** in CD_2Cl_2, $CDCl_3$, THF-d_8 and PhMe-d_8.

5.2 Determination of the Guest and Cavity Volume

The molecular structure for the determination of the cavity volume of the [4+4]-Cages was calculated starting from the obtained conformation from single-crystal X-ray diffraction data.[S5] The conformation was further optimized using quantum chemical calculations by employing the Gaussian09 program package.[S6] The theoretical approach is based on Kohn-Scham density functional methodologies[S7] using the B3LYP[S8] functional. As basis set the double-ζ-basis (6-31G)[S9] was used. The geometries of the regarded species were fully optimized using ultra-tight convergence criteria of the representative computational method. For solvent modelling, the polarized continuum model (PCM) was used.[S10]

The determination of the cavity and the guest volume was carried out using SwissPdbViewer[S11] 4.1.0 at the highest quality level (Surface Preferences: Quality 6). Six dummy atoms were added to the **3-H**-Cage and positioned in front of the windows of the cage to prevent the 1.4 Å radius measuring probe from “falling out” of the cavity of the cage.

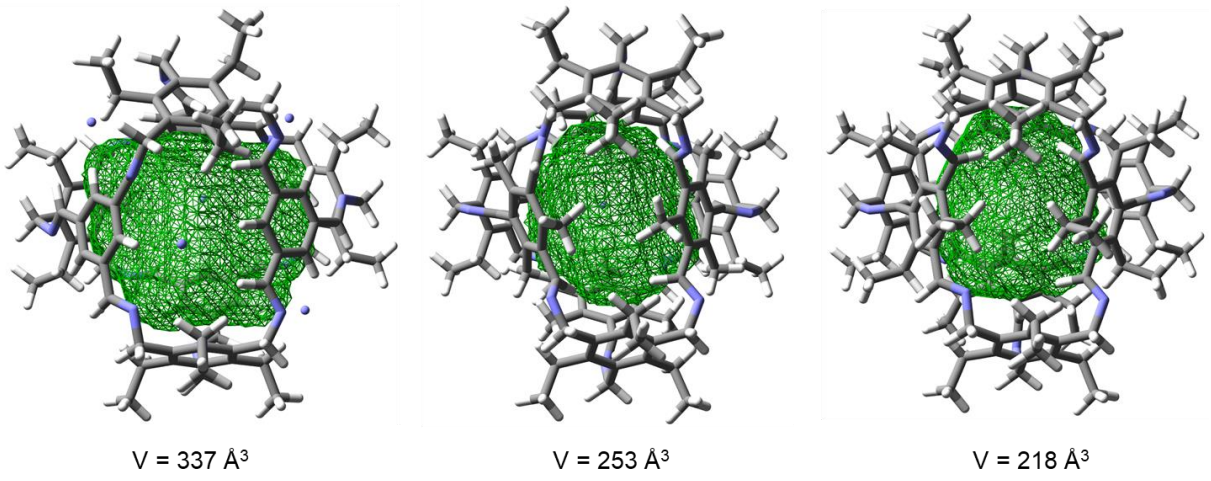

Figure S27: Representation of cavity volumes of the cages **3-H**, **3-Me** and **3-Et** as determined by a spherical probe of 1.4 Å. .

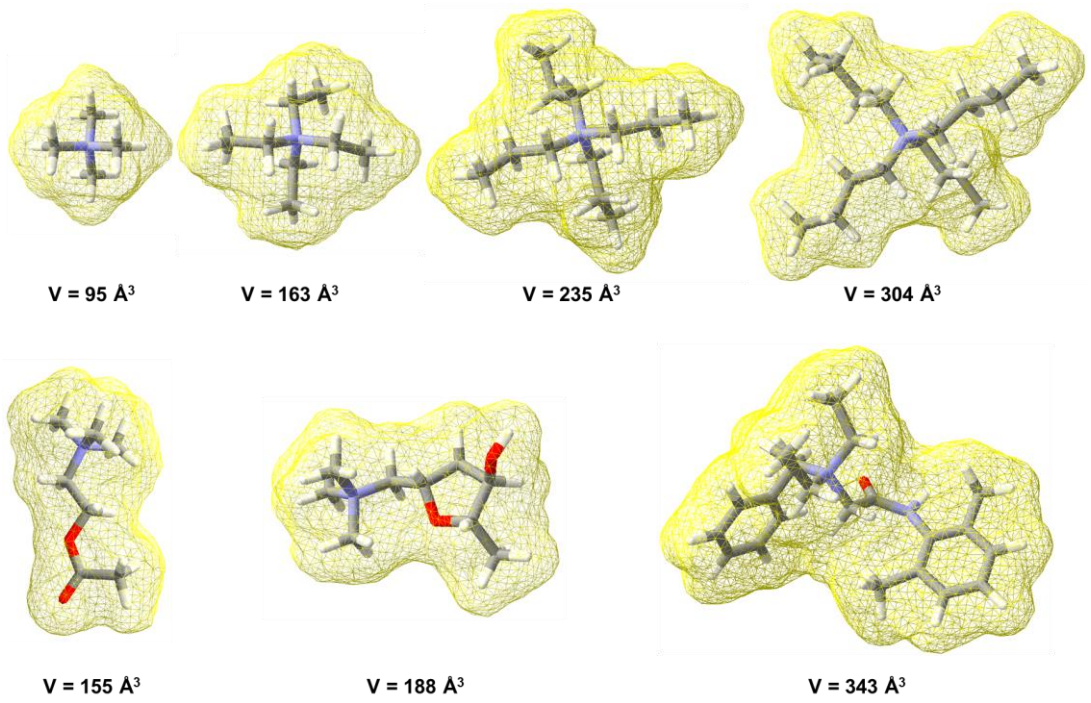

Figure S28: Representation of guest volumes.

Table S2: Calculated occupancys.

guest	occupancy of the space in the cavity by guest (%)		
	3-H	**3-Me**	**3-Et**
NMe_4^+	28	38	44
NEt_4^+	48	64	75
NPr_4^+	70	93	108
NBu_4^+	90	120	139
Acetylcholine$^+$	46	61	71
(±)-Muscarine$^+$	56	74	86
Denatonium$^+$	102	136	157

5.3 Evaluation of the Binding Constants

All ^{1}H NMR studies were performed in J-Young NMR tubes from stock solutions of the desired cages and guests. Association constants were evaluated in THF-d_8, $CDCl_3$ and CD_2Cl_2 at 298 K from the integration of characteristic signals observed in NMR experiments using different concentrations of cage and of guests according to the equations:

K_A =[$Guest@C$age]/[Cag$e$][$Guest$]

K_A is the association constant between the capsule and the guest (M^{-1})

[Guest@Cage] is the concentration of host-guest complex containing one guest (M)

[Cage] is the concentration of the free cage

[*Guest*] is the concentration of the free guest (M)

The mixtures were allowed to rest at room temperature until no change in ^{1}H-NMR was observed anymore measurements were recorded, the average of at least three measurements are reported as K_a values with standard deviations (σ) as uncertainty.

5.4 Host Guest Experiments in DCM-d_2

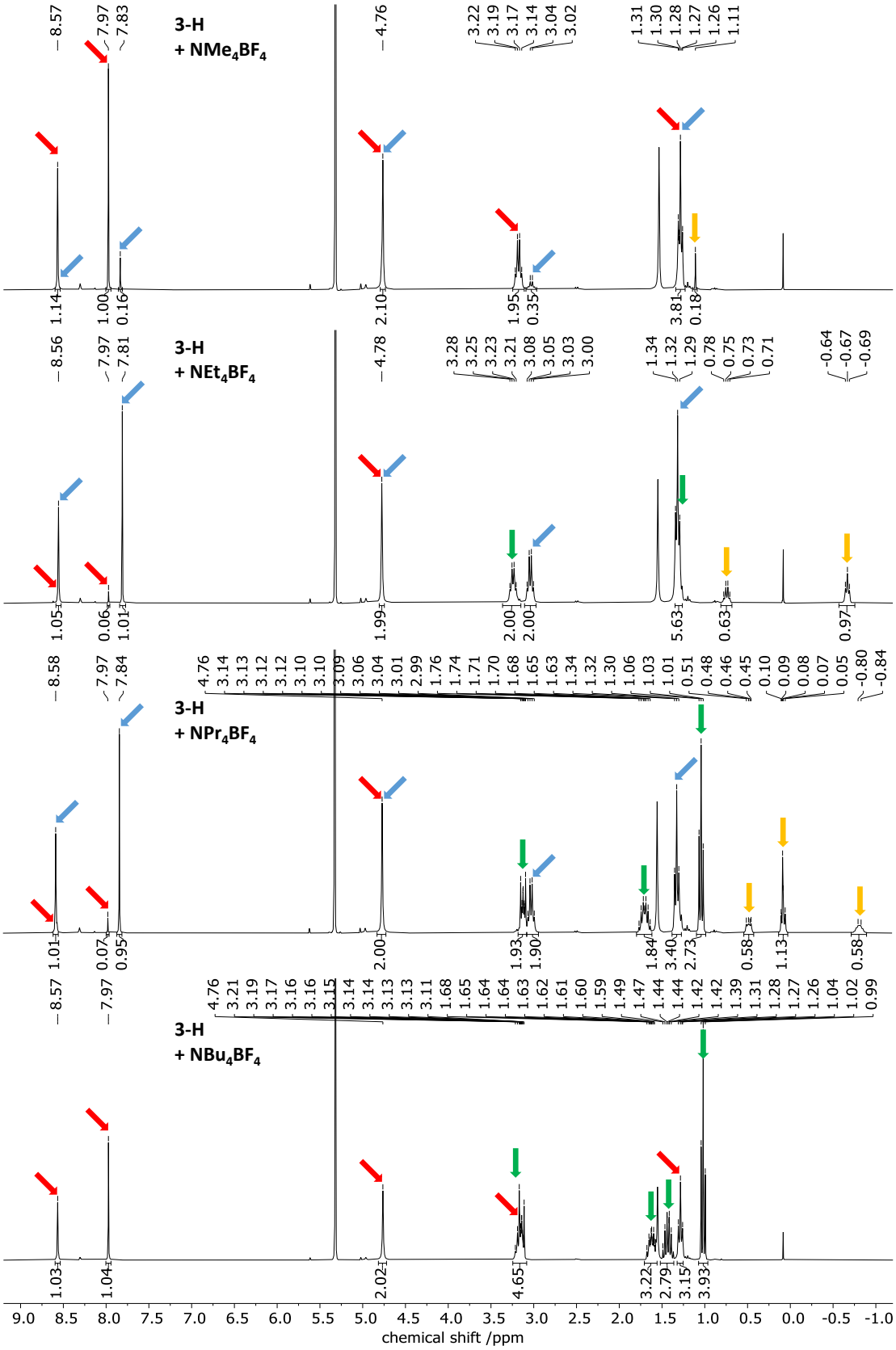

Figure S29: ^{1}H NMR spectra (CD_2Cl_2, 300 MHz) of **3-H** with tetraalkylammonium tetrafluoroborate added. Arrows highlight characteristic signal(s) from the host cage (blue), the free cage (red), the free guest (green) and the bound guest (yellow).

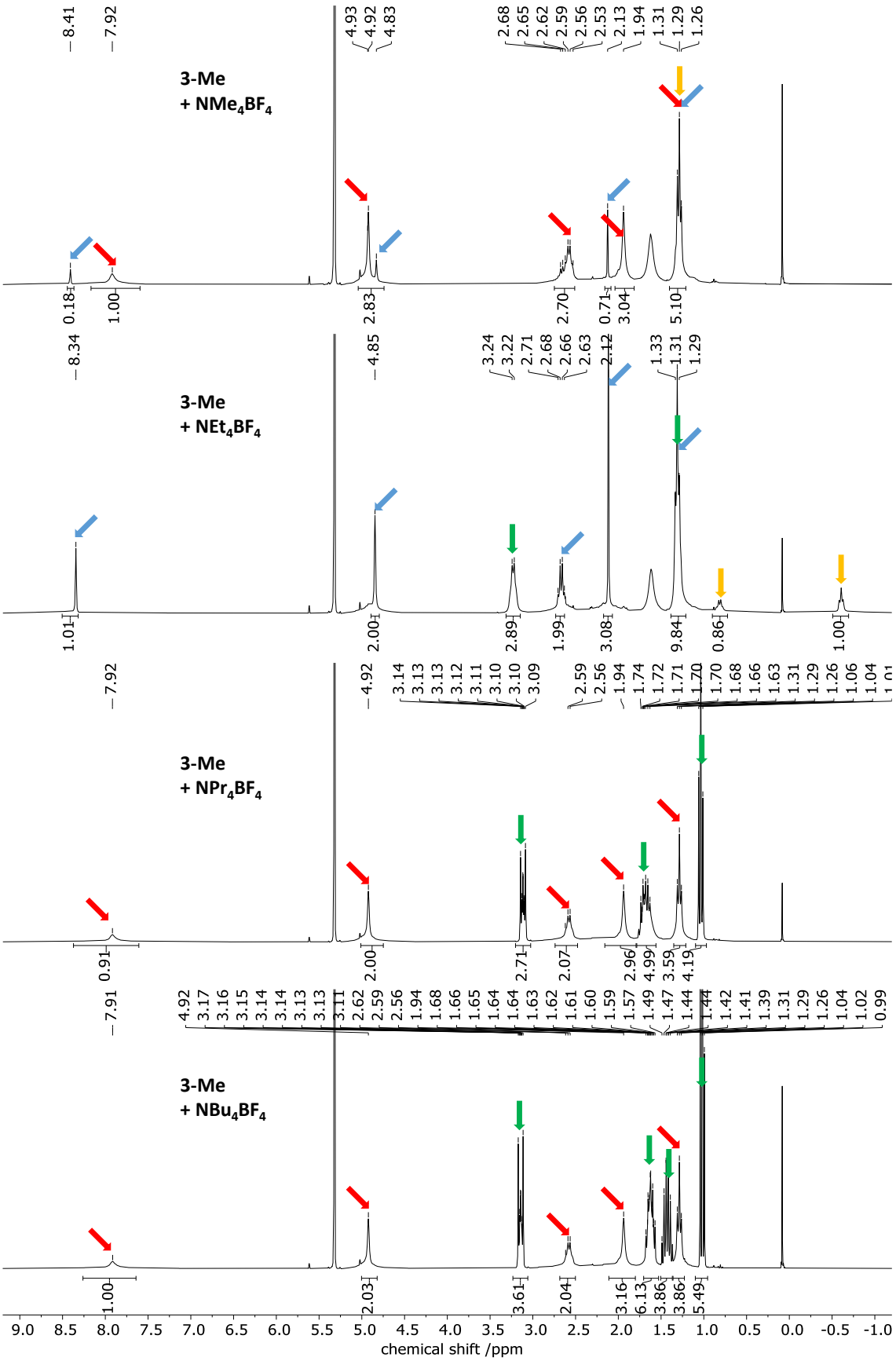

Figure S30: ^{1}H NMR spectra (CD_2Cl_2, 300 MHz) of **3-Me** with tetraalkylammonium tetrafluoroborate added. Arrows highlight characteristic signal(s) from the host cage (blue), the free cage (red), the free guest (green) and the bound guest (yellow).

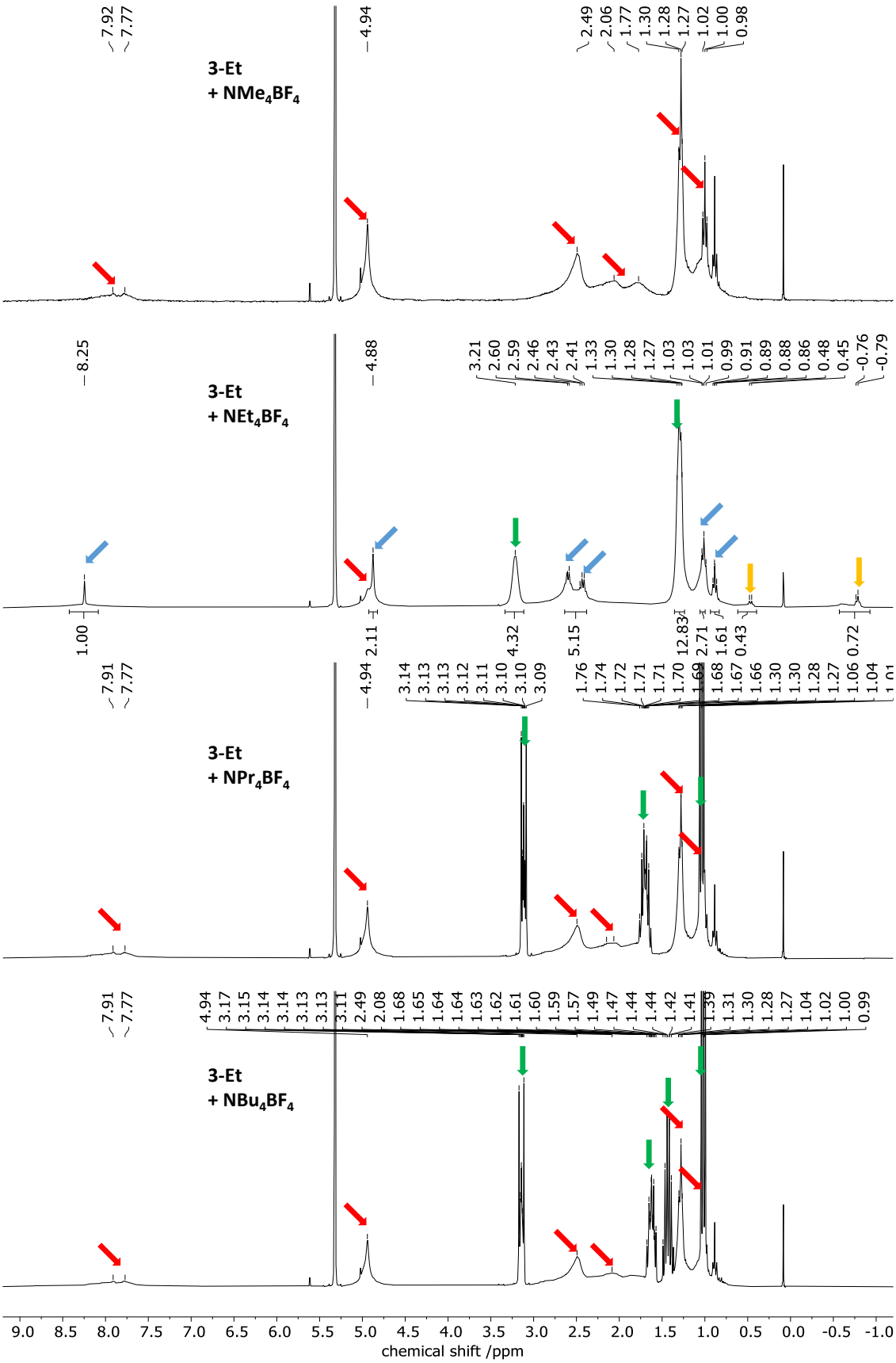

Figure S31: ^{1}H NMR spectra (CD_2Cl_2, 300 MHz) of **3-Et** with tetraalkylammonium tetrafluoroborate added. Arrows highlight characteristic signal(s) from the host cage (blue), the free cage (red), the free guest (green) and the bound guest (yellow).

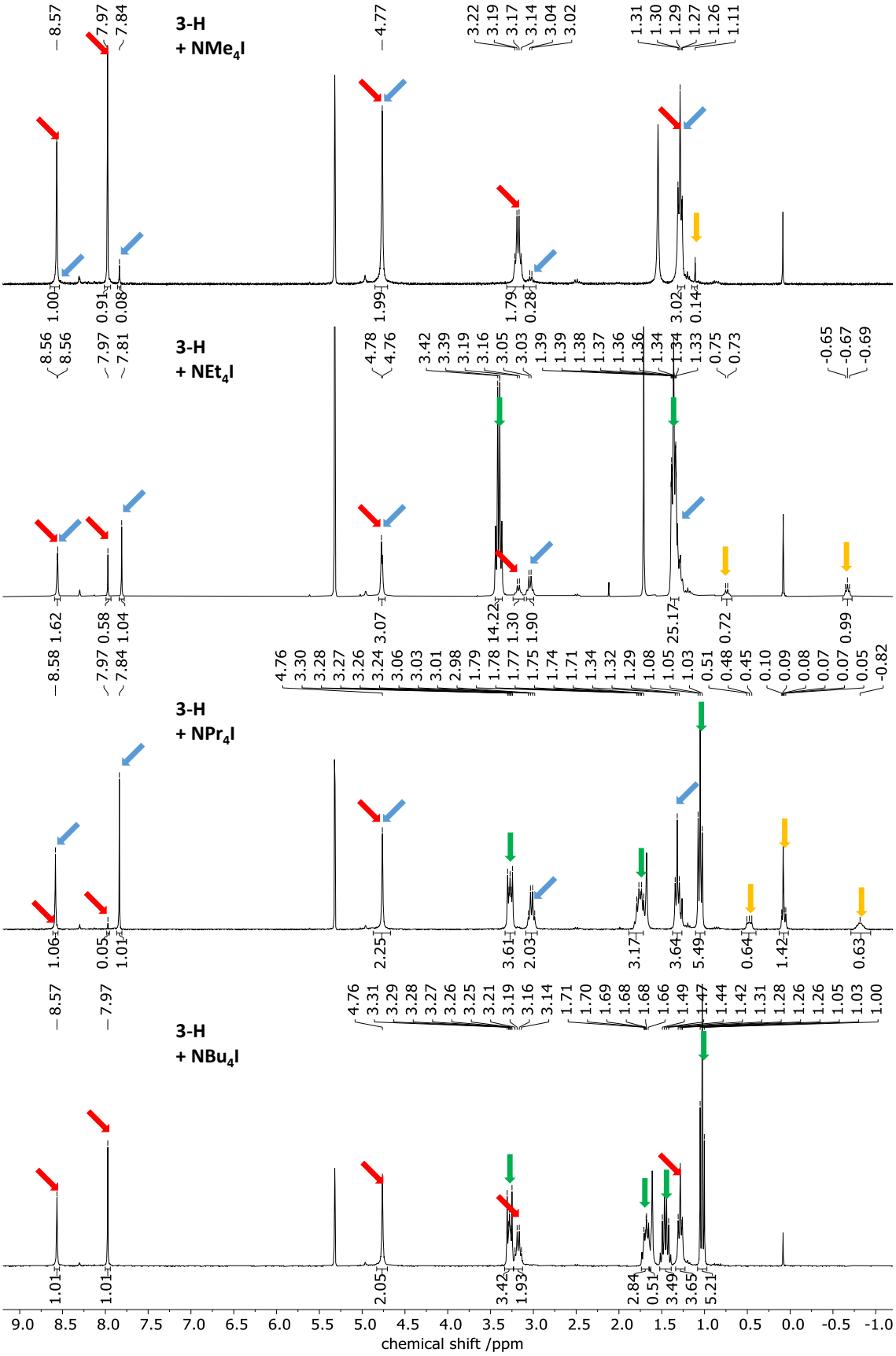

Figure S32: ^{1}H NMR spectra (CD_2Cl_2, 300 MHz) of **3-H** with tetraalkylammonium iodides added. Arrows highlight characteristic signal(s) from the host cage (blue), the free cage (red), the free guest (green) and the bound guest (yellow).

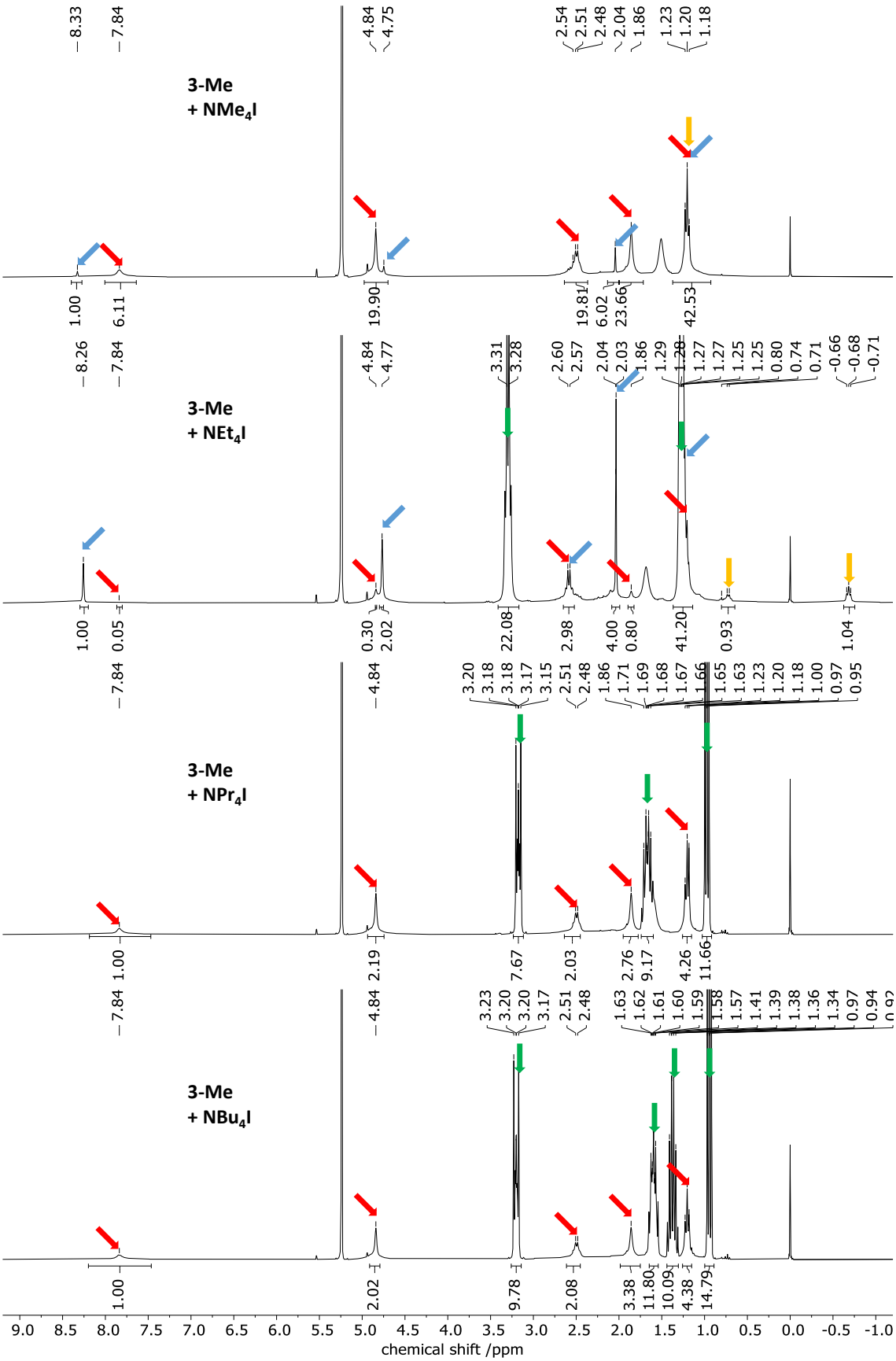

Figure S33: ^{1}H NMR spectra (CD_2Cl_2, 300 MHz) of **3-Me** with tetraalkylammonium iodides added. Arrows highlight characteristic signal(s) from the host cage (blue), the free cage (red), the free guest (green) and the bound guest (yellow).

Figure S34: ^{1}H NMR spectra (CD_2Cl_2, 300 MHz) of **3-Et** with tetraalkylammonium iodides added. Arrows highlight characteristic signal(s) from the host cage (blue), the free cage (red), the free guest (green) and the bound guest (yellow).

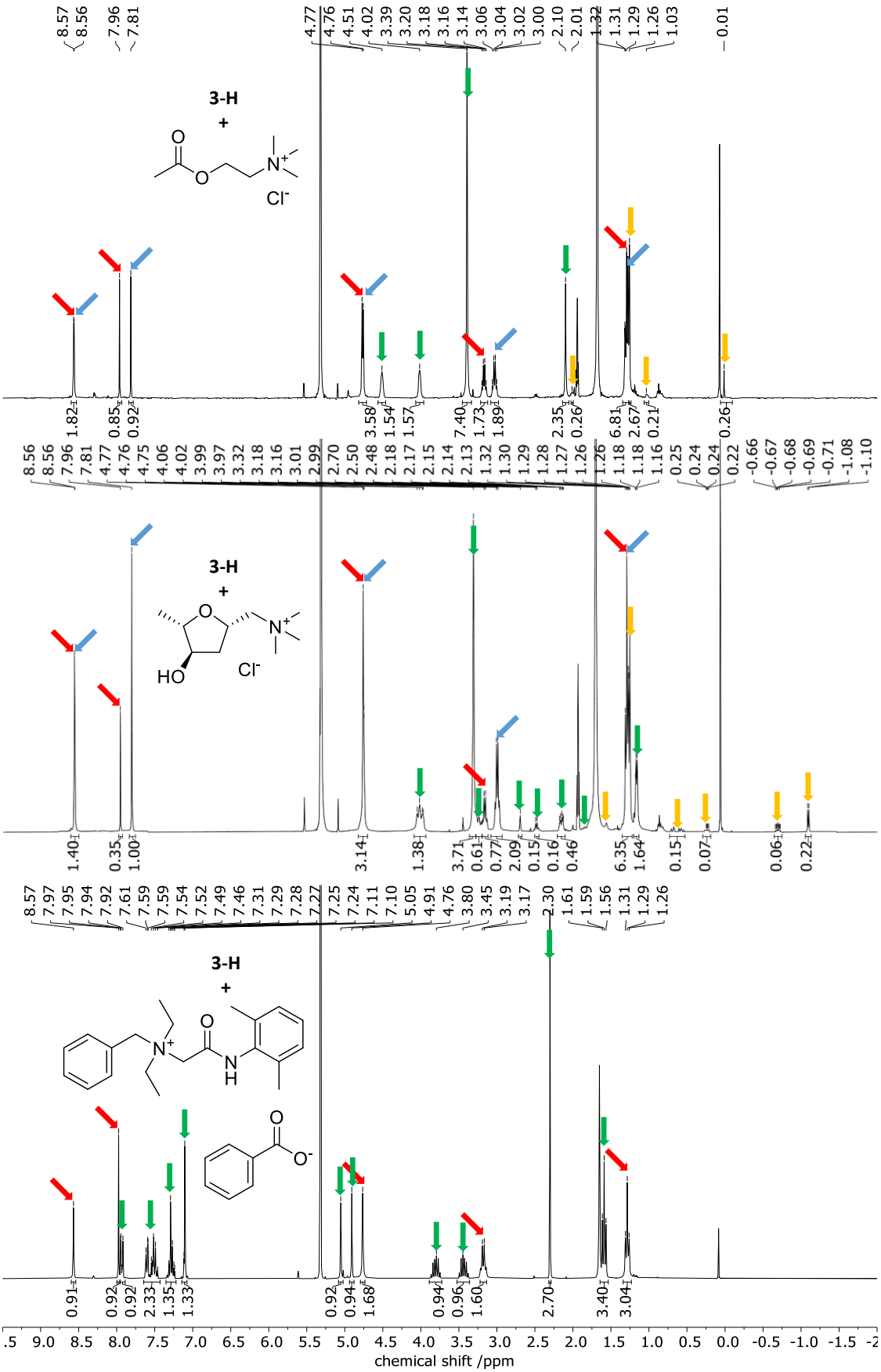

Figure S35: ^{1}H NMR spectra (CD_2Cl_2, 300 MHz) of **3-H** with different ammonia salts added. Arrows highlight characteristic signal(s) from the host cage (blue), the free cage (red), the free guest (green) and the bound guest (yellow).

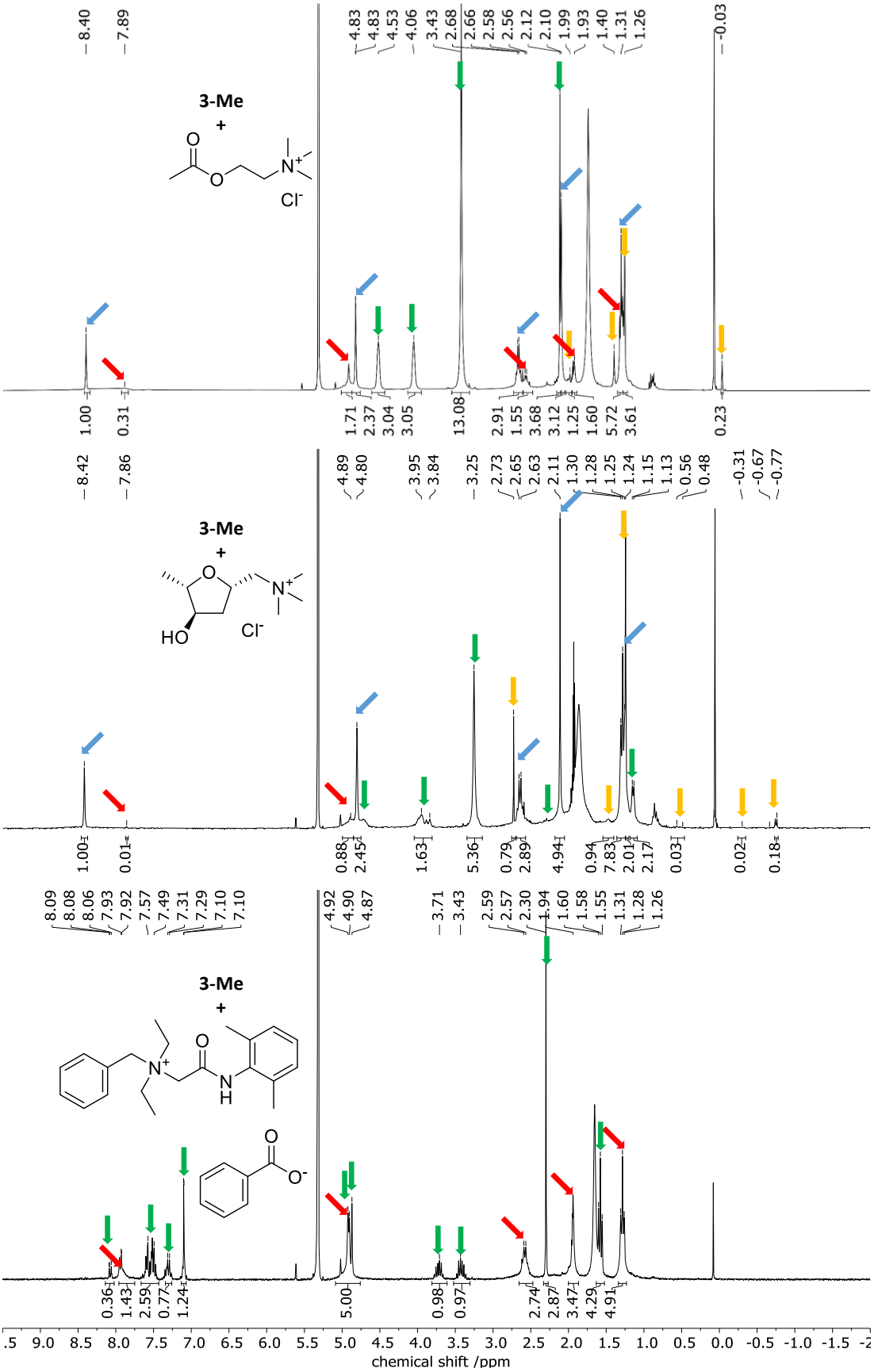

Figure S36: ^{1}H NMR spectra (CD_2Cl_2, 300 MHz) of **3-Me** with different ammonia salts added. Arrows highlight characteristic signal(s) from the host cage (blue), the free cage (red), the free guest (green) and the bound guest (yellow).

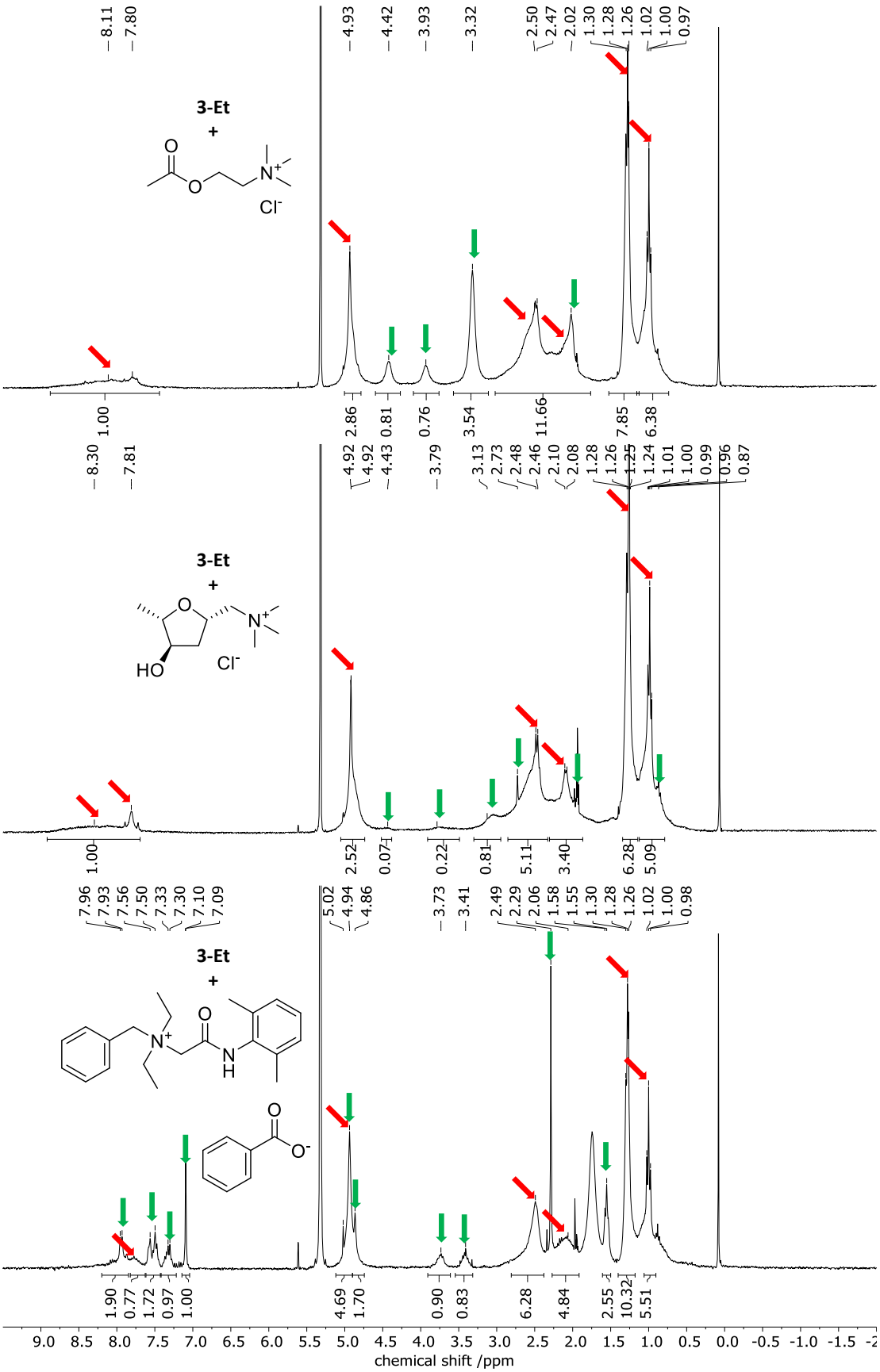

Figure S37: ^{1}H NMR spectra (CD_2Cl_2, 300 MHz) of **3-Et** with different ammonia salts added. Arrows highlight characteristic signal(s) from the host cage (blue), the free cage (red), the free guest (green) and the bound guest (yellow).

Table S3: Evaluation of the association constant (K_A) for the guest-inclusion process measured by ^{1}H NMR at 298 K in CD_2Cl_2.

Guest	Cage	Qnt Cage (μmol)	Qnt Guest (μmol)	Vol. CD_2Cl_2 (μL)	Fraction [Cage]/ [Guest@Cage]	Fraction [Guest]/ [Guest@Cage]	[Cage] (mM)	[Guest @Cage] (mM)	[Guest] (mM)	K'_A (M^{-1})	K_A (M^{-1})	σ
NMe_4BF_4	3-H	2	6	750	0.863 : 0.137	N/A [a]	2.301	0.365	7.635	21	19	1
NMe_4BF_4	3-H	2	6	750	0.875 : 0.125	N/A [a]	2.333	0.333	7.667	19		
NMe_4BF_4	3-H	2	6	750	0.876 : 0.124	N/A [a]	2.336	0.330	7.670	18		
NMe_4BF_4	3-H	2	6.4	500+125[b]	0.771 : 0.229	0.863 : 0.137	2.467	0.733	8.837	34	32	1
NMe_4BF_4	3-H	2	6.3	500+125[b]	0.777 : 0.223	0.870 : 0.130	2.486	0.714	8.770	33		
NMe_4BF_4	3-H	2	6.8	500+125[b]	0.768 : 0.232	0.857 : 0.143	2.458	0.742	9.324	32		
NMe_4BF_4	3-H	2	6.8	500+125[b]	0.778 : 0.222	0.862 : 0.138	2.490	0.710	9.379	30		
NMe_4I	3-H	2	6	500	0.921 : 0.079	N/A [a]	3.684	0.316	11.684	7.3	7.3	0.5
NMe_4I	3-H	2	7	500	0:915 : 0.085	N/A [a]	3.660	0.340	13.660	6.8		
NMe_4I	3-H	2	8	500	0.893 : 0.107	N/A [a]	3.572	0.428	15.572	7.7		
NEt_4BF_4	3-H	2	4.7	750	0.095 : 0.905	0.625 : 0.375	0.253	2.414	3.916	2.44×10^3	2.4×10^3	0.1×10^3
NEt_4BF_4	3-H	2	4.8	750	0.104 : 0.896	0.615 : 0.385	0.277	2.390	3.926	2.20×10^3		
NEt_4BF_4	3-H	2	6.7	750	0.055 : 0.945	0.761 : 0.239	0.147	2.520	6.900	2.48×10^3		
NEt_4BF_4	3-H	2	6.8	750	0.057 : 0.943	0.757 : 0.243	0.152	2.515	6.863	2.41×10^3		
NEt_4BF_4	3-H	2	6.9	750	0.054 : 0.946	0.753 : 0.247	0.144	2.523	6.827	2.57×10^3		
NEt_4I	3-H	2	25	500	0.360 : 0.640	0.961 : 0.039	1.440	2.560	48.05	3.70×10^1	3.5×10^1	0.2×10^1
NEt_4I	3-H	2	26	500	0.376 : 0.624	0.959 : 0. 41	1.504	2.496	49.87	3.33×10^1		
NEt_4I	3-H	2	27	500	0.359 : 0.641	0.954 : 0.046	1.436	2.564	51.52	3.46×10^1		
NPr_4BF_4	3-H	2	6.4	750	0.074 : 0.926	0.729 : 0.271	0.197	2.470	6.220	2.01×10^3	1.9×10^3	0.1×10^3
NPr_4BF_4	3-H	2	6.6	750	0.079 : 0.921	0.719 : 0.281	0.211	2.456	6.33	1.83×10^3		
NPr_4BF_4	3-H	2	7.1	750	0.074 : 0.926	0.756 : 0.244	0.197	2.470	7.258	1.73×10^3		
NPr_4BF_4	3-H	2	7.2	750	0.069 : 0.931	0.761 : 0.239	0.184	2.483	7.306	1.85×10^3		
NPr_4BF_4	3-H	2	7.3	750	0.070 : 0.930	0.762 : 0.238	0.187	2.480	7.315	1.81×10^3		
NPr_4I	3-H	2	12	500	0.065 : 0.935	0.850 : 0.150	0.26	3.740	20.400	7.05×10^2	9.21×10^2	1.9×10^2
NPr_4I	3-H	2	11.6	500	0.045 : 0.955	0.845 : 0.155	0.180	3.820	19.604	1.08×10^3		
NPr_4I	3-H	2	10.5	500	0.055 : 0.945	0.838 : 0.162	0.220	3.78	17.598	9.76×10^2		
NBu_4BF_4	3-H	2	7.7	750	1 : 0	1 : 0	2.667	0	10.4	0	0	0
NBu_4I	3-H	2	11.2	600	1 : 0	1 : 0	3.333	0	18.7	0	0	0
NMe_4BF_4	3-Me	2	6	750	0.780 : 0.220	N/A [a]	2.080	0.587	5.920	48	47	3
NMe_4BF_4	3-Me	2	6	750	0.772 : 0.228	N/A [a]	2.059	0.608	5.941	50		
NMe_4BF_4	3-Me	2	6	750	0.792 : 0.208	N/A [a]	2.112	0.555	5.888	45		
NMe_4BF_4	3-Me	2	3	500+125[b]	0.829 : 0.171	0.932 : 0.068	2.653	0.547	4.474	46	53	7
NMe_4BF_4	3-Me	2	2.5	500+125[b]	0.817 : 0.183	0.903 : 0.097	2.614	0.586	3.612	62		
NMe_4BF_4	3-Me	2	2.8	500+125[b]	0.832 : 0.168	0.932 : 0.068	2.662	0.538	4.175	48		
NMe_4BF_4	3-Me	2	2.5	500+125[b]	0.825 : 0.175	0.906 : 0.094	2.640	0.560	3.624	58		
NMe_4I	3-Me	1	6	500	0.822 : 0.178	N/A [a]	1.644	0.356	11.64	19	15	3
NMe_4I	3-Me	1	7	500	0.856 : 0.144	N/A [a]	1.712	0.288	13.71	12		
NMe_4I	3-Me	1	8	500	0.812 : 0.188	N/A [a]	1.624	0.376	15.62	15		
NEt_4BF_4	3-Me	2	13.4	750	0.001 : 0.999 [c]	0.792 : 0.208	<0.003	>2.663	10.61	$>1 \times 10^5$	$>10^5$	-
NEt_4I	3-Me	1	17.3	500	0.011 : 0.989	0.980 : 0.120	0.022	1.978	32.62	2.76×10^3	2.4×10^3	0.3×10^3
NEt_4I	3-Me	1	5.3	500	0.045 : 0.955	0.820 : 0.180	0.090	1.910	8.690	2.44×10^3		
NEt_4I	3-Me	1	12.8	500	0.020 : 0.980	0.923 : 0.077	0.040	1.960	23.64	2.07×10^3		
NPr_4BF_4	3-Me	2	7.6	750	1 : 0	1 : 0	2.667	0	10.1	0	0	0
NPr_4I	3-Me	1	11.5	500	1 : 0	1 : 0	2	0	23.1	0	0	0
NBu_4BF_4	3-Me	2	9	750	1 : 0	1 : 0	2.667	0	12	0	0	0
NBu_4I	3-Me	2	14.7	500	1 : 0	1 : 0	2	0	29.4	0	0	0
NMe_4BF_4	3-Et	2	6	750	1 : 0	1 : 0	2.667	0	8	0	0	0
NMe_4BF_4	3-Et	2	6.4	500+125[b]	1 : 0	1 : 0	3.200	0	10.2	0	0	0
NMe_4I	3-Et	2	6	600	1 : 0	1 : 0	3.333	0	10	0	0	0
NEt_4BF_4	3-Et	2	17	750	0.001 : 0.999 [c]	0.792 : 0.208	<0.003	>2.663	10.801	$>1 \times 10^5$	$> 10^5$	-
NEt_4I	3-Et	2	16.3	500	0.392 : 0.608	0.925 : 0.075	1.568	2.432	30.17	5.14×10^1	4.8×10^1	0.5×10^1
NEt_4I	3-Et	2	17.3	500	0.423 : 0.577	0.933 : 0.067	1.692	2.308	32.29	4.22×10^1		
NEt_4I	3-Et	2	17.5	500	0.386 : 0.614	0.930 : 0.070	1.544	2.456	32.544	4.89×10^1		
NPr_4BF_4	3-Et	2	10	750	1 : 0	1 : 0	2.667	0	13.3	0	0	0

NPr_4I	3-Et	1	19.7	600	1 : 0	1 : 0	2	0	39.4	0	0	0
NBu_4BF_4	3-Et	2	12	750	1 : 0	1 : 0	2.667	0	16	0	0	0
NBu_4I	3-Et	1	13.6	600	1 : 0	1 : 0	2	0	27.2	0	0	0

[a] suspension. [b] MeCN was added to get a clear solution. [c] Concentration of free cage is under the detection limit of the ^{1}H NMR.[S12]

Table S4: Evaluation of the association constant (K_A) of the pharmaceutically active guests-measured by ^{1}H NMR at 298 K in CD_2Cl_2-MeCN-d_3 (9:1, v/v).

Ac.coline	3-H	1	6.1	450+50	0.498 : 0.502	0.919 : 0.081	0.996	1.004	11.21	8.99×10^1	8.3×10^1	0.9×10^1
Ac.coline	3-H	1	5.7	450+50	0.565 : 0.436	0.928 : 0.072	1.130	0.870	10.58	7.28×10^1		
Ac.coline	3-H	1	6.8	450+50	0.479 : 0.521	0.923 : 0.076	0.958	1.042	12.56	8.66×10^1		
Muscarine	3-H	1	4.5	450+50	0.270 : 0.730	0.836 : 0.163	0.540	1.460	7.491	3.61×10^2	3.67×10^2	0.06×10^2
Muscarine	3-H	1	4.4	450+50	0.266 : 0.734	0.835 : 0.165	0.532	1.468	7.415	3.72×10^2		
Muscarine	3-H	1	4.5	450+50	0.268 : 0.732	0.836 : 0.164	0.536	1.464	7.440	3.67×10^2		
Bitrex	3-H	2	12.2	500	1 : 0	1 : 0	4	0	24.4	0	0	0
Ac.coline	3-Me	1	13.3	450+50	0.237 : 0.763	0.946 : 0.054	0.474	1.526	25.16	1.28×10^2	1.2×10^2	0.1×10^2
Ac.coline	3-Me	1	13.5	450+50	0.275 : 0.725	0.945 : 0.055	0.550	1.45	25.55	1.03×10^2		
Ac.coline	3-Me	1	14	450+50	0.238 : 0.762	0.946 : 0.054	0.476	1.524	26.48	1.25×10^2		
Muscarine	3-Me	1	4	450+50	0.015 : 0.985	0.753 : 0.247	0.030	1.970	6.03	1.09×10^4	7.7×10^3	2.9×10^3
Muscarine	3-Me	1	4.5	450+50	0.026 : 0.974	0.783 : 0.217	0.052	1.948	7.05	5.3×10^3		
Muscarine	3-Me	1	5	450+50	0.018 : 0.982	0.804 : 0.196	0.036	1.964	8.04	6.8×10^3		
Bitrex	3-Me	1	2.1	450+50	1 : 0	1 : 0	2	0	4.2	0	0	0
Ac.coline	3-Et	1	1.4	450+50	1 : 0	1 : 0	2	0	2.8	0	0	0
Muscarine	3-Et	1	3.3	450+50	1 : 0	1 : 0	2	0	6.6	0	0	0
Bitrex	3-Et	1	2	450+50	1 : 0	1 : 0	2	0	4	0	0	0

5.5 Host Guest Experiments in Tetrahydrofuran-d$_8$

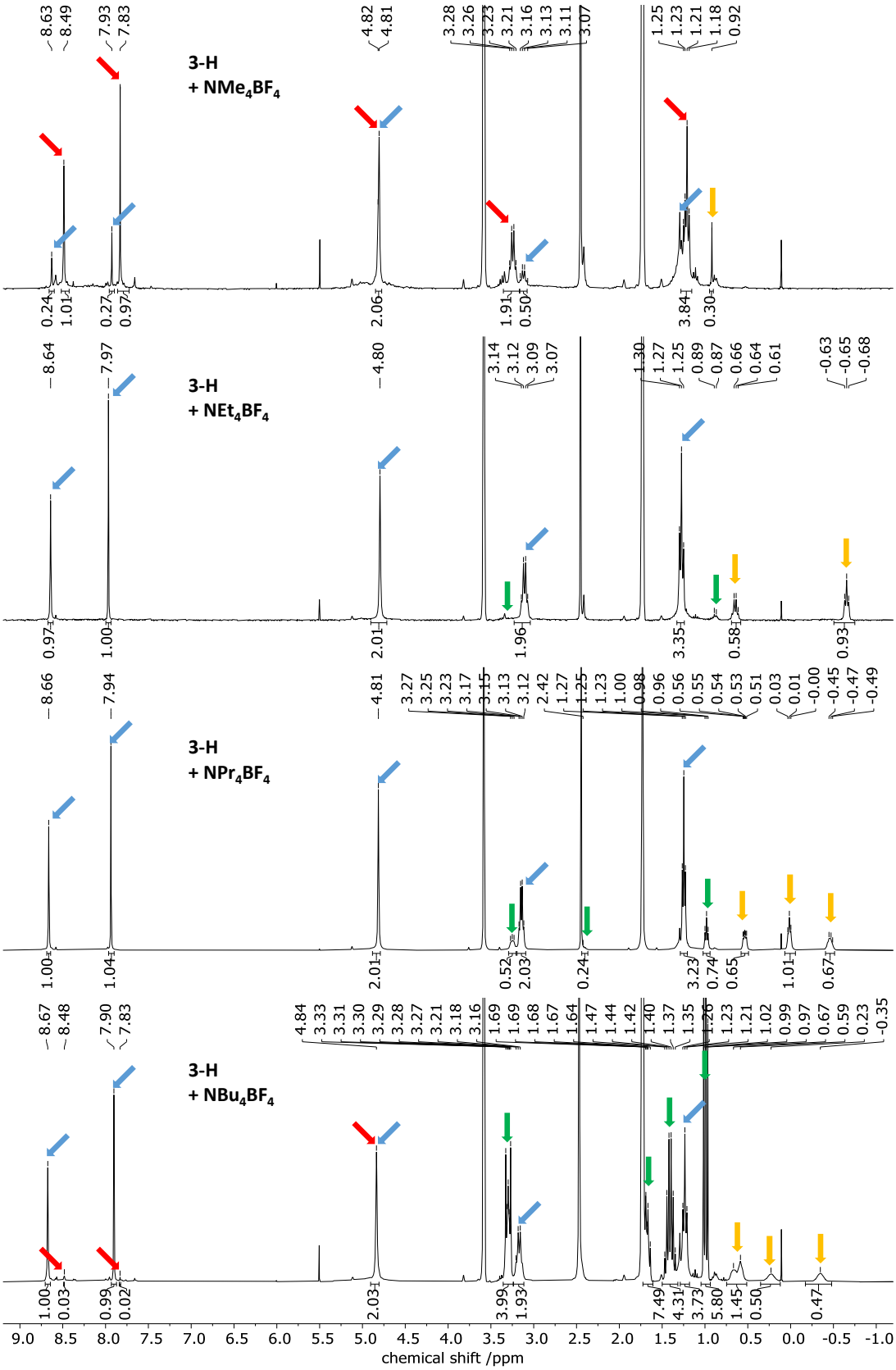

Figure S38: ^{1}H NMR spectra (THF-d$_8$, 300 MHz) of **3-H** with tetraalkylammonium tetrafluoroborate added. Arrows highlight characteristic signal(s) from the host cage (blue), the free cage (red), the free guest (green) and the bound guest (yellow).

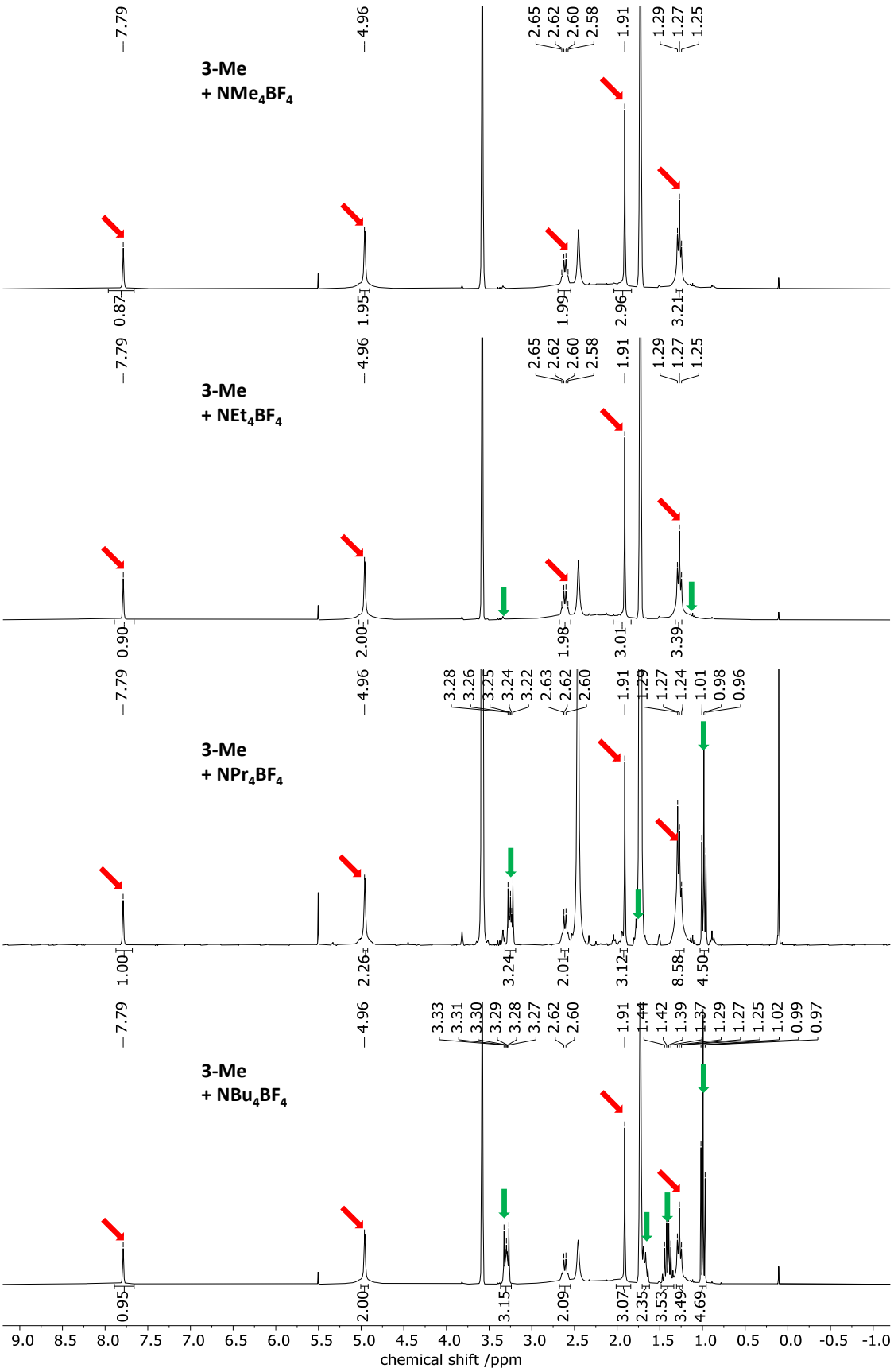

Figure S39: ^{1}H NMR spectra (THF-d_8, 300 MHz) of **3-Me** with tetraalkylammonium tetrafluoroborate added. Arrows highlight characteristic signal(s) from the host cage (blue), the free cage (red), the free guest (green) and the bound guest (yellow).

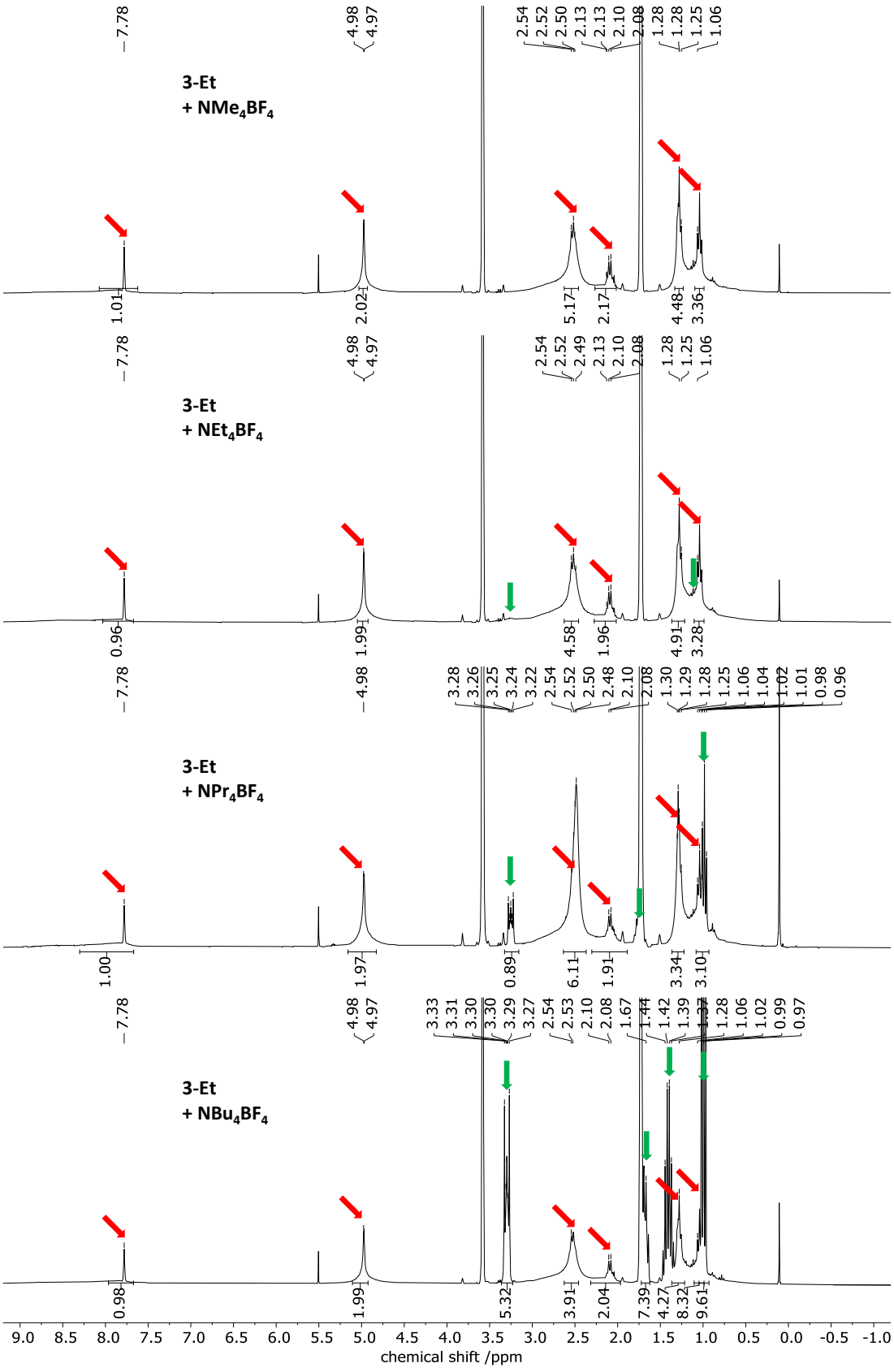

Figure S40: ^{1}H NMR spectra (THF-d_8, 300 MHz) of **3-Et** with tetraalkylammonium tetrafluoroborate added. Arrows highlight characteristic signal(s) from the host cage (blue), the free cage (red), the free guest (green) and the bound guest (yellow).

Table S5: Evaluation of the association constant (K_A) for the guest-inclusion process measured by ^{1}H NMR at 298 K in THF-d_8.

Guest	Cage	Qnt Cage (µmol)	Qnt Guest (µmol)	Vol. THF-d_8 (µL)	Fraction [Cage]/ [Guest@Cage]	Fraction [Guest]/ [Guest@Cage]	[Cage] (mM)	[Guest@Cage] (mM)	[Guest] (mM)	K'_A (M^{-1})	K_A (M^{-1})	σ
NMe_4BF_4	3t-H	2	12	750	0.771 : 0.229	N/A [a]	2.056	0.611	15.39	19	21	3
NMe_4BF_4	3-H	2	12	750	0.775 :0.224	N/A [a]	2.067	0.597	15.40	19		
NMe_4BF_4	3-H	2	24	750	0.768 : 0.232	N/A [a]	2.048	0.619	15.38	20		
NMe_4BF_4	3-H	2	24	750	0.716 : 0.284	N/A [a]	1.910	0.757	15.24	26		
NEt_4BF_4	3-H	2	6	750	0.001 : 0.999 [b]	N/A [a]	<0.003	>2.663	5.337	>1x10^5	>1 x 10^5	-
NEt_4BF_4	3-H	2	6	750	0.001 : 0.999 [b]	N/A [a]	<0.003	>2.663	5.337	>1x10^5		
NEt_4BF_4	3-H	2	6	750	0.001 : 0.999 [b]	N/A [a]	<0.003	>2.663	5.337	>1 x 10^5		
NPr_4BF_4	3-H	2	3.5	750	0.001 : 0.999 [b]	0.423 : 0.577	<0.003	>2.663	1.974	>1 x 10^5	>1 x 10^5	-
NPr_4BF_4	3-H	2	4.2	750	0.001 : 0.999 [b]	0.518 : 0.483	<0.003	>2.663	2.901	>1 x 10^5		
NPr_4BF_4	3-H	2	2.4	750	0.001 : 0.999 [b]	0.220 : 0.780	<0.003	>2.663	0.704	>1 x 10^5		
NBu_4BF_4	3-H	2	11.2	750	0.039 : 0.961	0.839 : 0.161	0.104	2.563	12.529	1.97 x 10^3	2.13 x 10^3	0.29 x 10^3
NBu_4BF_4	3-H	2	11.2	750	0.035 : 0.965	0.836 : 0.164	0.093	2.574	12.484	2.22 x 10^3		
NBu_4BF_4	3-H	2	8.4	750	0.055 : 0.955	0.788 : 0.122	0.147	2.547	8.826	1.96 x 10^3		
NBu_4BF_4	3-H	2	11.4	750	0.028 : 0.972	0.846 : 0.154	0.075	2.592	12.859	2.69 x 10^3		
NBu_4BF_4	3-H	2	12.8	750	0.033 : 0.967	0.862 : 0.138	0.088	2.579	14.711	1.99 x 10^3		
NBu_4BF_4	3-H	2	13.8	750	0.031 : 0.969	0.868 : 0.132	0.083	2.584	15.971	1.96 x 10^3		
NMe_4BF_4	3-Me	2	12	750	1 : 0	N/A [a]	2.667	0	16	0	0	0
NEt_4BF_4	3-Me	2	6	750	1 : 0	N/A [a]	2.667	0	8	0	0	0
NPr_4BF_4	3-Me	1	4.9	750	1 : 0	1 : 0	1.334	0	6.5	0	0	0
NBu_4BF_4	3-Me	2	9.5	750	1 : 0	1 : 0	2.667	0	12.7	0	0	0
NMe_4BF_4	3-Et	2	12	750	1 : 0	N/A [a]	2.667	0	16	0	0	0
NEt_4BF_4	3-Et	2	6	750	1 : 0	N/A [a]	2.667	0	8	0	0	0
NPr_4BF_4	3-Et	1	1.4	750	1 : 0	1 : 0	1.334	0	1.9	0	0	0
NBu_4BF_4	3-Et	2	15.9	750	1 : 0	1 : 0	2.667	0	21.2	0	0	0

[a] Suspension. [b] Concentration of free cage is under the detection limit of the ^{1}H NMR.[S12]

5.5.1 Folding of the Guest Inside the Cavity

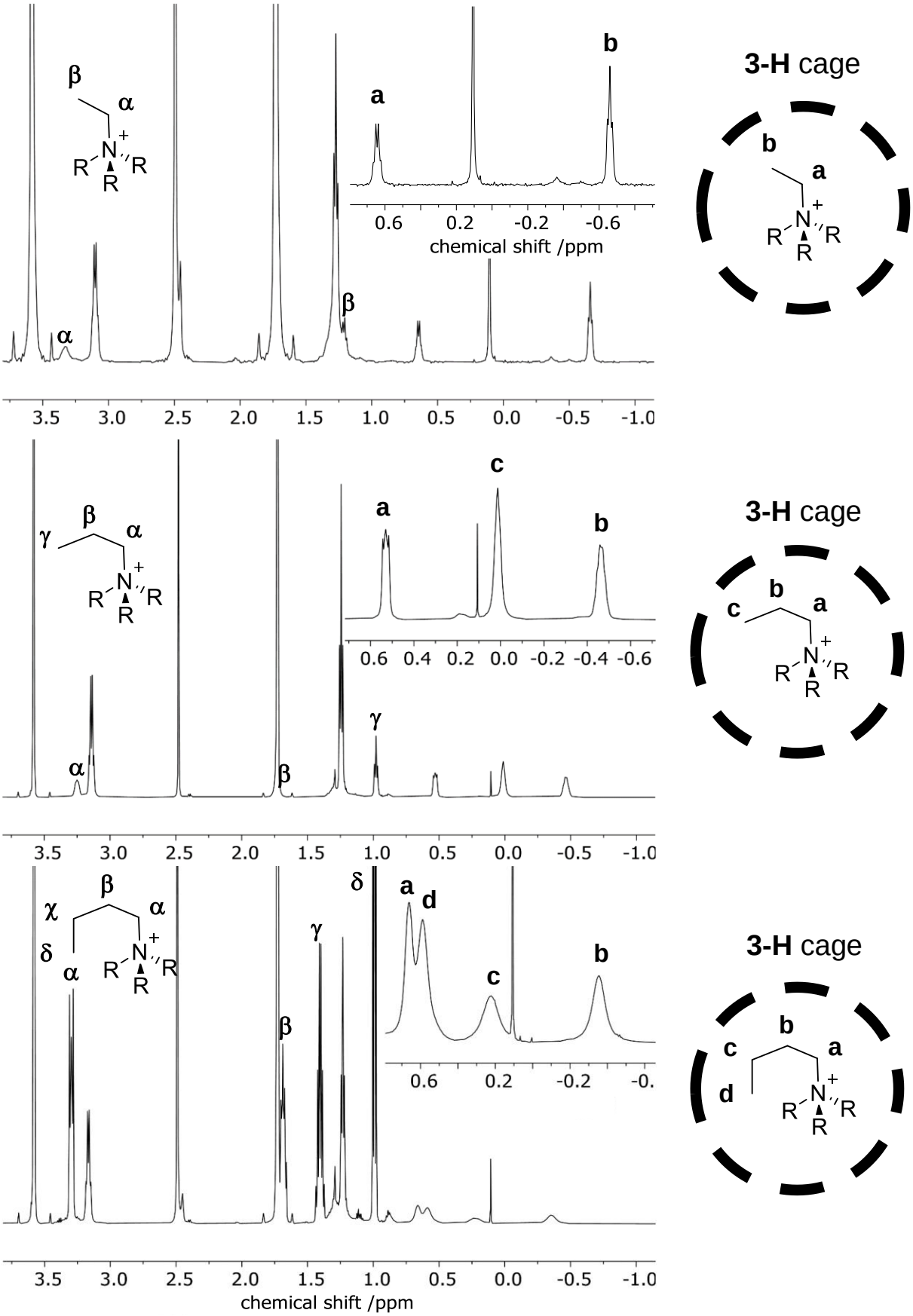

Figure S41: ^{1}H NMR spectra (THF-d_8; top: 500 MHz, middle and bottom 600 MHz) of **3-H** with tetraalkylammonium tetrafluoroborate added.

5.6 Host Guest Experiments in Chloroform-d

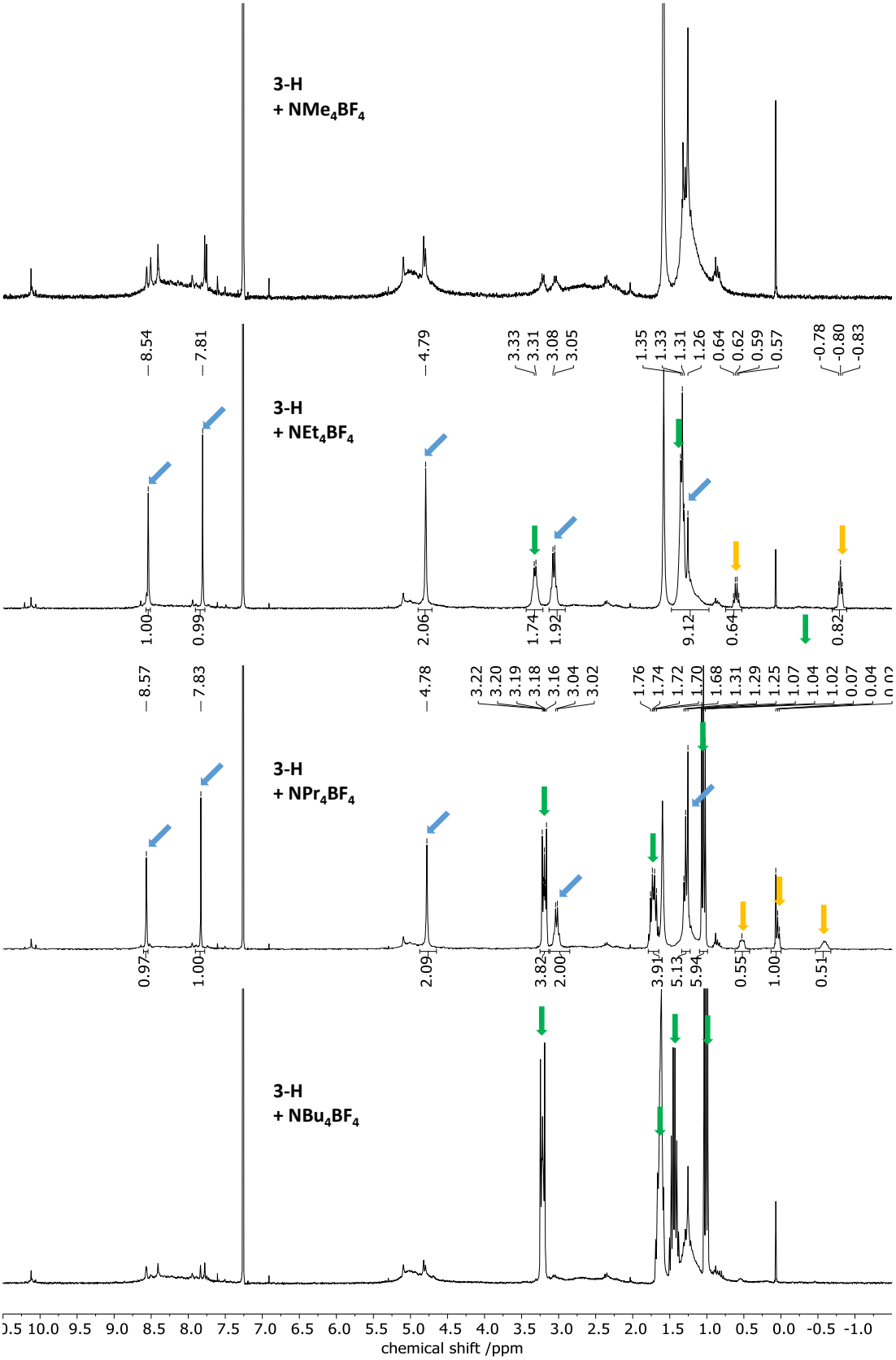

Figure S42: ^{1}H NMR spectra ($CDCl_3$, 300 MHz) of **3-H** with tetraalkylammonium tetrafluoroborate added. Arrows highlight characteristic signal(s) from the host cage (blue), the free cage (red), the free guest (green) and the bound guest (yellow).

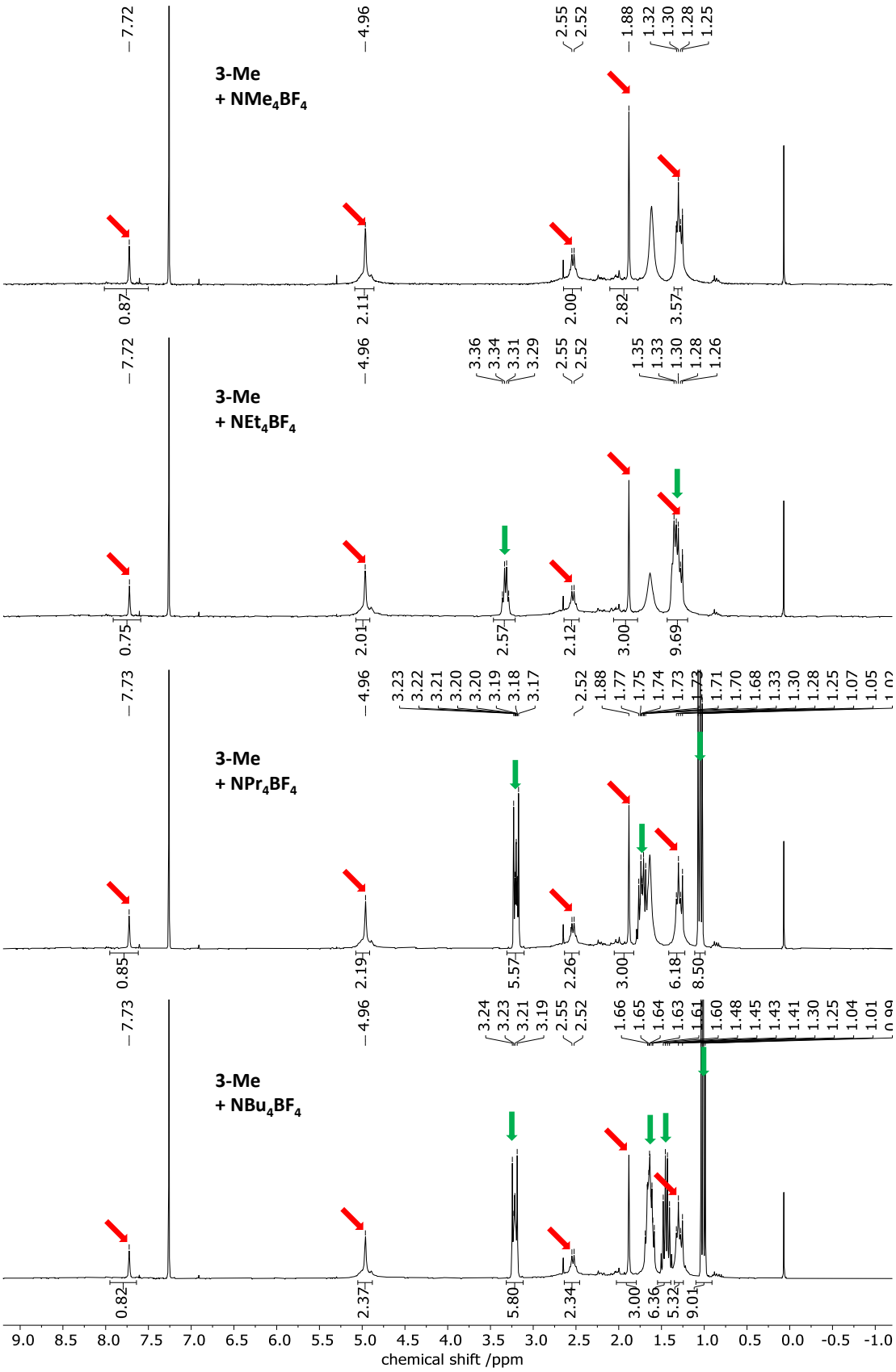

Figure S43: ^{1}H NMR spectra ($CDCl_3$, 300 MHz) of **3-Me** with tetraalkylammonium tetrafluoroborate added. Arrows highlight characteristic signal(s) from the host cage (blue), the free cage (red), the free guest (green) and the bound guest (yellow).

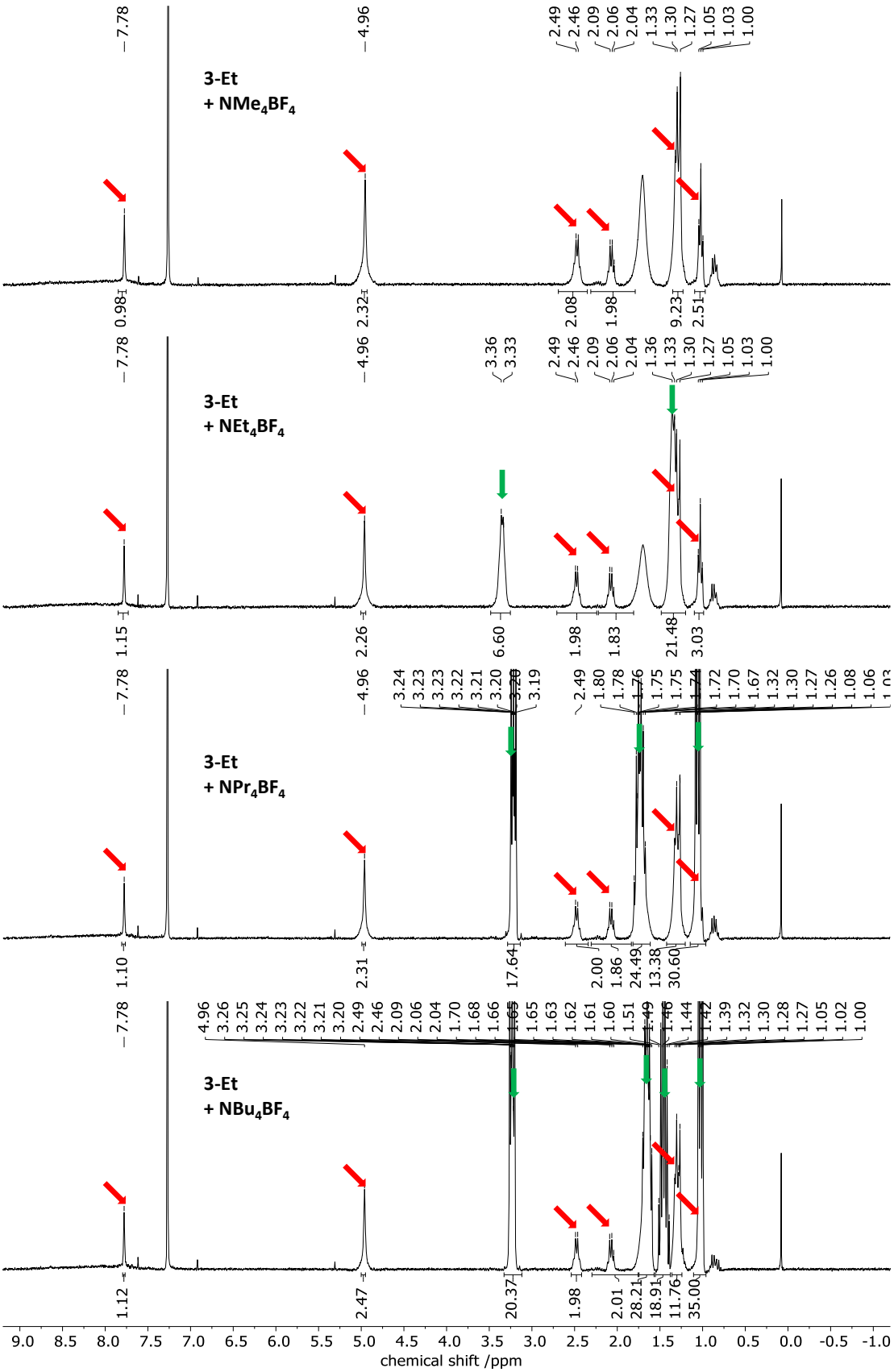

Figure S44: ^{1}H NMR spectra ($CDCl_3$, 300 MHz) of **3-Et** with tetraalkylammonium tetrafluoroborate added. Arrows highlight characteristic signal(s) from the host cage (blue), the free cage (red), the free guest (green) and the bound guest (yellow).

Table S6: Evaluation of the association constant (K_A) for the guest-inclusion process measured by ^{1}H NMR at 298 K in $CDCl_3$.

Guest	Cage	Qnt Cage (µmol)	Qnt Guest (µmol)	Vol. $CDCl_3$ (µL)	Fraction [Cage]/ [Guest@Cage]	Fraction [Guest]/ [Guest@Cage]	[Cage] (mM)	[Guest@Cage] (mM)	[Guest] (mM)	K'_A (M^{-1})	K_A (M^{-1})	σ
NMe_4BF_4	3-H	0.7	12	600	- [a]	- [a]	- [a]	- [a]	- [a]	- [a]	- [a]	-
NEt_4BF_4	3-H	0.7	2.5	600	0.001 : 0.999 [a][b]	0.745 : 0.255[a]	<0.001[a]	>1.165[a]	3.104[a]	>1 x 10^{5}[a]	>1 x 10^{5}[a]	-
NPr_4BF_4	3-H	0.7	5.4	600	0.001 : 0.999 [a][b]	0.868 : 0.132[a]	<0.001[a]	>1.165[a]	7.812[a]	>1 x 10^{5}[a]	>1 x 10^{5}[a]	-
NBu_4BF_4	3-H	0.7	6	600	- [a]	- [a]	- [a]	- [a]	- [a]	- [a]	- [a]	-
NMe_4BF_4	3-Me	0.7	6	600	1 : 0	1 : 0	1.167	0	10	0	0	0
NEt_4BF_4	3-Me	0.7	6	600	1 : 0	1 : 0	1.167	0	10	0	0	0
NPr_4BF_4	3-Me	0.7	6	600	1 : 0	1 : 0	1.167	0	10	0	0	0
NBu_4BF_4	3-Me	0.7	6	600	1 : 0	1 : 0	1.167	0	10	0	0	0
NMe_4BF_4	3-Et	0.7	6	600	1 : 0	1 : 0	1.167	0	10	0	0	0
NEt_4BF_4	3-Et	0.7	6	600	1 : 0	1 : 0	1.167	0	10	0	0	0
NPr_4BF_4	3-Et	0.7	6	600	1 : 0	1 : 0	1.167	0	10	0	0	0
NBu_4BF_4	3-Et	0.7	6	600	1 : 0	1 : 0	1.167	0	10	0	0	0

[a] Decomposition of free cage. [b] Concentration of free cage is under the detection limit of the ^{1}H NMR.[S12]

5.7 Host Guest Experiments in Toluene-d$_8$

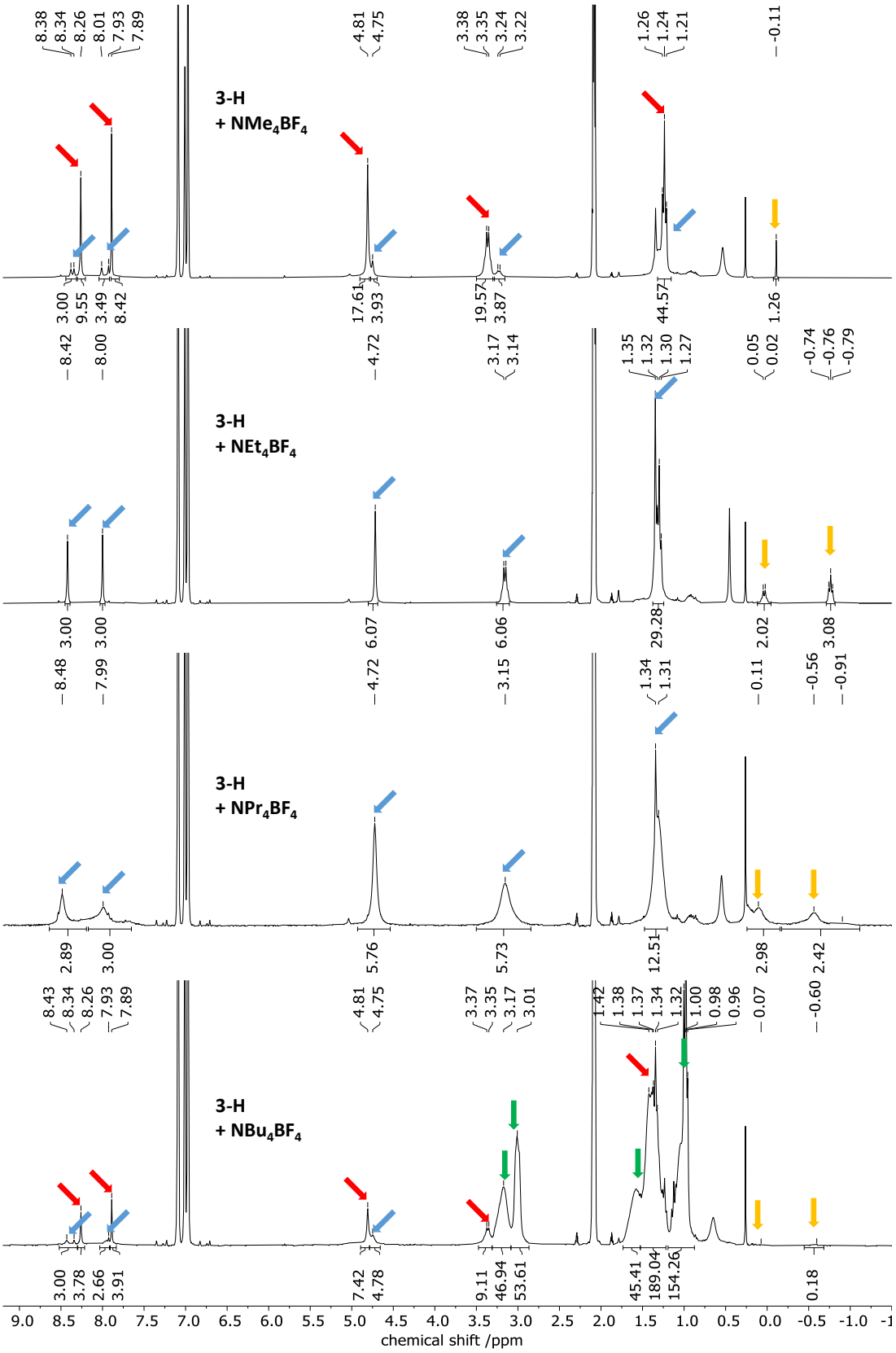

Figure S45: ^{1}H NMR spectra (PhMe-d$_8$, 300 MHz) of **3-H** with tetraalkylammonium tetrafluoroborate added. Arrows highlight characteristic signal(s) from the host cage (blue), the free cage (red), the free guest (green) and the bound guest (yellow).

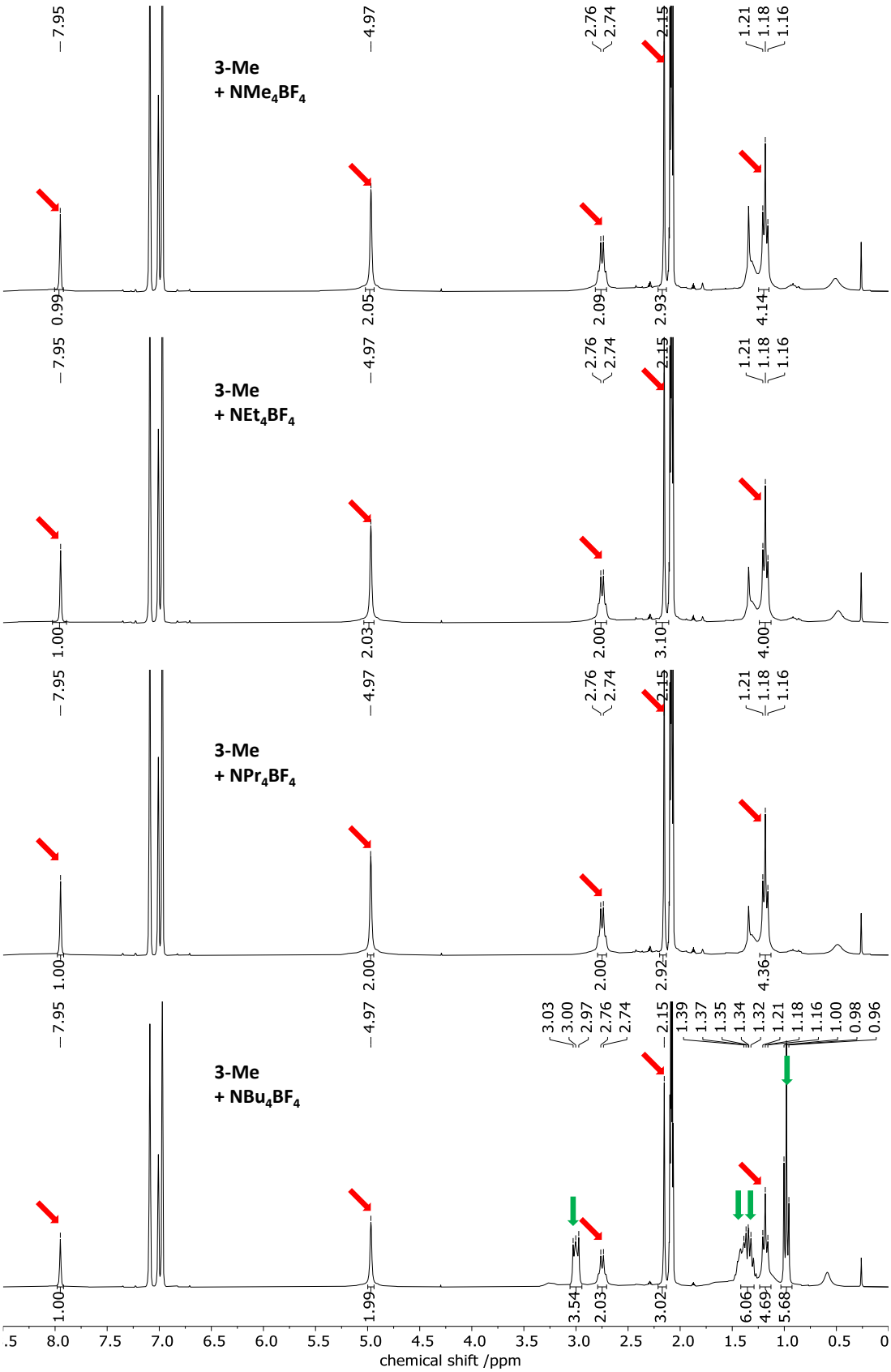

Figure S46: ^{1}H NMR spectra (PhMe-d_8, 300 MHz) of **3-Me** with tetraalkylammonium tetrafluoroborate added. Arrows highlight characteristic signal(s) from the host cage (blue), the free cage (red), the free guest (green) and the bound guest (yellow).

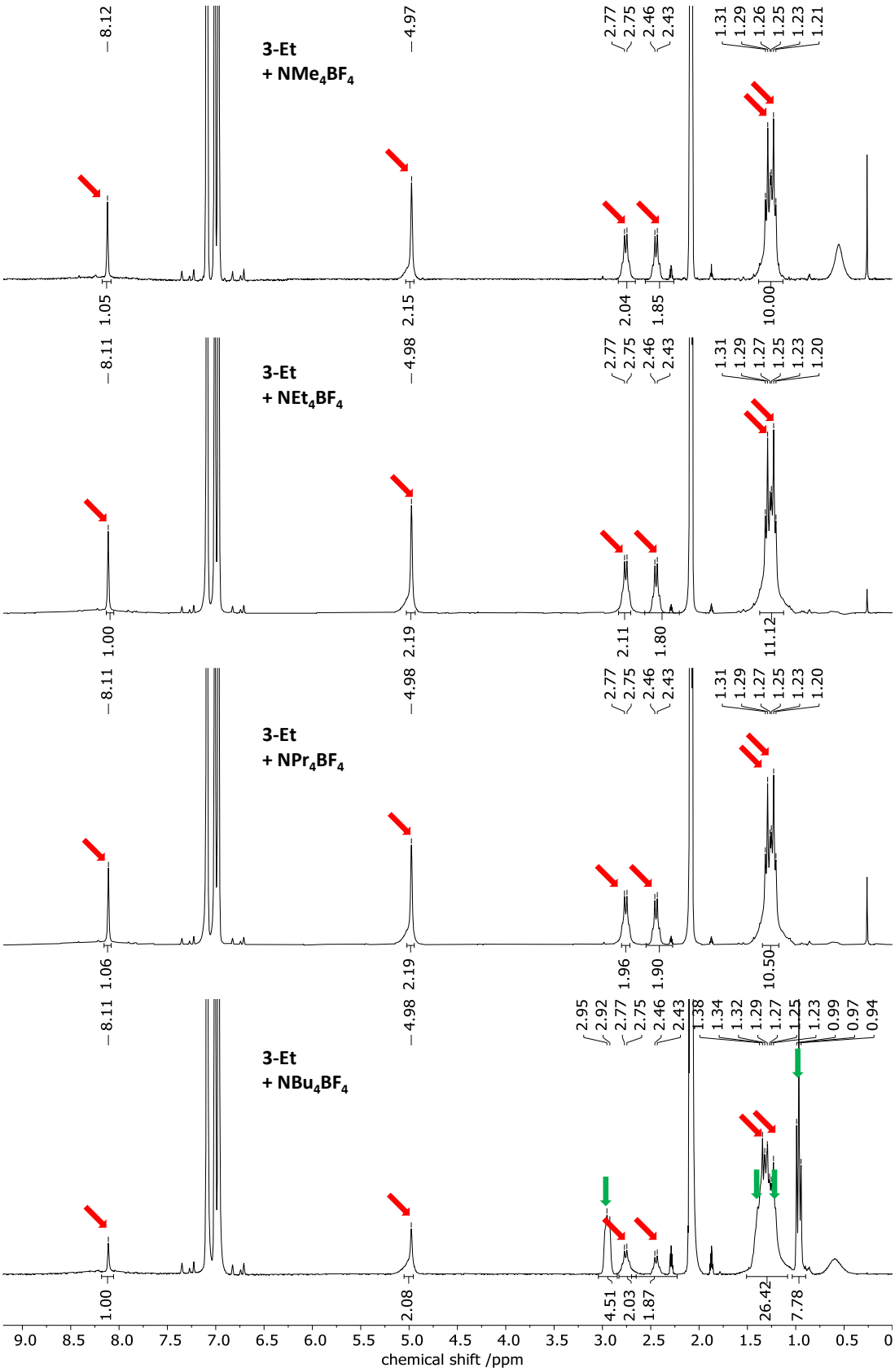

Figure S47: ^{1}H NMR spectra (PhMe-d_8, 300 MHz) of **3-Et** with tetraalkylammonium tetrafluoroborate added. Arrows highlight characteristic signal(s) from the host cage (blue), the free cage (red), the free guest (green) and the bound guest (yellow).

Table S7: Evaluation of the association constant (K_A) for the guest-inclusion process measured by ^{1}H NMR at 298 K in PhMe-d_8.

Guest	Cage	Qnt Cage (µmol)	Qnt Guest (µmol)	Vol. PhMe (µL)	Fraction [Cage]/ [Guest@Cage]	Fraction [Guest]/ [Guest@Cage]	[Cage] (mM)	[Guest@Cage] (mM)	[Guest] (mM)	K'_A (M^{-1})	K_A (M^{-1})	σ
NMe_4BF_4	3-H	0.7	4	600	0.835 : 0.165	N/A[a]	0.974	0.192	6.475	30	25	6
NMe_4BF_4	3-H	0.7	5	600	0.823 : 0.177	N/A[a]	0.960	0.207	8.126	27		
NMe_4BF_4	3-H	0.7	6	600	0.845 : 0.155	N/A[a]	0.986	0.181	9.819	19		
NEt_4BF_4	3-H	0.7	6	600	0.001 : 0.999 [b]	N/A[a]	<0.001	>1.165	8.835	>1 x 10^5	>1 x 10^5	-
NPr_4BF_4	3-H	0.7	6	600	0.01 : 0.99 [b][c]	N/A[a]	<0.01	>1.15	8.85	>1 x 10^5	>1 x 10^5	-
NBu_4BF_4	3-H	0.7	4.7	600	0.72 : 0.28 [c]	0.98 : 0.02	0.84	0.33	7.67	51	44	6
NBu_4BF_4	3-H	0.7	4.6	600	0.76 : 0.24 [c]	0.99 : 0.01	0.89	0.28	7.59	41		
NBu_4BF_4	3-H	0.7	10	600	0.61 : 0.39 [c]	0.99 : 0.01	0.71	0.46	16.49	39		
NMe_4BF_4	3-Me	0.7	6	600	1 : 0	1 : 0	1.167	0	10	0	0	0
NEt_4BF_4	3-Me	0.7	6	600	1 : 0	1 : 0	1.167	0	10	0	0	0
NPr_4BF_4	3-Me	0.7	6	600	1 : 0	1 : 0	1.167	0	10	0	0	0
NBu_4BF_4	3-Me	0.7	6	600	1 : 0	1 : 0	1.167	0	10	0	0	0
NMe_4BF_4	3-Et	0.7	6	600	1 : 0	1 : 0	1.167	0	10	0	0	0
NEt_4BF_4	3-Et	0.7	6	600	1 : 0	1 : 0	1.167	0	10	0	0	0
NPr_4BF_4	3-Et	0.7	6	600	1 : 0	1 : 0	1.167	0	10	0	0	0
NBu_4BF_4	3-Et	0.7	6	600	1 : 0	1 : 0	1.167	0	10	0	0	0

[a] Suspension. [b] Concentration of free cage is under the detection limit of the ^{1}H NMR.[S12]
[c] Broad Signals.

5.8 Mass Spectra of Host-Guest Compounds

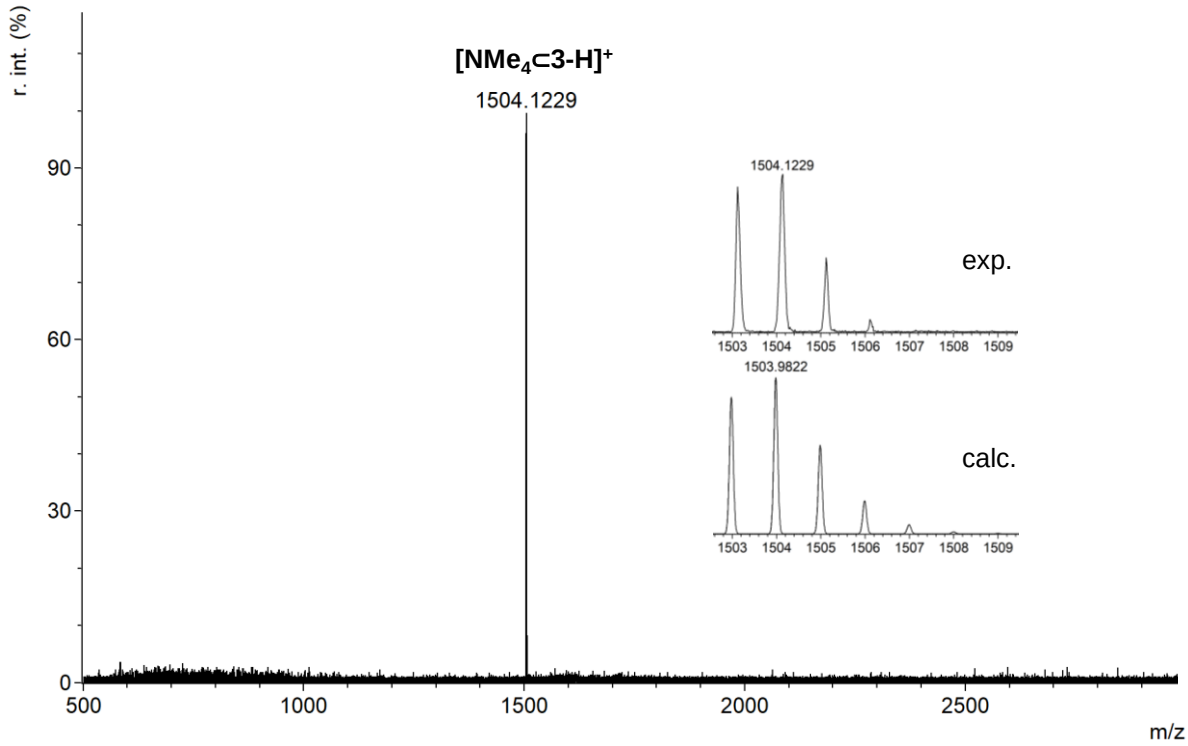

Figure S48: MALDI-TOF-MS of compound **[NMe$_4$⊂3-H]$^+$**.

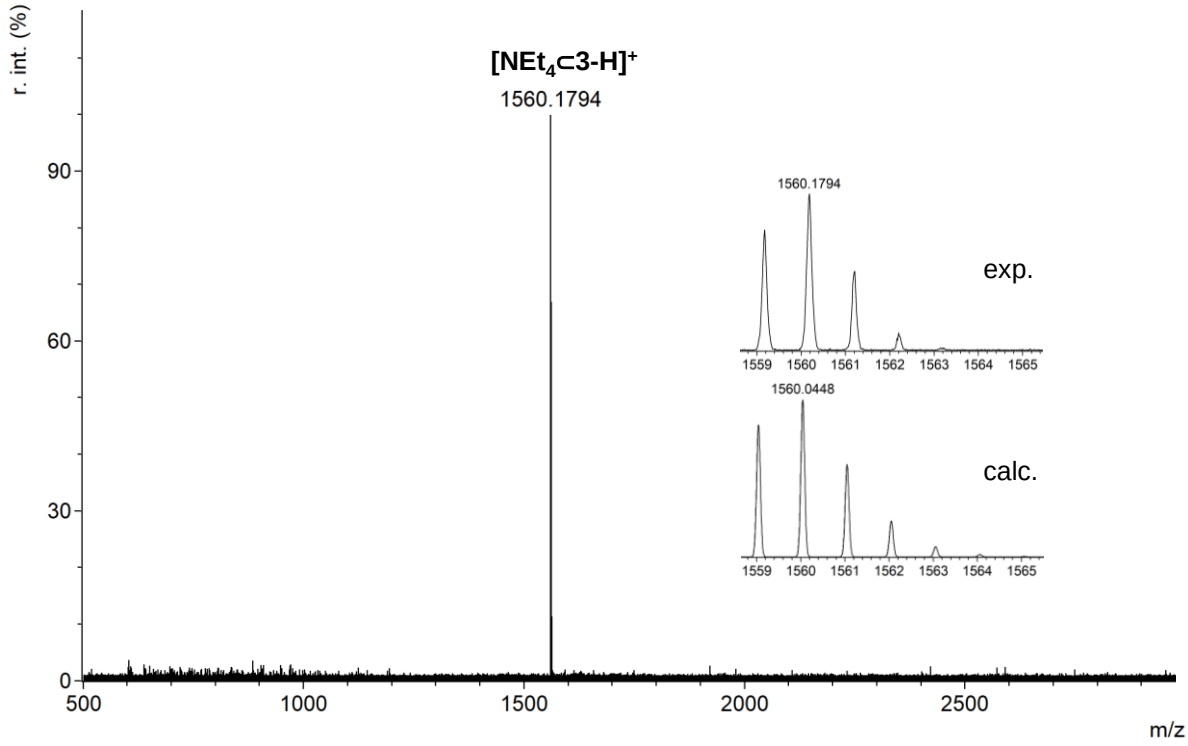

Figure S49: MALDI-TOF-MS of compound **[NEt$_4$⊂3-H]$^+$**.

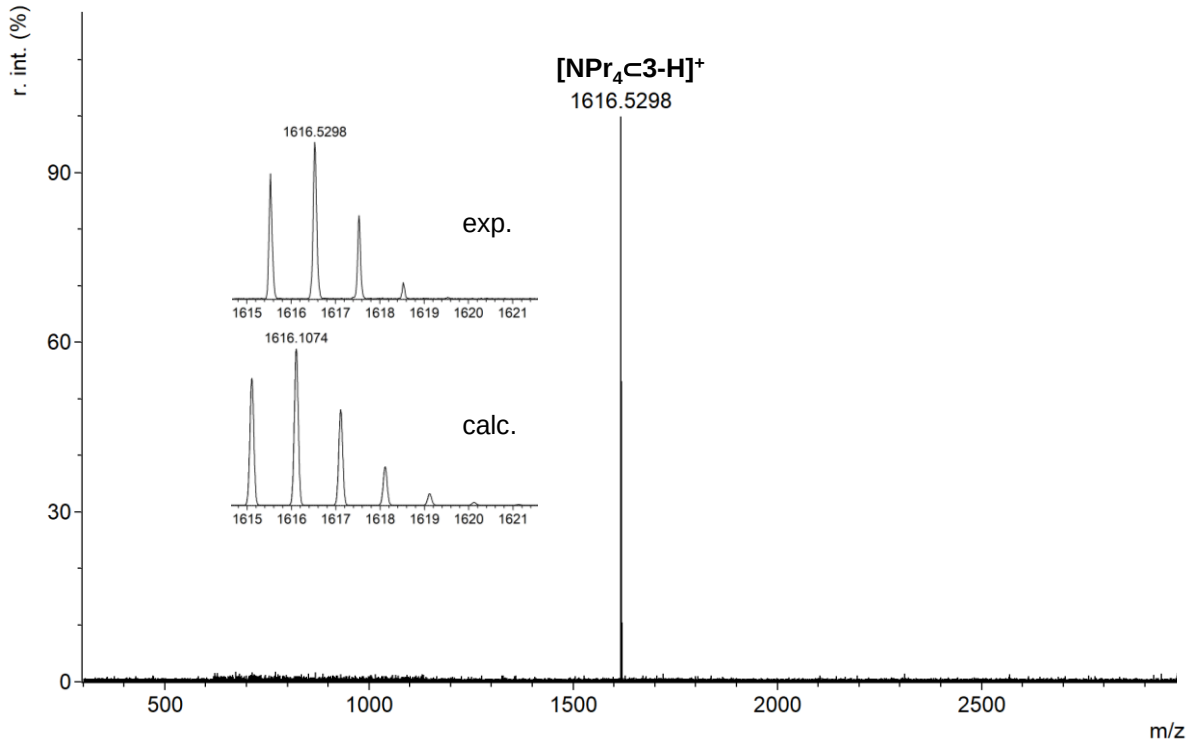

Figure S50: MALDI-TOF-MS of compound **[NPr$_4$⊂3-H]$^+$**.

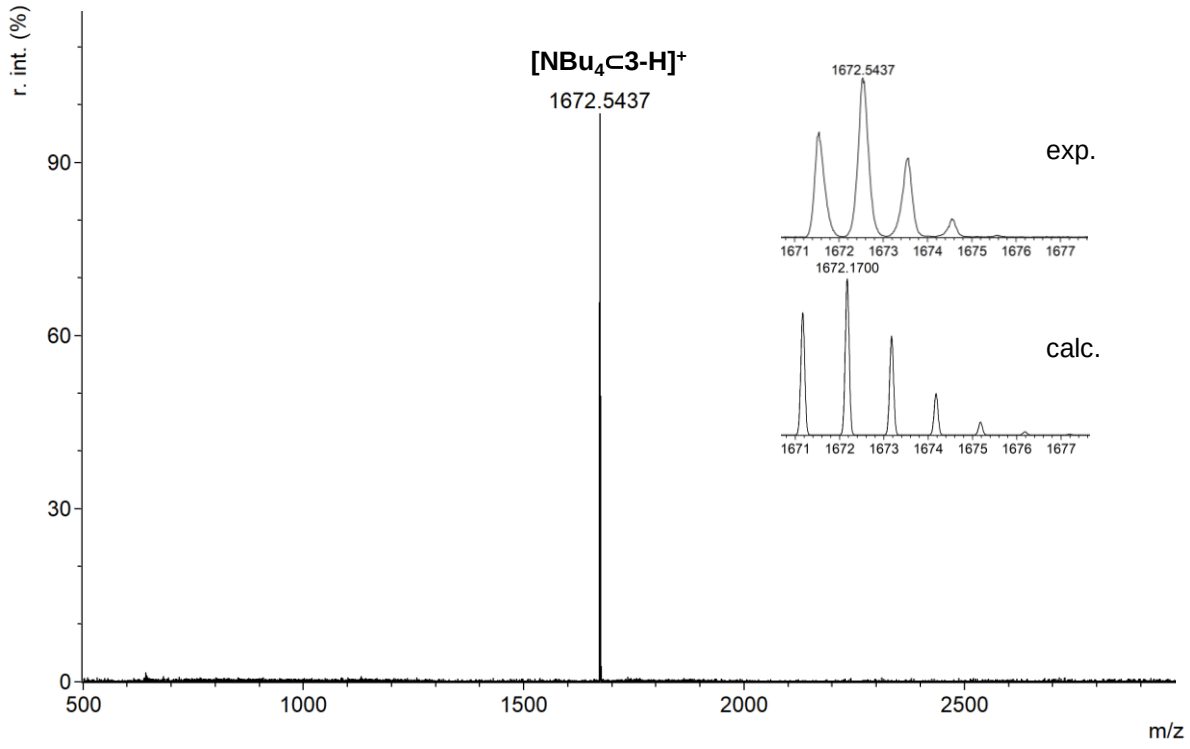

Figure S51: MALDI-TOF-MS of compound **[NBu$_4$⊂3-H]$^+$**.

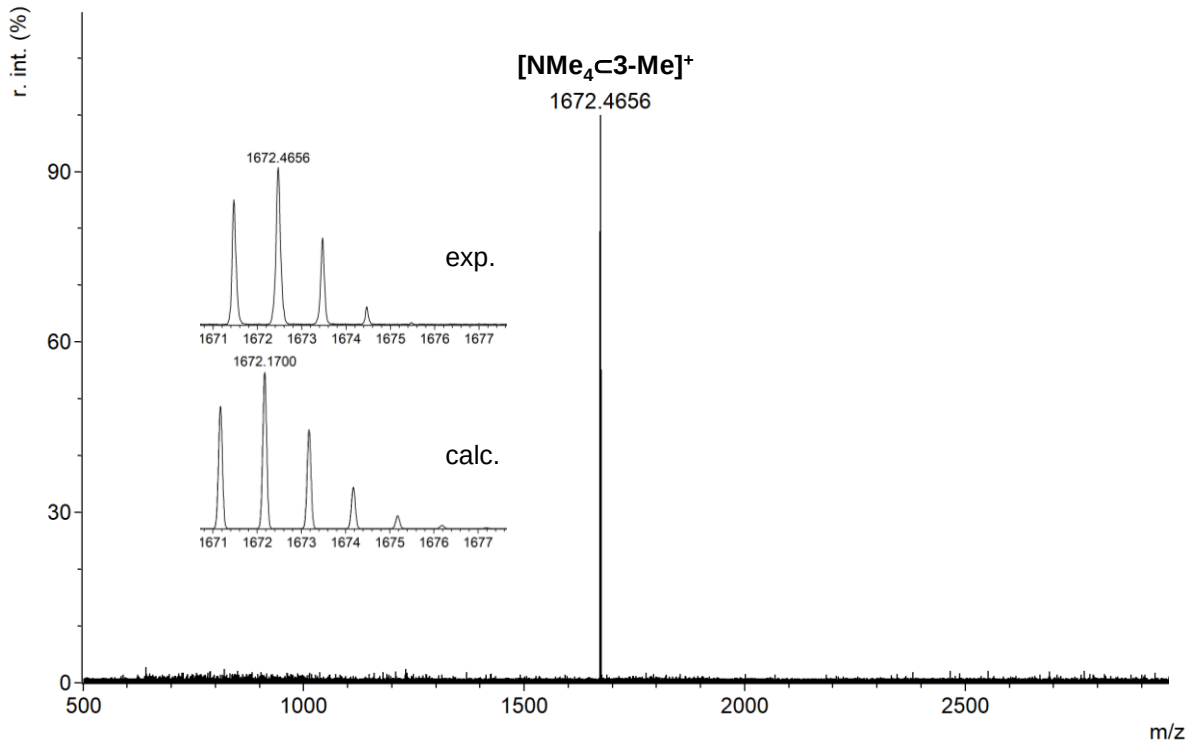

Figure S52: MALDI-TOF-MS of compound **[NMe$_4$⊂3-Me]$^+$**.

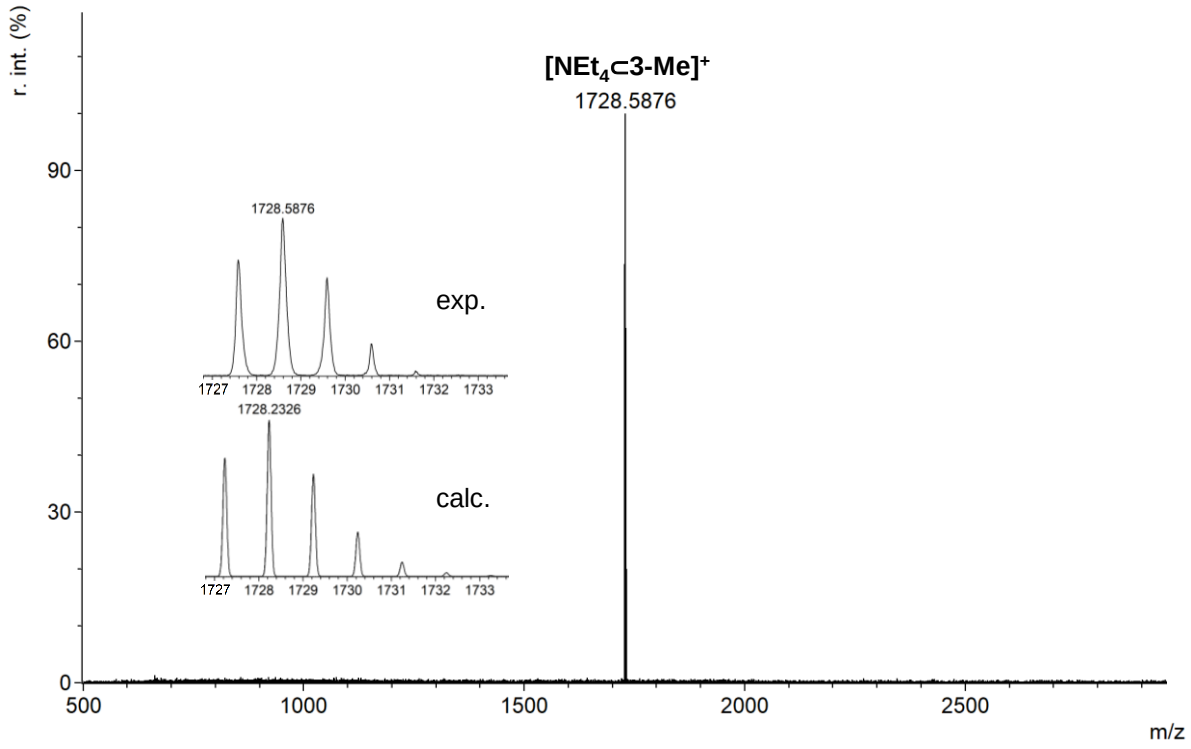

Figure S53: MALDI-TOF-MS of compound **[NEt$_4$⊂3-Me]$^+$**.

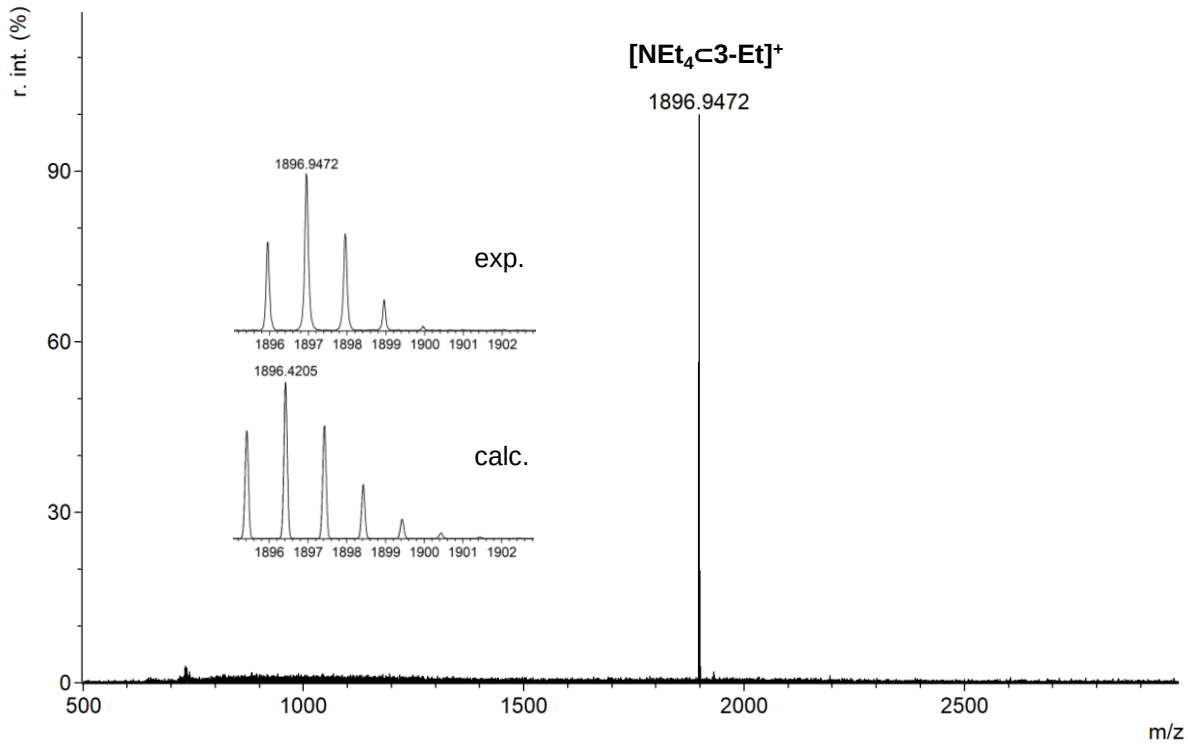

Figure S54: MALDI-TOF-MS of compound **[NEt_4⊂3-Et]$^+$**.

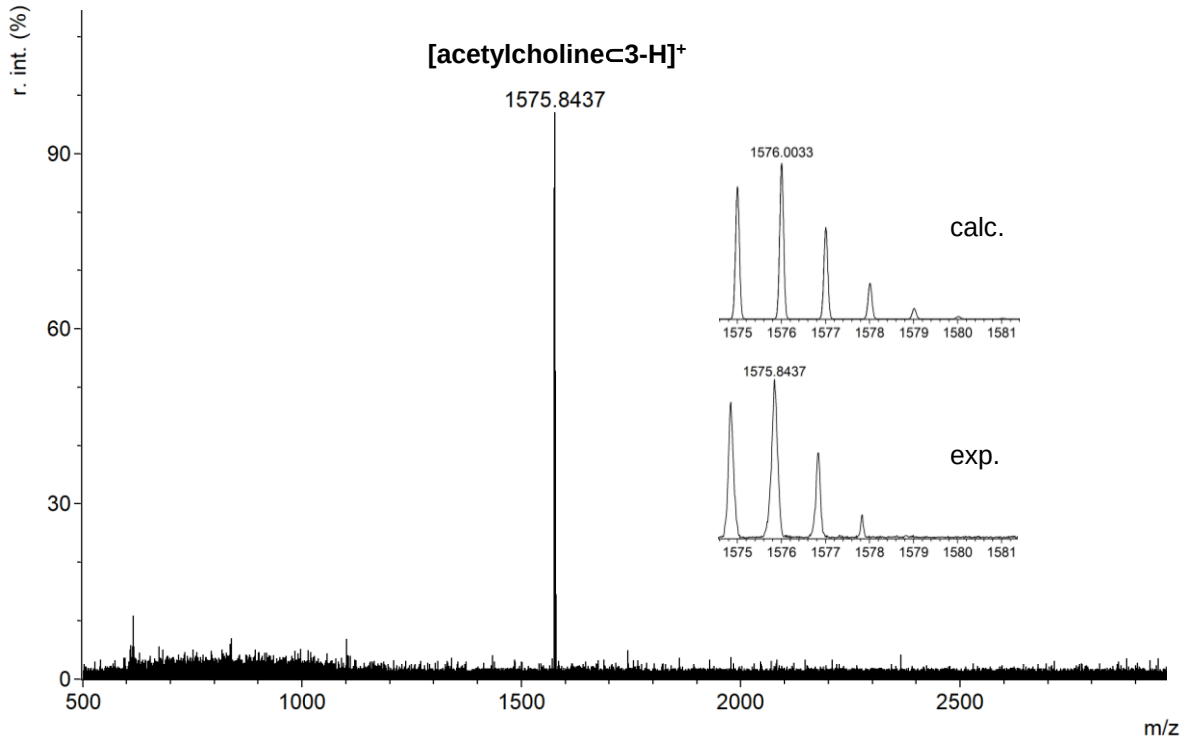

Figure S55: MALDI-TOF-MS of compound **[acetylcholine⊂3-H]$^+$.**

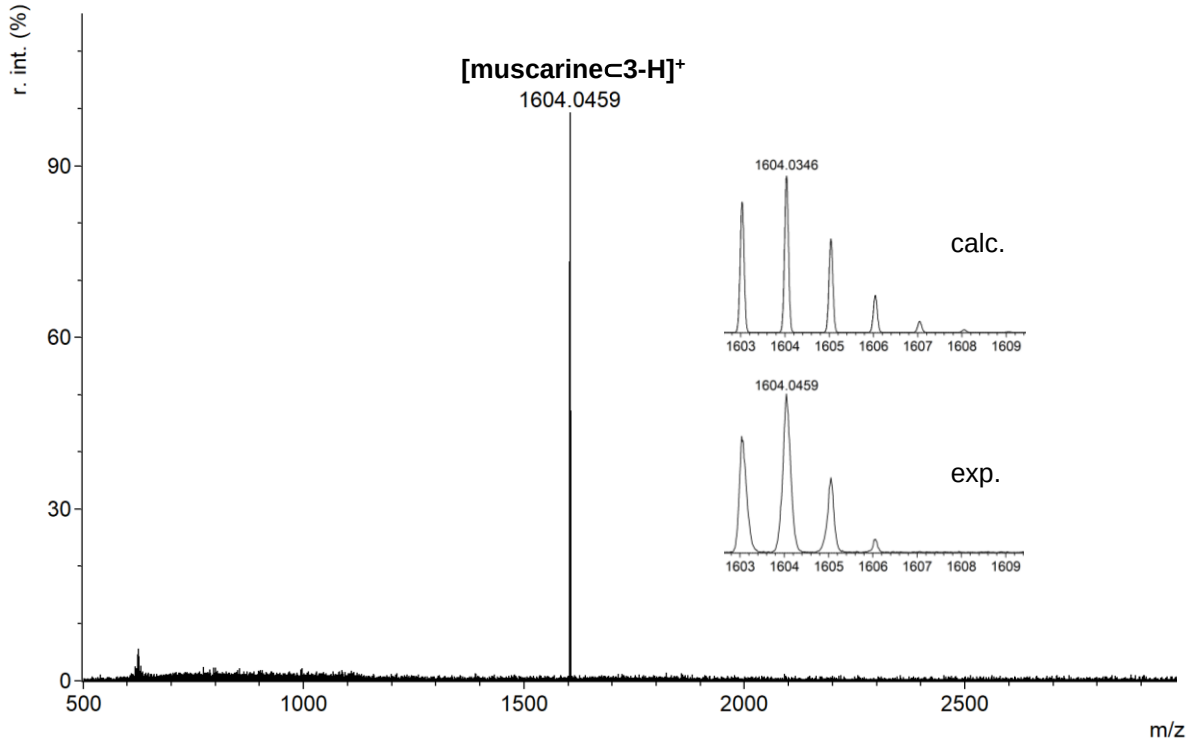

Figure S56: MALDI-TOF-MS of compound **[muscarine⊂3-H]⁺.**

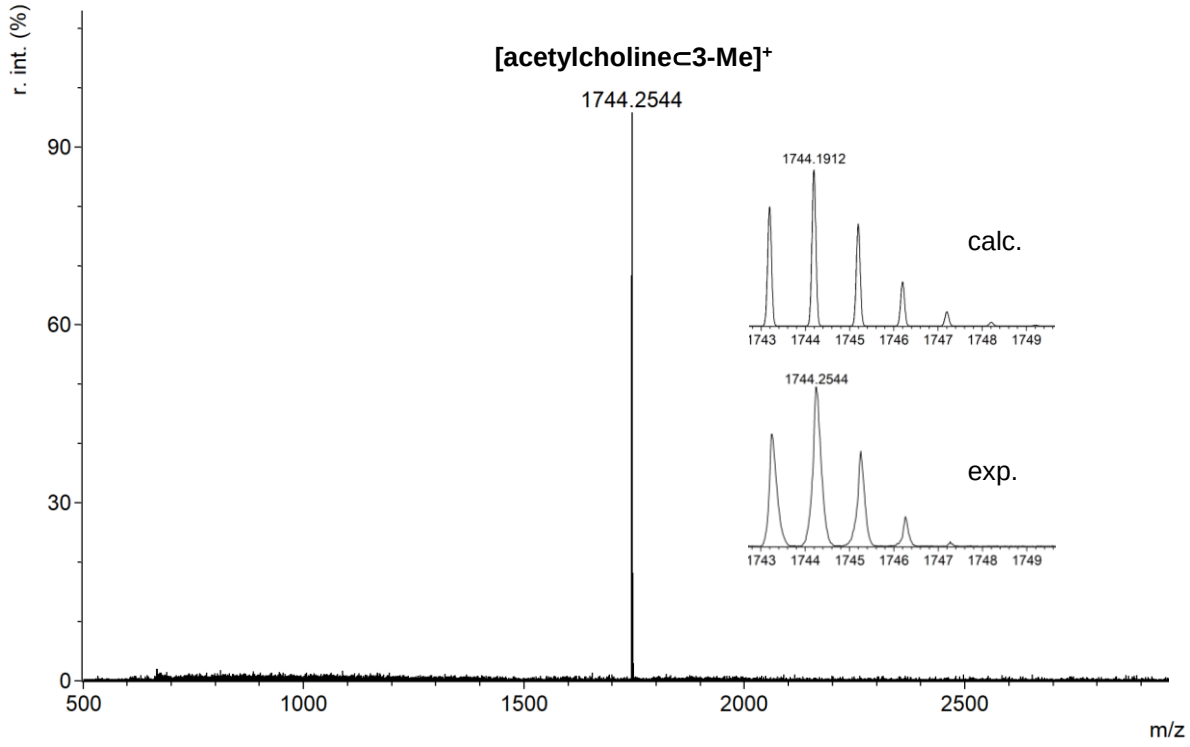

Figure S57: MALDI-TOF-MS of compound **[acetylcholine⊂3-Me]⁺.**

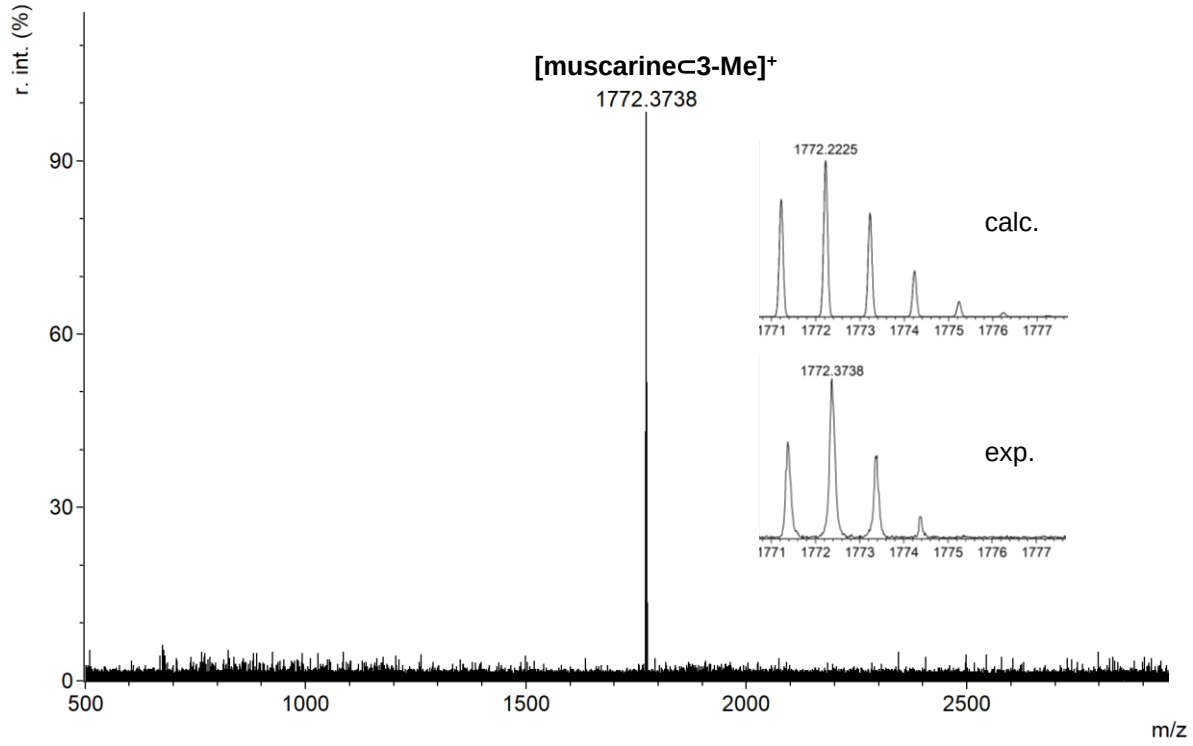

Figure S58: MALDI-TOF-MS of compound **[muscarine⊂3-Me]$^+$.**

5.9 ^{19}F-NMR Analytics

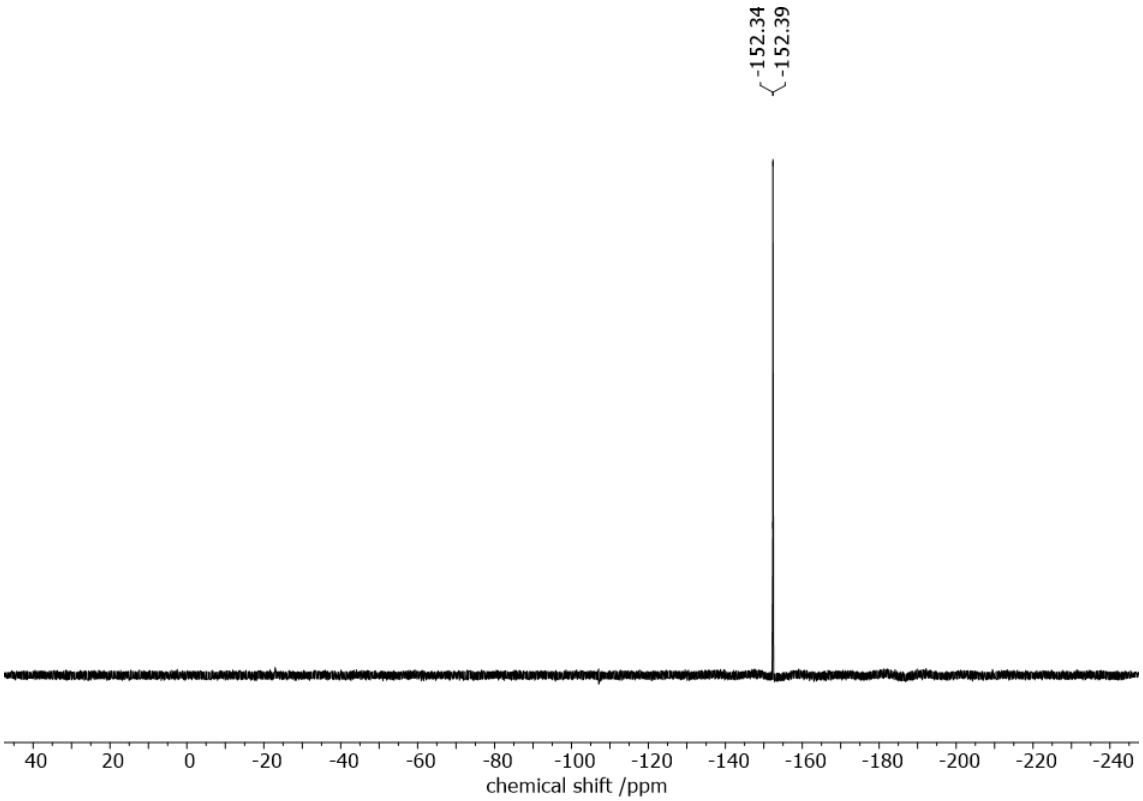

Figure S59: ^{19}F NMR spectrum (471 MHz, CD_2Cl_2) of compound **(NMe$_4$⊂3-H)BF$_4$**.

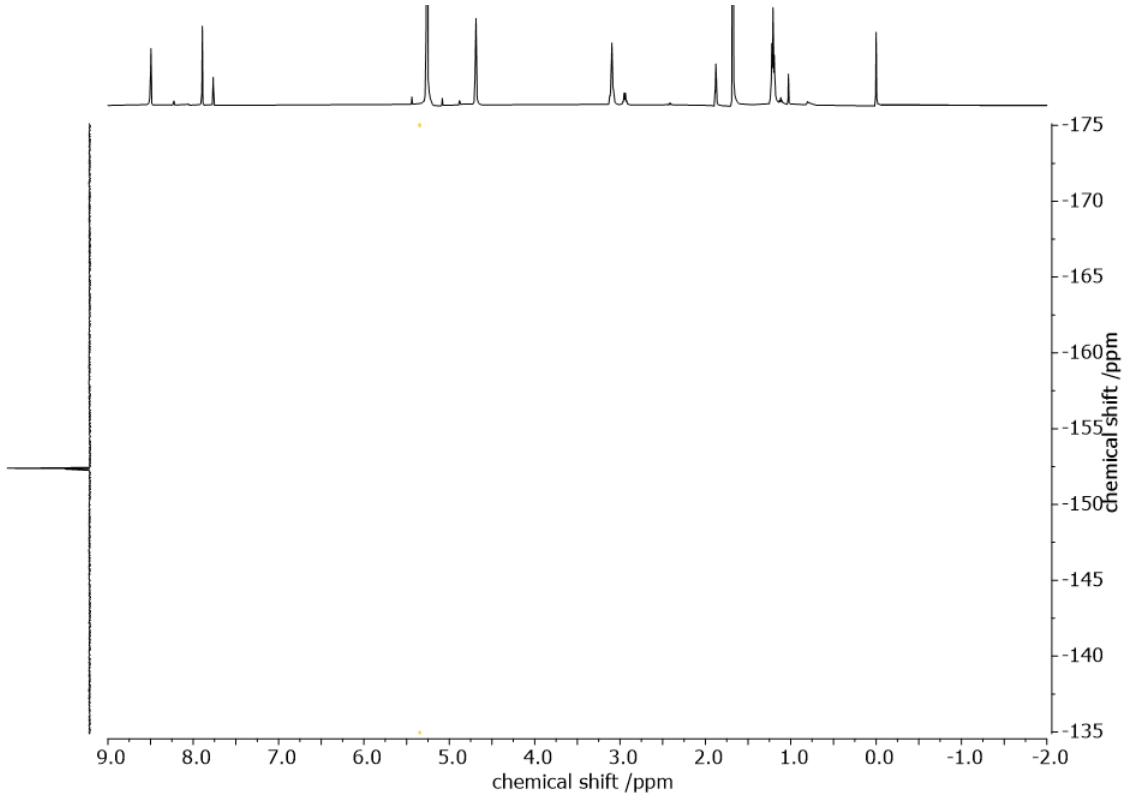

Figure S60: ^{1}H-^{19}F HOESY NMR spectrum (500/471 MHz, CD_2Cl_2) of compound **(NMe$_4$⊂3-H)BF$_4$**.

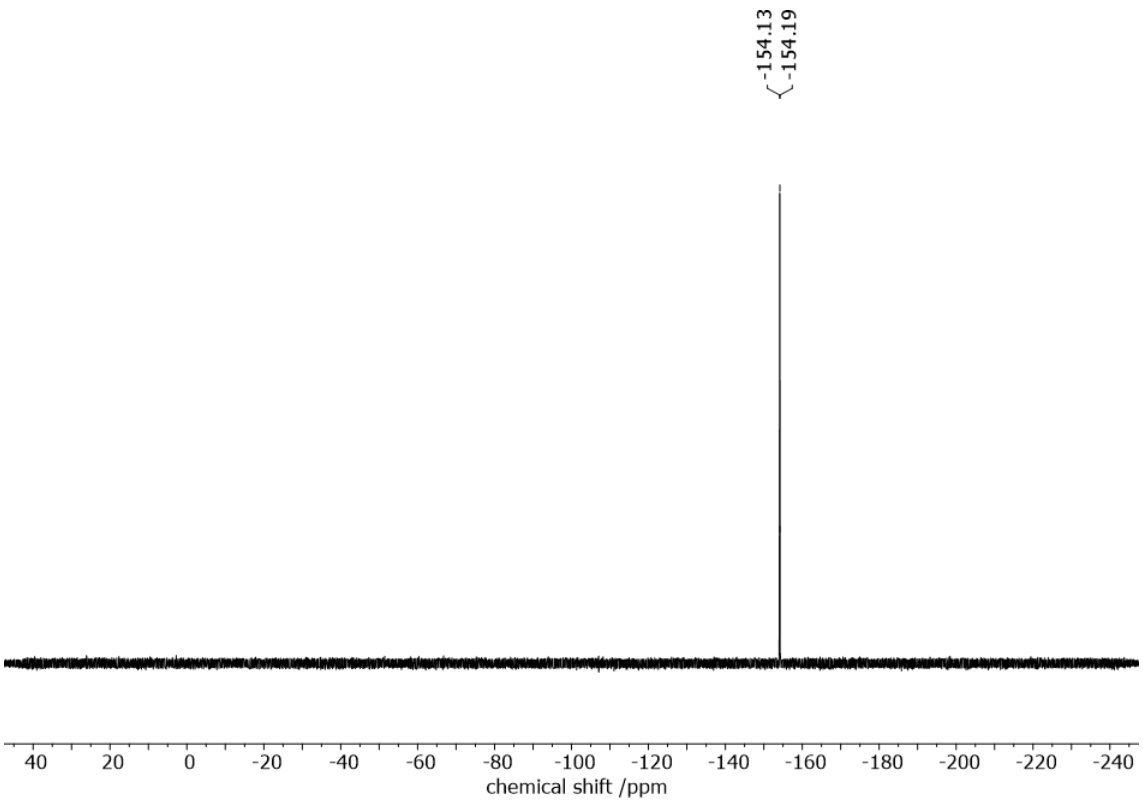

Figure S61: ^{19}F NMR spectrum (471 MHz, THF-d_8) of compound **(NEt$_4$⊂3-H)BF$_4$**.

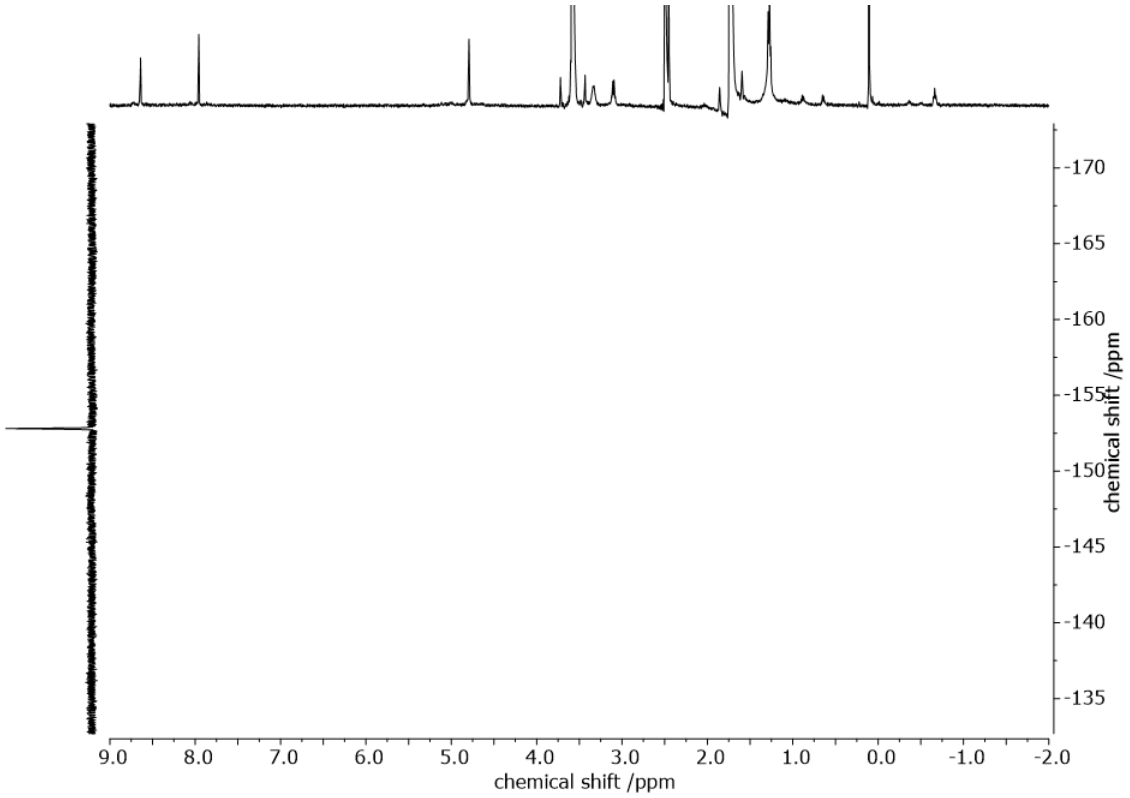

Figure S62: ^{1}H-^{19}F HOESY NMR spectrum (500/471 MHz, THF-d_8) of compound **(NEt$_4$⊂3-H)BF$_4$**.

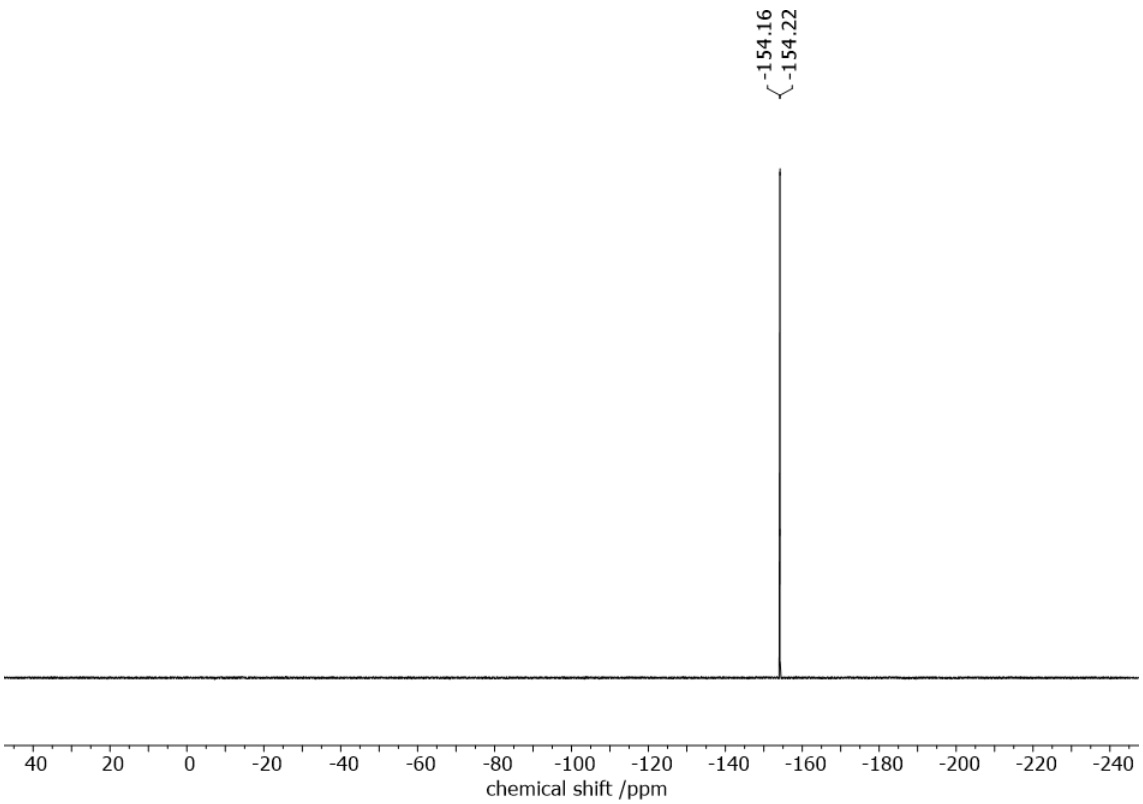

Figure S63: ^{19}F NMR spectrum (471 MHz, THF-d_8) of compound **(NPr$_4$⊂3-H)BF$_4$**.

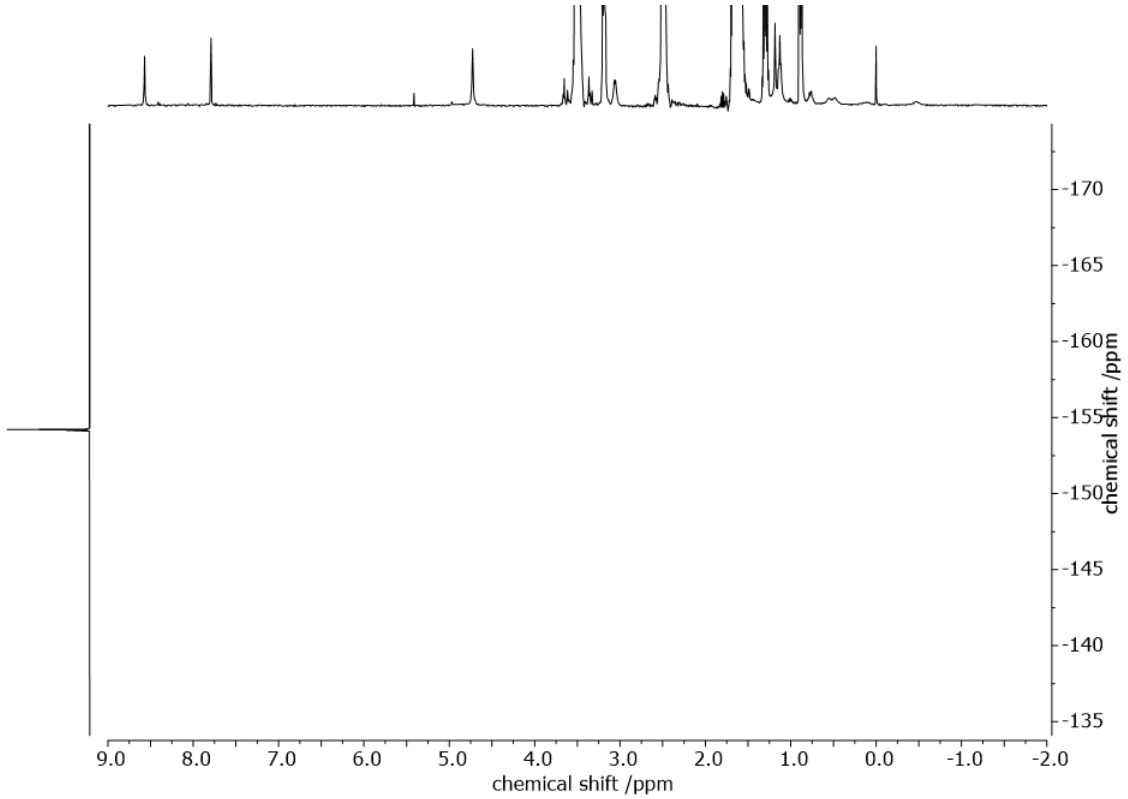

Figure S64: ^{1}H-^{19}F HOESY NMR spectrum (500/471 MHz, THF-d_8) of compound **(NPr$_4$⊂3-H)BF$_4$**.

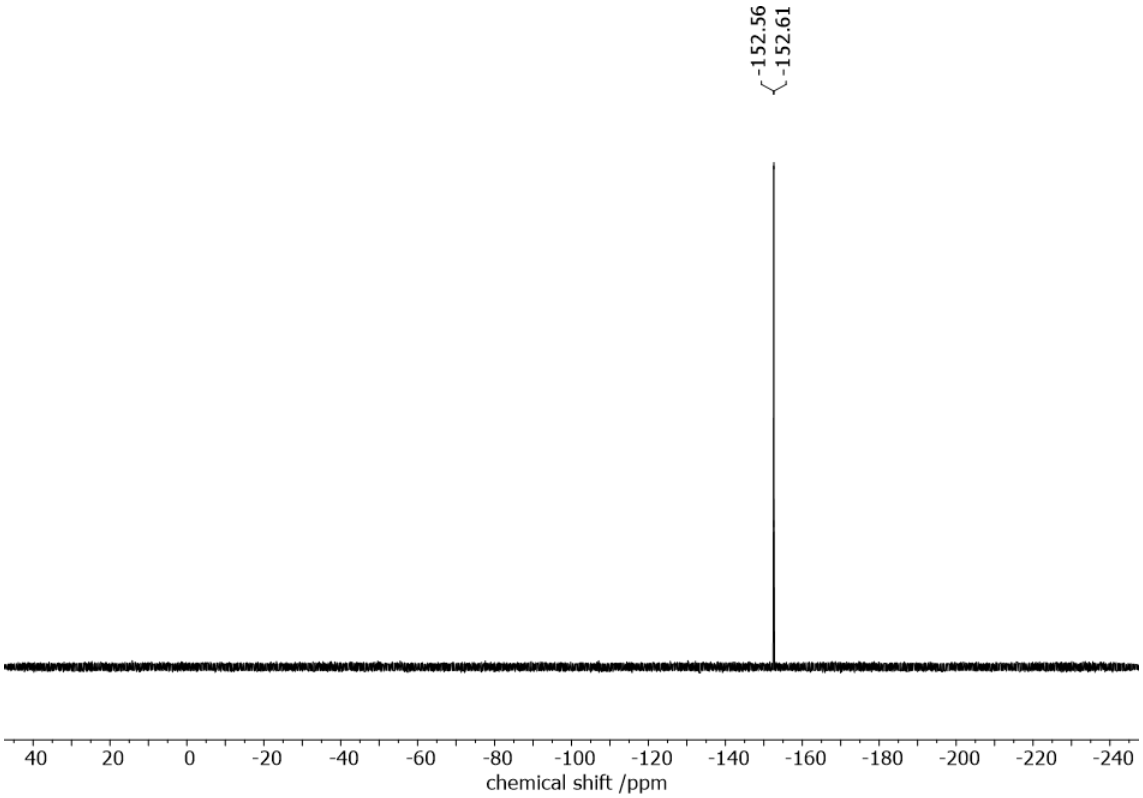

Figure S65: ^{19}F NMR spectrum (471 MHz, THF-d_8) of compound **(NBu$_4$⊂3-H)BF$_4$**.

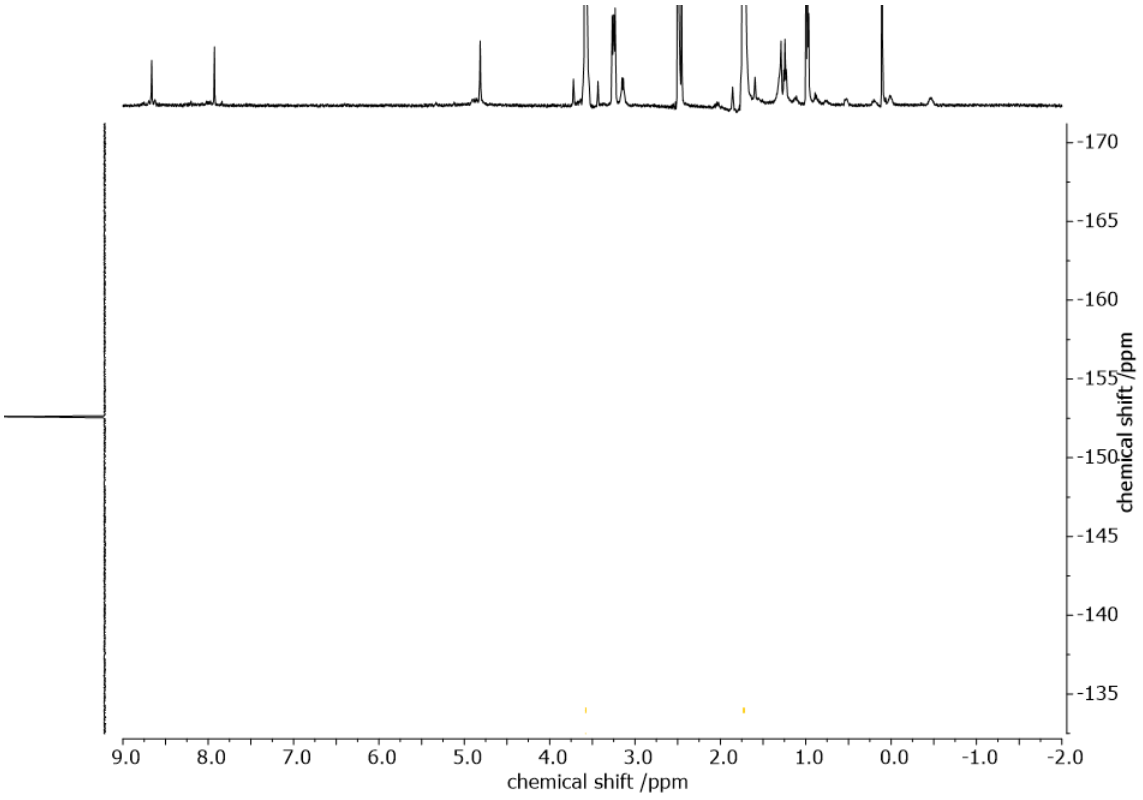

Figure S66: ^{1}H-^{19}F HOESY NMR spectrum (500/471 MHz, THF-d_8) of compound **(NBu$_4$⊂3-H)BF$_4$**.

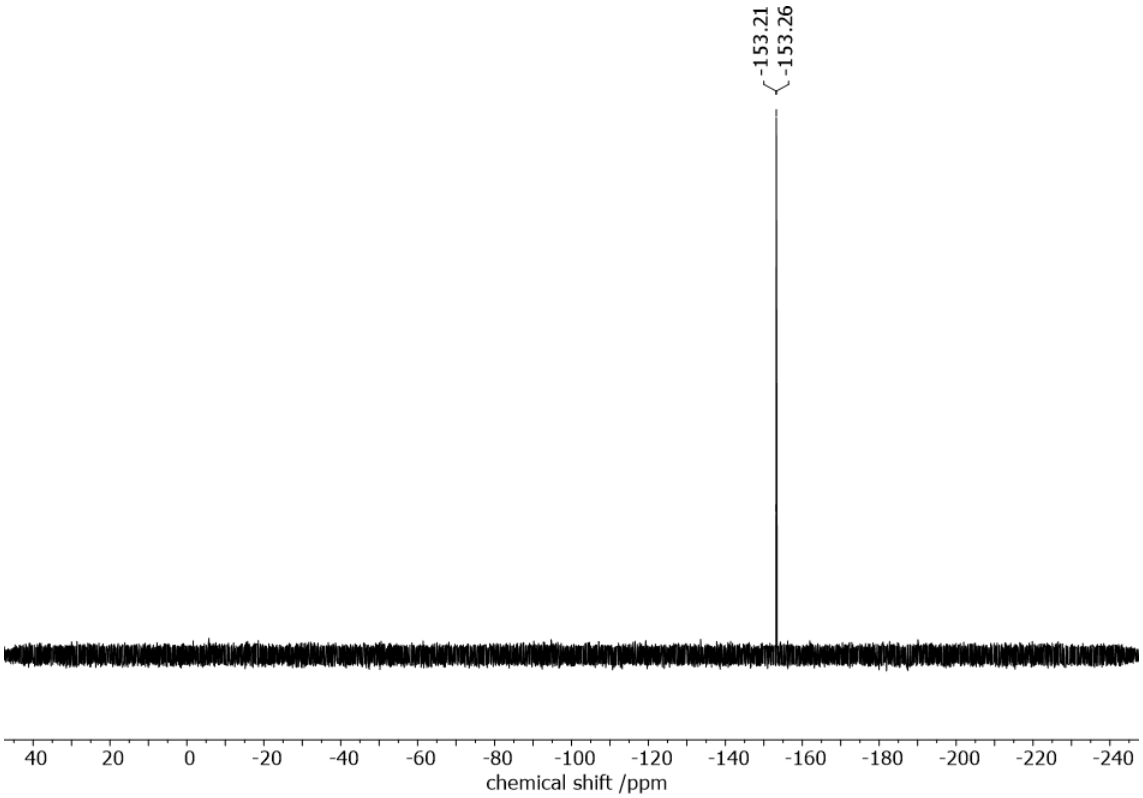

Figure S67: ^{19}F NMR spectrum (471 MHz, CD_2Cl_2) of compound **(NMe$_4$⊂3-Me)BF$_4$**.

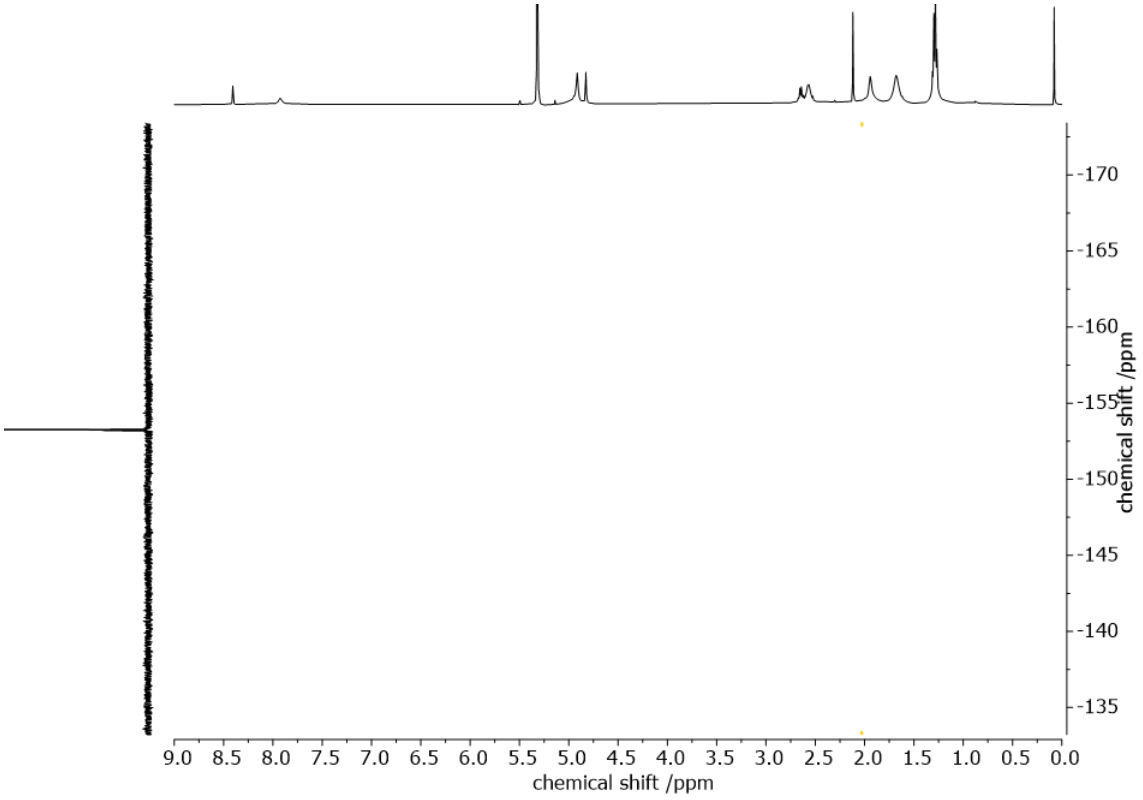

Figure S68: ^{1}H-^{19}F HOESY NMR spectrum (500/471 MHz, CD_2Cl_2) of compound **(NMe$_4$⊂3-Me)BF$_4$**.

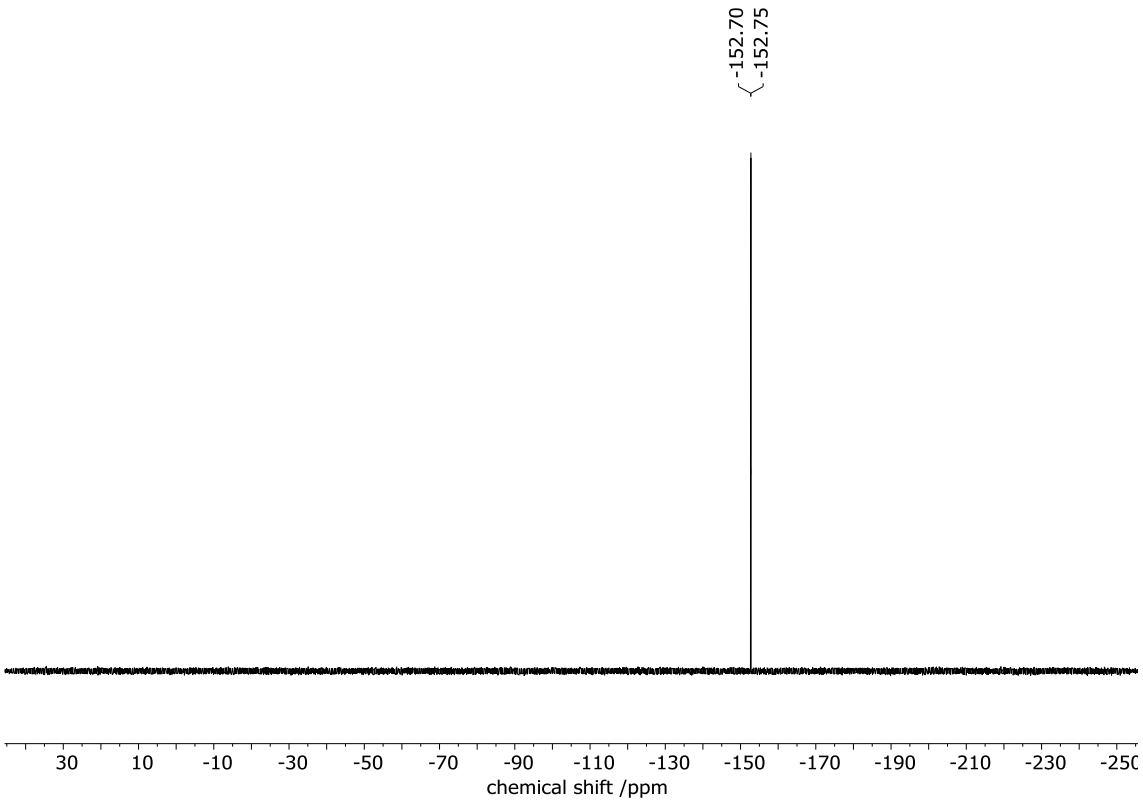

Figure S69: ^{19}F NMR spectrum (471 MHz, CD_2Cl_2) of compound **$(NEt_4 \subset 3\text{-}Me)BF_4$**.

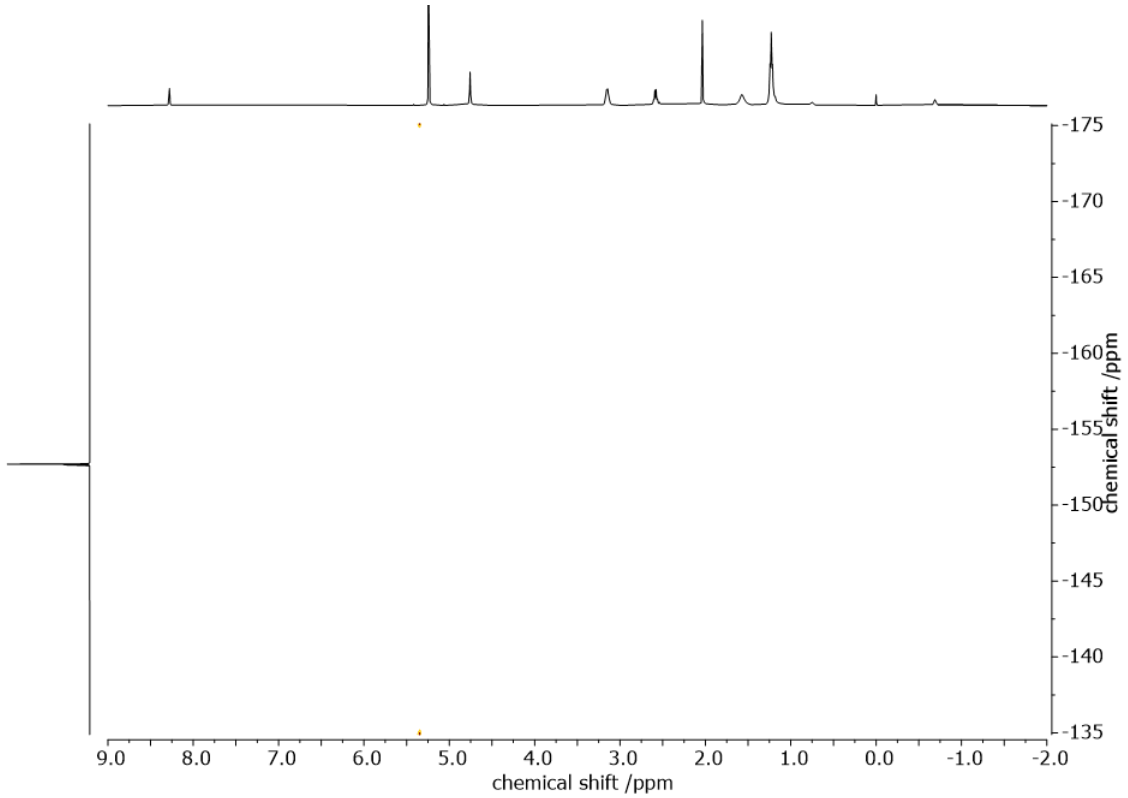

Figure S70: ^{1}H-^{19}F HOESY NMR spectrum (500/471 MHz, CD_2Cl_2) of compound **$(NEt_4 \subset 3\text{-}Me)BF_4$**.

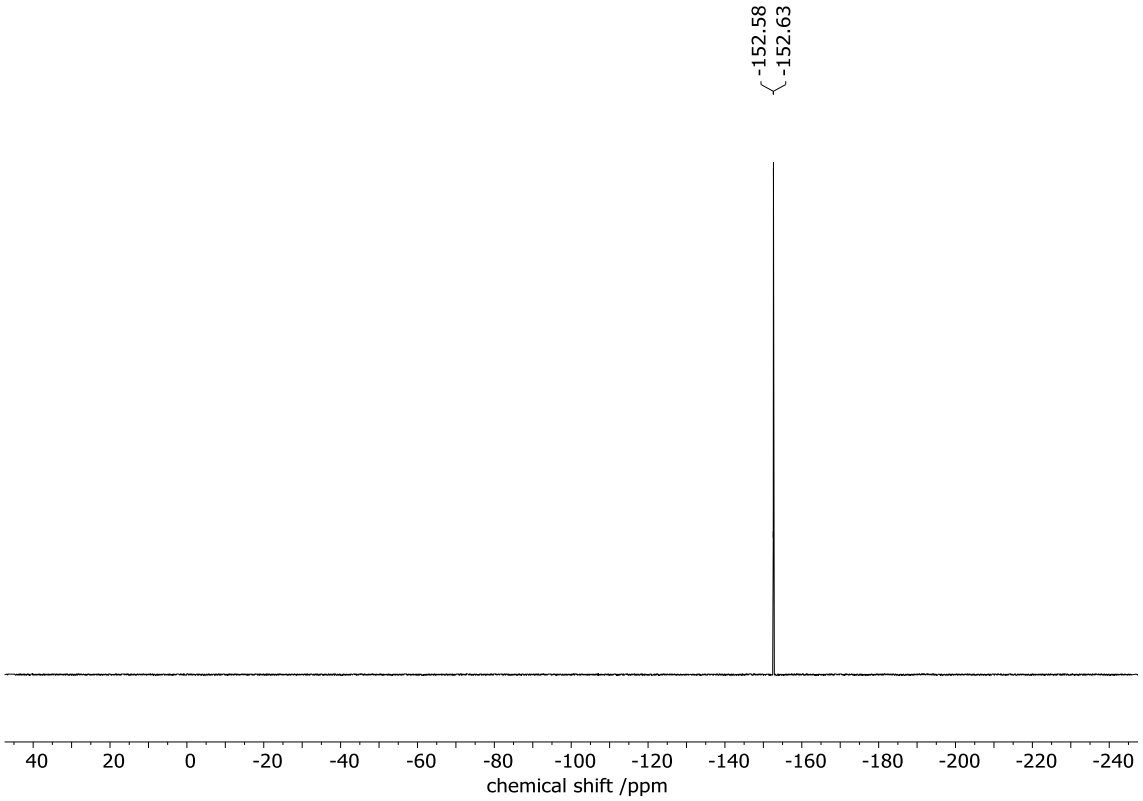

Figure S71: ^{19}F NMR spectrum (471 MHz, CD_2Cl_2) of compound **$(NEt_4 \subset 3\text{-}Et)BF_4$**.

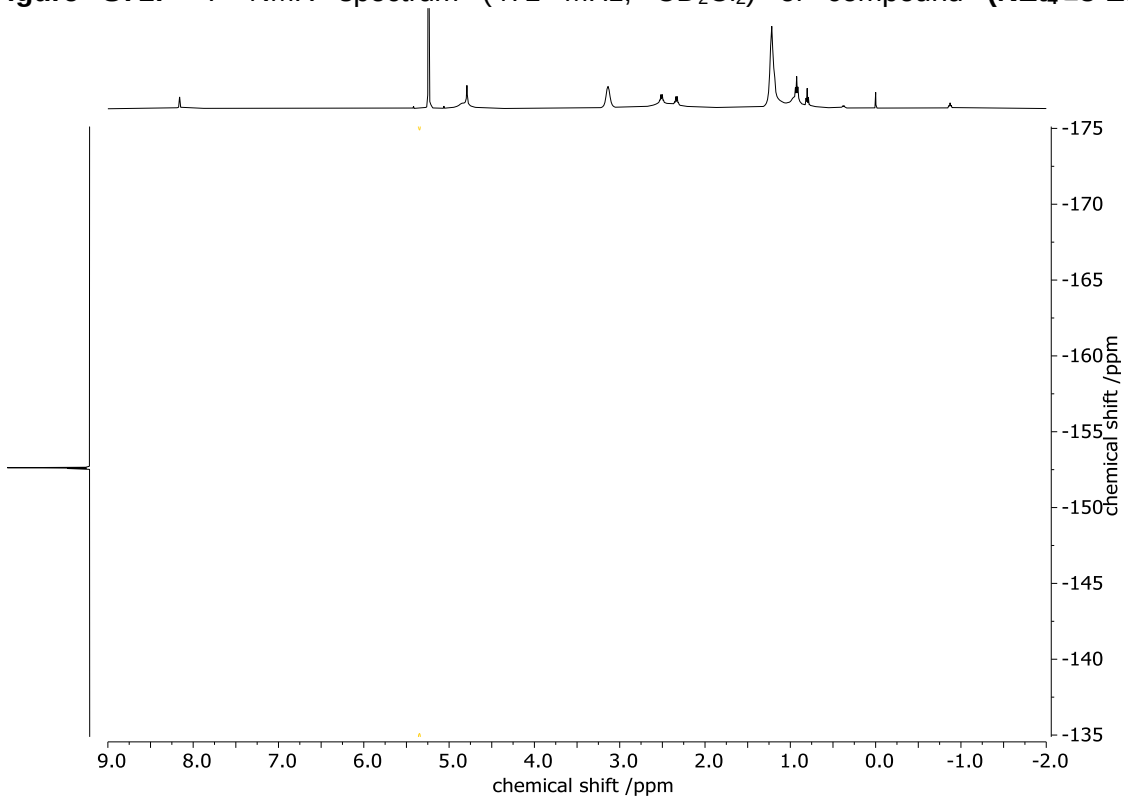

Figure S72: ^{1}H-^{19}F HOESY NMR spectrum (500/471 MHz, CD_2Cl_2) of compound **$(NEt_4 \subset 3\text{-}Et)BF_4$**.

5.10 ^{1}H NMR Kinetic Experiments

All ^{1}H NMR (300 MHz, CD_2Cl_2) kinetic experiments were performed in J-Young NMR tubes from stock solutions of the desired cages and guests, following literature procedures for similar host-guest systems.[S13] At least two solutions were monitored for each experiment. The reactions were treated as reaction of second order. The rate constant $\boldsymbol{k_1}$ was determined by graphical evaluation of the slope with the following equation:

$$\boldsymbol{k_1}t = \frac{1}{[Cage]_0 - [Guest]_0} ln \frac{[Cage][Guest]_0}{[Cage]_0[Guest]}$$

The average of at least two measurements are reported as k_1 values with standard deviations (σ) as uncertainty using the STABW.N function of Microsoft Excel 2016.

Table S8: Experimental details of the kinetic experiments. The counter ion is BF_4^-.

Compound	Solvent	Qnt cage [µmol]	Qnt guest [µmol]	T [K	$\acute{k}_1$ [$M^{-1}s^{-1}$]	k_1 [$M^{-1}s^{-1}$]
NMe_4^+⊂3-H	540 µL DCM + 60 µL MeCN	0.2	2.0	303	6.3 x 10^{-2}	6.4(2) x 10^{-2}
		0.2	2.0	303	6.3 x 10^{-2}	
		0.2	2.0	303	6.8 x 10^{-2}	
		0.2	2.0	303	6.1 x 10^{-2}	
		0.2	2.0	303	6.3 x 10^{-2}	
NEt_4^+⊂3-H	600 µL DCM	0.2	2.0	303	1.8 x 10^{-3}	2.5(2) x 10^{-3}
		0.2	2.0	303	2.1 x 10^{-3}	
NPr_4^+⊂3-H	600 µL DCM	0.2	1.2	303	1.7 x 10^{-3}	1.9(2) x 10^{-3}
		0.2	1.2	303	2.0 x 10^{-3}	
NMe_4^+⊂3-Me	600 µL DCM	0.2	2.0	314	1.8 x 10^{-4}	1.8(1) x 10^{-4}
		0.2	2.0	314	1.7 x 10^{-4}	
NEt_4^+⊂3-Me	600 µL DCM	0.2	1.0	314	2.0 x 10^{-3}	2.0(1) x 10^{-3}
		0.2	1.2	314	1.9 x 10^{-3}	
NEt_4^+⊂3-Et	600 µL DCM	0.5	12	314	6.4 x 10^{-5}	6.1(4) x 10^{-5}
		0.5	11	314	5.7 x 10^{-5}	

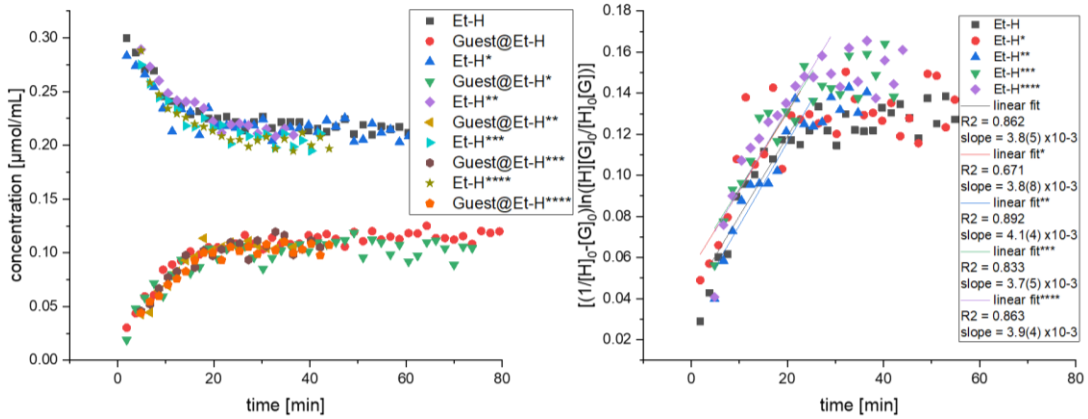

Figure S73: Left: Concentration-time diagram of the formation of **(NMe$_4$⊂3-H)BF$_4$** at 303 K. Right: Graphical evaluation of ***k*$_1$**.

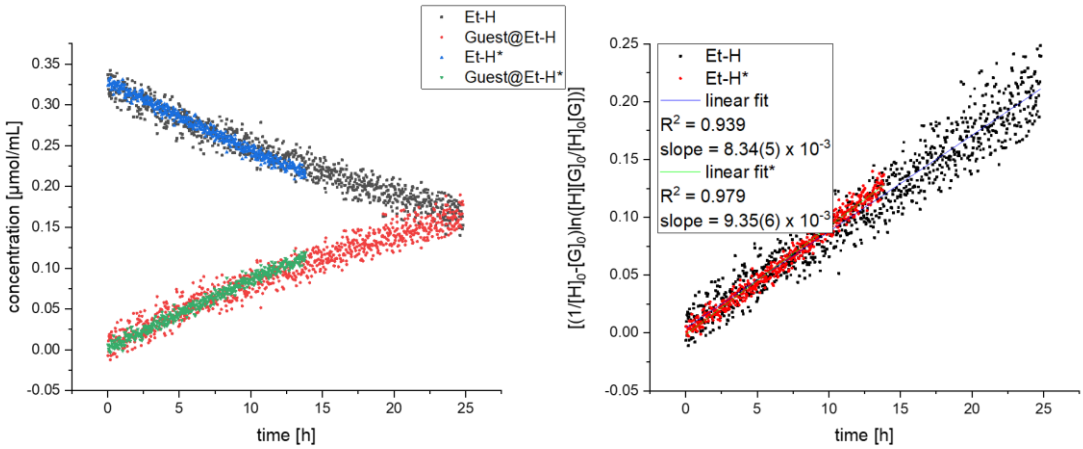

Figure S74: Left: Concentration-time diagram of the formation of (NEt4⊂3-H)BF4 at 303 K. Right: Graphical evaluation of k1.

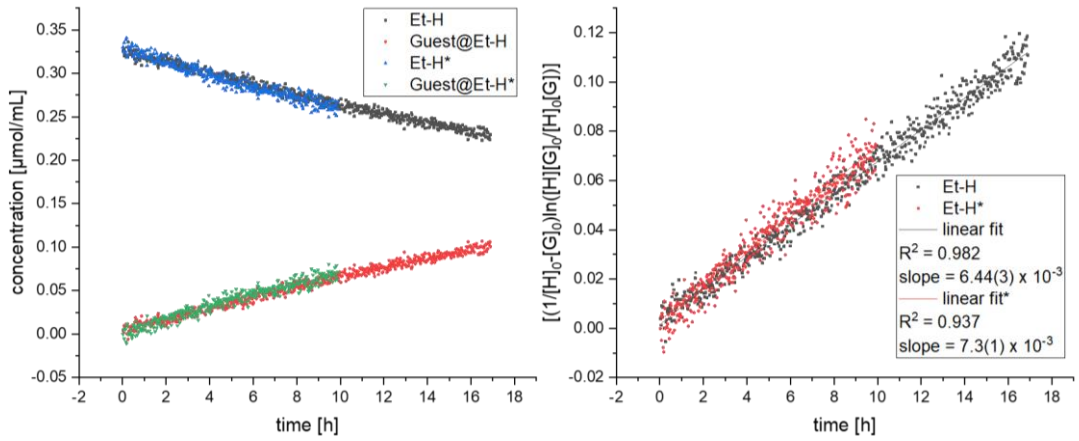

Figure S75: Left: Concentration-time diagram of the formation of **(NPr$_4$⊂3-H)BF$_4$** at 303 K. Right: Graphical evaluation of ***k*$_1$**.

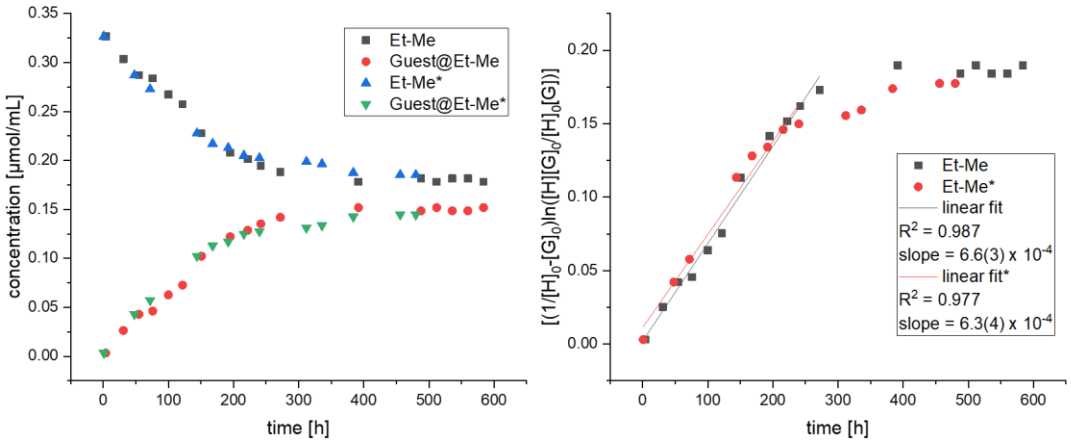

Figure S76: Left: Concentration-time diagram of the formation of **(NMe$_4$⊂3-Me)BF$_4$** at 314 K. Right: Graphical evaluation of k_1.

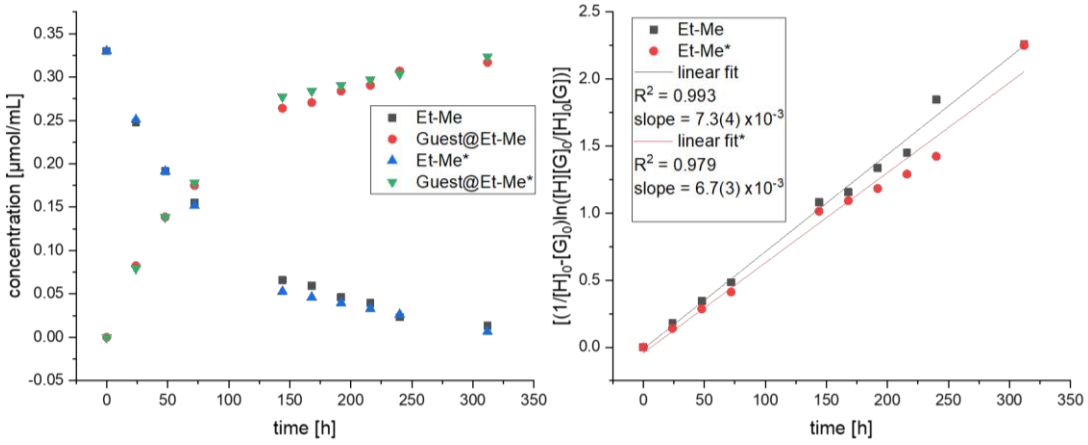

Figure S77: Left: Concentration-time diagram of the formation of **(NEt$_4$⊂3-Me)BF$_4$** at 314 K. Right: Graphical evaluation of k_1.

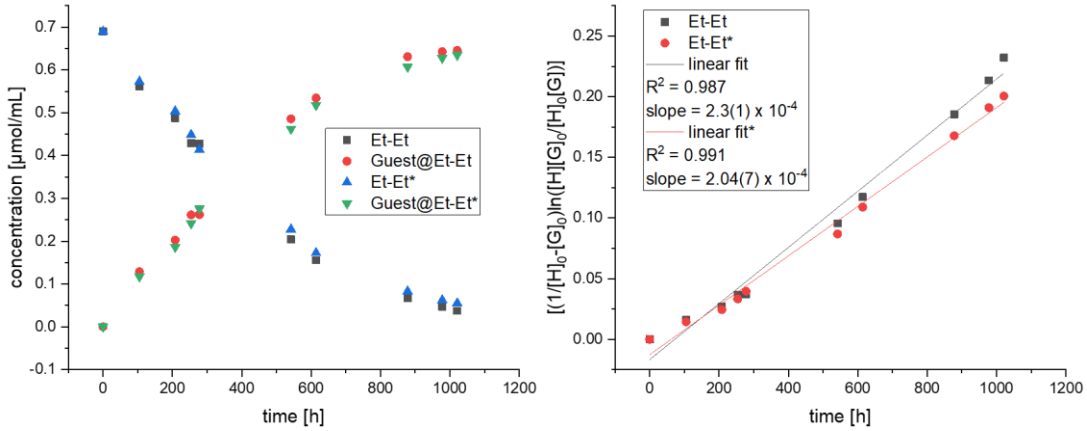

Figure S78: Left: Concentration-time diagram of the formation of **(NEt$_4$⊂3-Et)BF$_4$** at 314 K. Right: Graphical evaluation of k_1.

5.10.1 Decomposition of 3-H

The decomposition of **3-H**, **$(NEt_4⊂3\text{-}H)BF_4$** and **$(NPr_4⊂3\text{-}H)BF_4$** in $CDCl_3$ were monitored by ^1H NMR (300 MHz). The kinetic experiments were performed in three separate J-Young NMR tubes. **3-H**, **$(NEt_4⊂3\text{-}H)BF_4$** and **$(NPr_4⊂3\text{-}H)BF_4$**. (each 2 µmol) were dissolved in $CDCl_3$ (0.5 mL) and 1,3,5-trimethoxybenzene (50µmol/mL; 100 µL) was added. The reaction mixture was monitored for 74 hours by ^1H NMR at r.t. The reaction rate constant k_1 was determined by evaluating the reaction as reaction of *pseudo* first order.

Table S9: Decomposition of Et-H.

Compound	Guest	T [K]	k_1 [s^{-1}]
3-H	-	298	1.6×10^{-5}
3-H	**NEt_4^+**	298	1.3×10^{-6}
3-H	**NPr_4^+**	298	3.3×10^{-7}

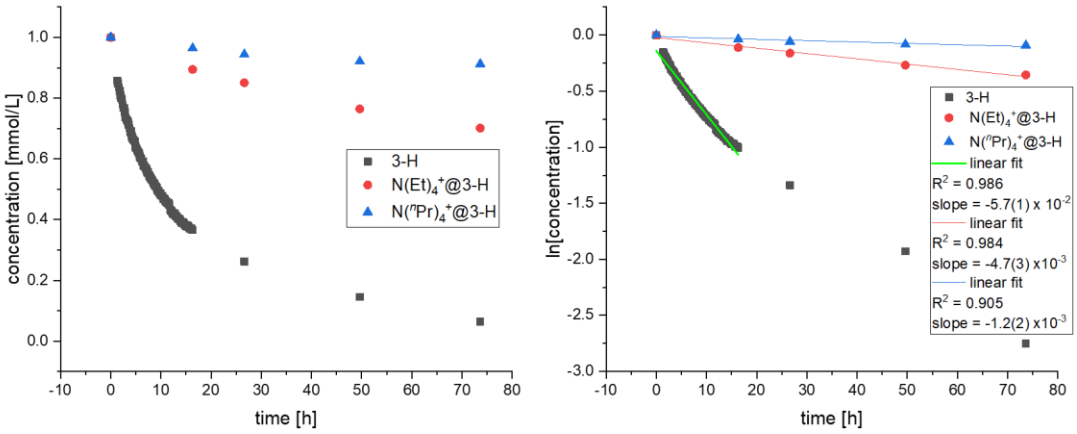

Figure S79: Left: Concentration-time diagram of the decomposition of **3-H**, **$(NEt_4⊂3\text{-}H)BF_4$** and **$(NPr_4⊂3\text{-}H)BF_4$** in $CDCl_3$ at 298 K. Right: Graphical evaluation of k_1.

6 Computational Studies

6.1 Initial Structural Model

Models of all cage structures, as well as cationic ligands NEt_4^+ and NMe_4^+, were constructed with xLeap tool from the AmberTools package[S14] employing the general Amber force field (GAFF)[S15]. The atomic charge of models were calculated by the Hartree-Fock method using GAUSSIAN09[S6] with 6-31G* basis set[S16]. The force field parameters of the solvent molecule dichloromethane and the Cl^- counter ions were also selected from the GAFF.

Different cage structures with corresponding cationic ligands were separately settled in a 5×5×5 $Å^3$ simulation box with periodic boundary conditions. Afterwards, dichloromethane molecules were inserted into the box, and one of those solvent molecules were subsequently replaced by the Cl^- to achieve electroneutrality. A total of 6 systems were set up and each of them comprised ca. 4000 atoms, which contained one cage molecule, one cationic ligand molecule, ca. 750 dichloromethane molecules and one counter ions.

6.2 All-atom MD Simulations

All the systems were firstly undergone steepest descents energy minimization and 2 ns NVT simulation at 298 K in sequence. Afterwards, an 2 ns NPT simulation were performed at 298 K and 1 bar with the Berendsen barostat[S17] and was followed by 2 ns further NPT simulation with Parrinello-Rahman barostat[S18] under the same thermodynamic conditions. Then, to further stabilize the system and to collect optimized structure, we performed 100 ns MD simulations for each system. In order to increase the accuracy, two groups (one comprised the cages molecule, the other one contained the ligand, solvent and counter ions) were set for temperature coupling in all simulations.

6.3 Free Energy Simulations

The free energies of the center-of-mass distance between the cage and its corresponding cationic ligands were calculated with classical well-tempered metadynamics simulations[S19]. The initial structure was taken from the result of the 100 ns MD simulations for each system. The Gaussian bias potential was initially set with height = 0.5 kJ/mol, width σ = 0.2 Å, and was deposited each picosecond. Since the higher energy barriers to be crossed for the cage with the $\mathbf{NEt_4^+}$, for those who have $\mathbf{NEt_4^+}$, the bias factor was 100, and for systems with $\mathbf{NMe_4^+}$, the bias factor was 50. To enhance the sampling efficiency, based on the estimation of the cage radius (r ≈ 4.5 Å) the ligand was restricted to move within 7 Å from the mass centre of the cage. According to the experiments, we never saw the counter ions BF_4^- enter into the cage, the counter ions Cl^- was restrained to move 5 Å away from the cage centre.

The initial systems were set up with GROMACS in version 4.6.7 and the following all-atom simulations were performed with GROMACS in version 2018.3.[S20] The well-tempered

metadynamics simulations were performed and analyzed via GROMACS 2018.3 interfaced with the Plumed 2.5.1 package.[S21] Molecular structures were visualized with VMD 1.9.2.[S22]

6.4 Data

Table S10: Activation energy $\Delta G_d^{\ddagger}$ (kJ/mol) from simulations.

Host	Guest	*simulations*
3-H	**NMe_4^+**	61
3-H	**NEt_4^+**	141
3-H	**NPr_4^+**	-
3-Me	**NMe_4^+**	123
3-Me	**NEt_4^+**	241
3-Et	**NMe_4^+**	91
3-Et	**NEt_4^+**	359

Table S11: Solvation effects**.**

Host	Guest	*Number of solvent molecules per state*		
		A	***B***	***C***
3-H	**NMe_4^+**	6	3	4
3-H	**NEt_4^+**	6	2	3
3-Me	**NMe_4^+**	2	2	2
3-Me	**NEt_4^+**	0	1	1
3-Et	**NMe_4^+**	0	0	0
3-Et	**NEt_4^+**	0	0	0

6.4.1 Conformational Changes During De-encapsulation

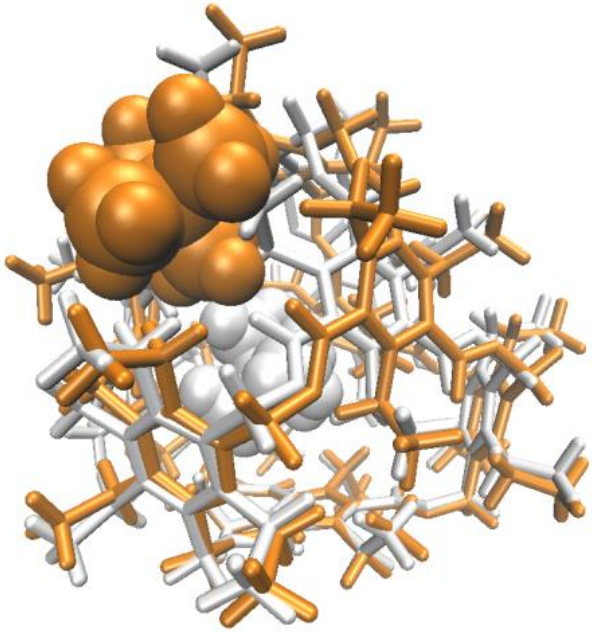

Figure S80: Representation of the conformational change during de-encapsulation (example for 3-Et with NEt_4^+). White: Guest in the middle of the host; Orange: Guest is leaving the host.

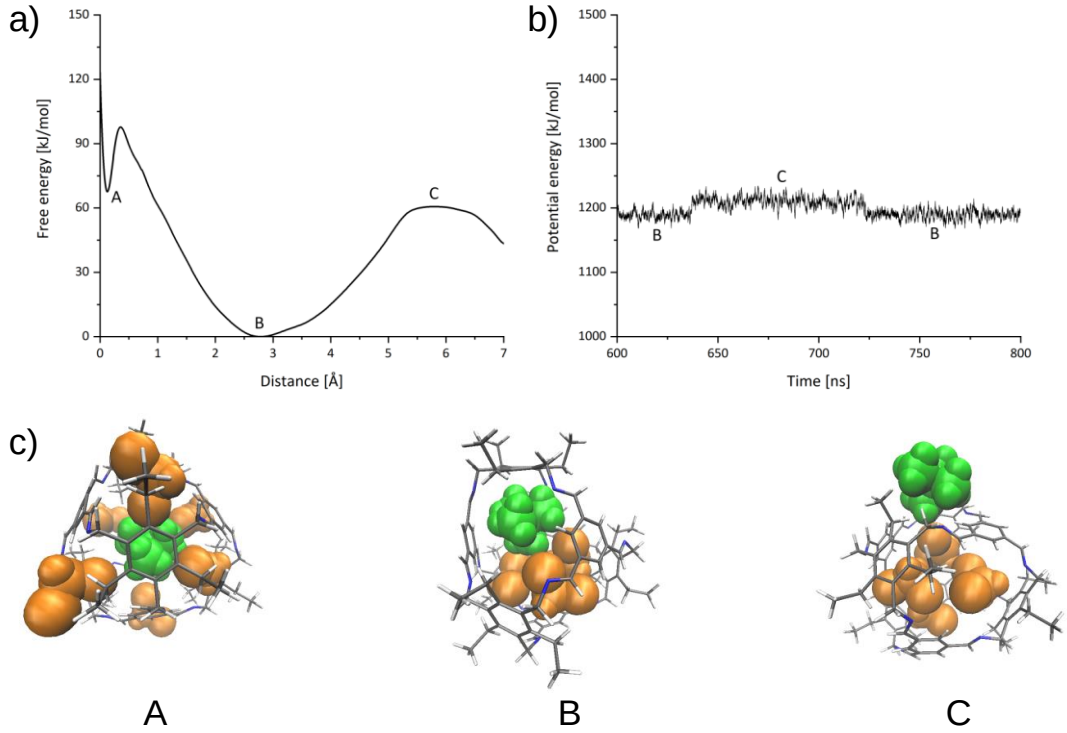

Figure S81: Computed decapsulation process for **3-H** with $\mathbf{NMe_4^+}$: a) Free energy surface, $\Delta G_d^{\ddagger}$= 61 kJ/mol b) Host potential energy changes when guest leaves and comes back once. c) Different conformations at state A, B and C. Due to solvation effects, the guest is not favoured at the center of the cage (A), the most stable position is at the cage walls (B).

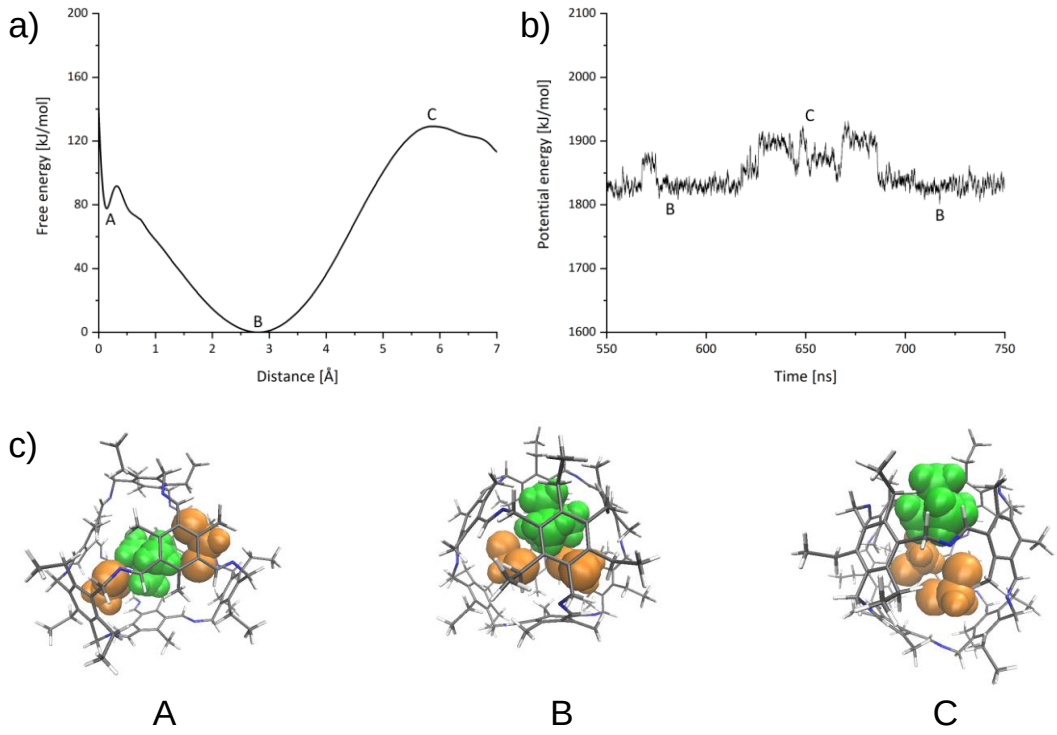

Figure S82: Computed decapsulation process for **3-Me** with $\mathbf{NMe_4^+}$: a) Free energy surface, $\boldsymbol{\Delta G_d^{\ddagger}}$= 123 kJ/mol b) Host potential energy changes when guest leaves and comes back once. c) Different conformations at state A, B and C. Due to solvation effects, the guest is not favoured at the center of the cage (A), the most stable position is at the cage walls (B). Since no solvent molecule is found in the cage during the simulation time, the most favourable position is in the center of the cage (A).

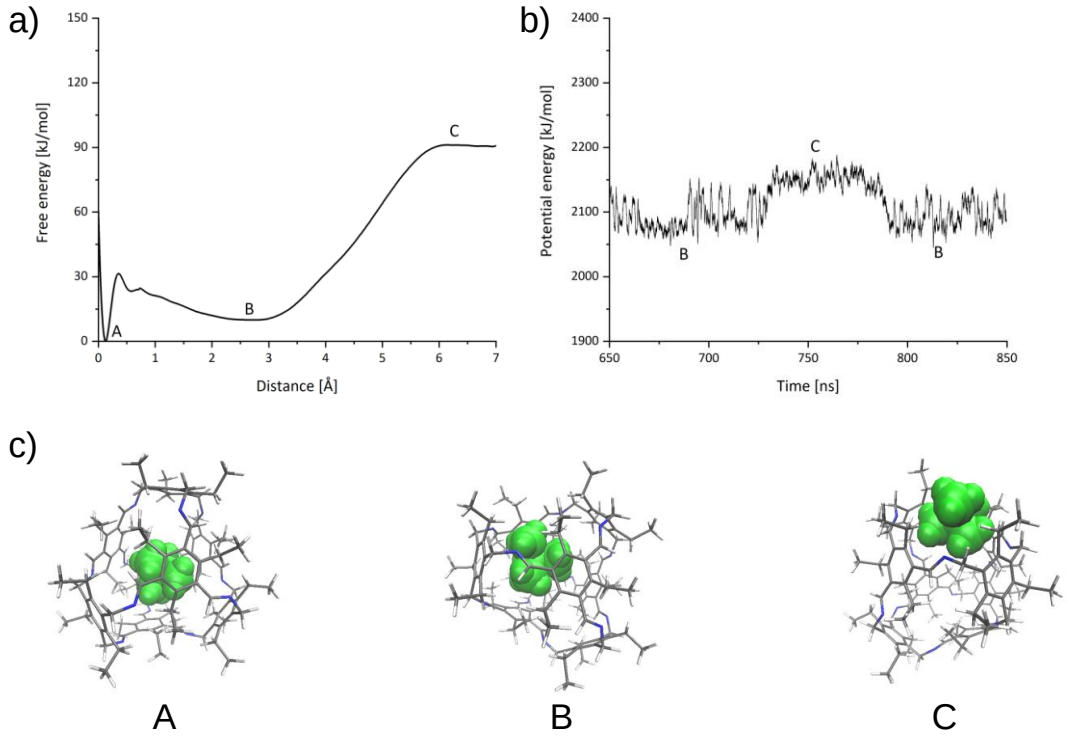

Figure S83: Computed decapsulation process for **3-Et** with NMe_4^+: a) Free energy surface, $\Delta G_d^{\ddagger}$= 91 kJ/mol b) Host potential energy changes when guest leaves and comes back once. c) Different conformations at state A, B and C.

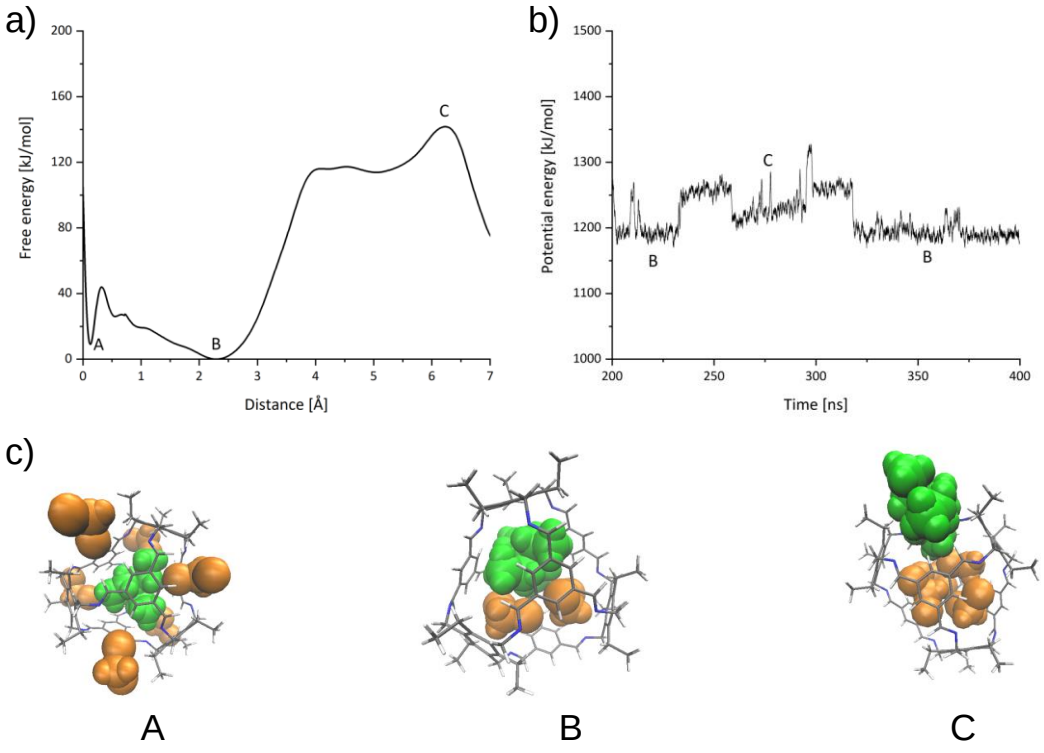

Figure S84: Computed decapsulation process for **3-H** with NEt_4^+: a) Free energy surface, $\Delta G_d^{\ddagger}$= 141 kJ/mol b) Host potential energy changes when guest leaves and comes back once. c) Different conformations at state A, B and C

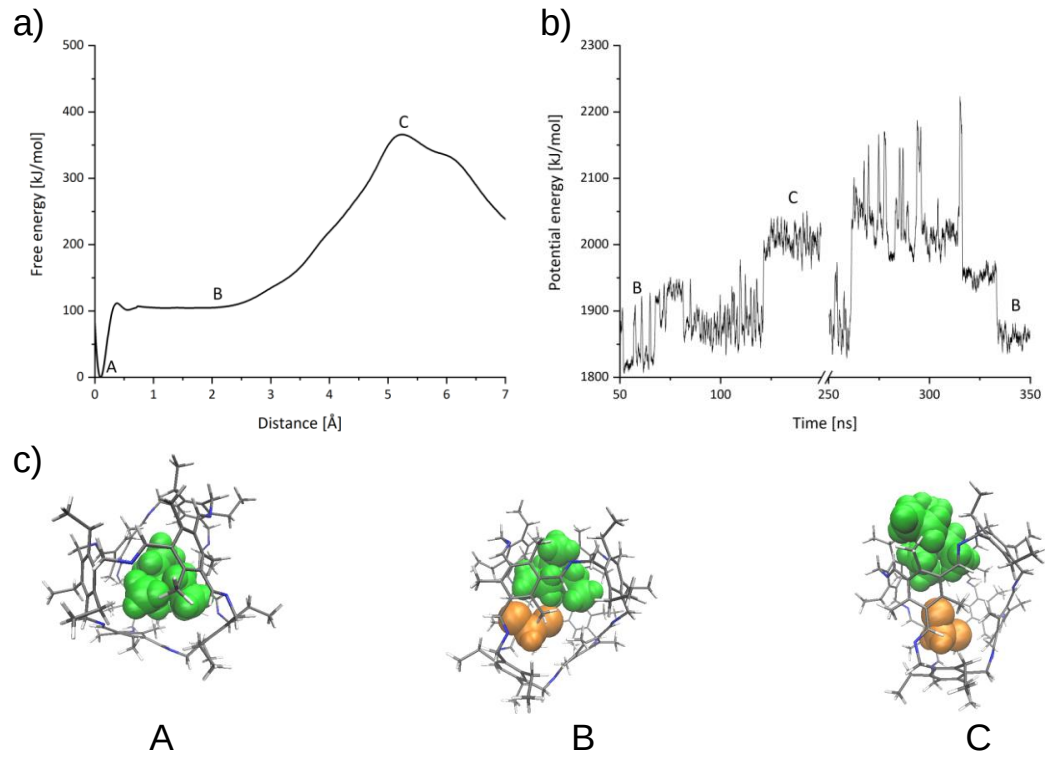

Figure S85: Computed decapsulation process for **3-Me** with NEt_4^+: a) Free energy surface, $\Delta G_d^{\ddagger}$= 357 kJ/mol b) Host potential energy changes when guest leaves and comes back once. c) Different conformations at state A, B and C.

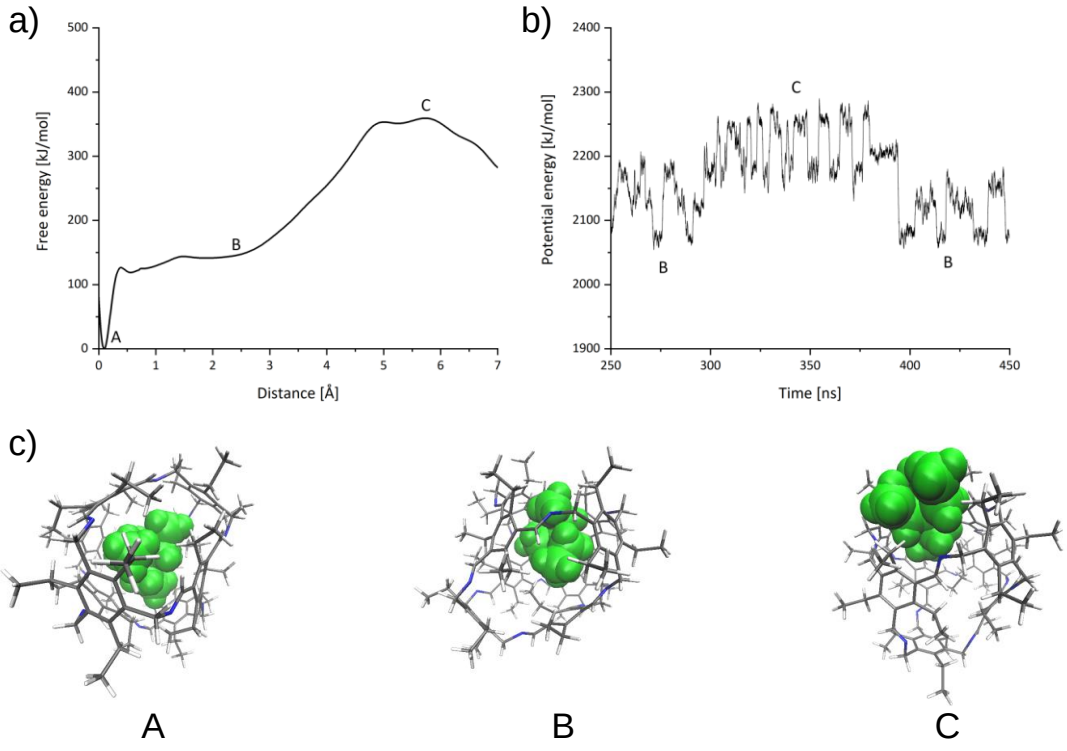

Figure S86: Computed decapsulation process for **3-Et** with NEt_4^+: a) Free energy surface, $\Delta G_d^{\ddagger}$= 359 kJ/mol b) Host potential energy changes when guest leaves and comes back once. c) Different conformations at state A, B and C.

7 Single-Crystal X-ray Diffraction Data

General remarks

All crystals were obtained in closed flat bottom tubes (35 x 7.8 mm) by slow evaporation of the appropriate solvent through a PE-plug (1-4 weeks). The crystallisation batches were protected from light.

Crystal structure of cage compound 3-Me

Crystals were obtained by slow evaporation of Dichloromethane.

CCDC-number : 1970309

Crystal data and structure refinement for **3-Me**.

Identification code	jol32
Empirical formula	$C_{108}H_{132}Cl_{0.25}N_{12}$
Formula weight	1607.11
Temperature	200(2) K
Wavelength	1.54178 Å
Crystal system	orthorhombic
Space group	Ama2
Z	4
Unit cell dimensions	a = 26.6462(17) Å α = 90 deg. b = 15.9453(13) Å β = 90 deg. c = 27.420(3) Å γ = 90 deg.
Volume	11650.0(16) $Å^3$
Density (calculated)	0.92 g/cm^3
Absorption coefficient	0.46 mm^{-1}
Crystal shape	brick
Crystal size	0.128 x 0.050 x 0.038 mm^3
Crystal colour	colourless
Theta range for data collection	3.6 to 44.5 deg.
Index ranges	$-16 \le h \le 24$, $-14 \le k \le 13$, $-24 \le l \le 23$
Reflections collected	10662
Independent reflections	4073 (R(int) = 0.0644)
Observed reflections	2088 ($I > 2\sigma(I)$)
Absorption correction	Semi-empirical from equivalents
Max. and min. transmission	1.31 and 0.75
Refinement method	Full-matrix least-squares on F^2
Data/restraints/parameters	4073 / 893 / 585
Goodness-of-fit on F^2	0.95
Final R indices (I>2sigma(I))	R1 = 0.062, wR2 = 0.135
Absolute structure parameter	2.8(5)
Largest diff. peak and hole	0.14 and -0.12 $eÅ^{-3}$

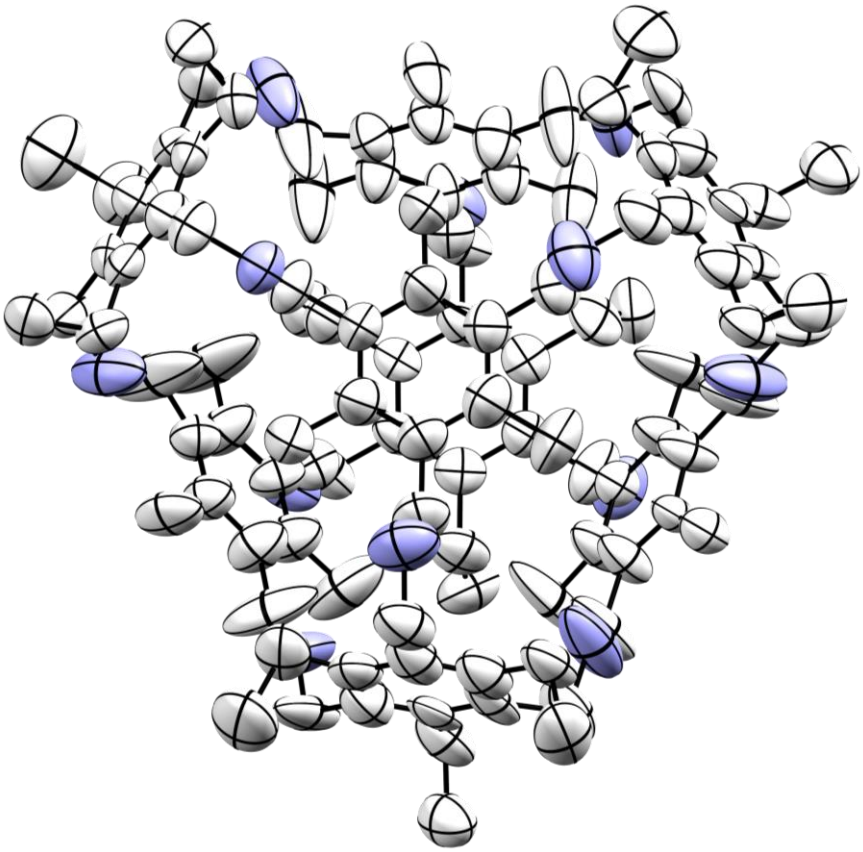

Figure S87: Crystal structure of compound **3-Me**. Atoms of carbon are depicted in white and nitrogen in blue.

Crystal structure of cage compound (NPr_4⊂3-H)BF_4.

Crystals were obtained by slow evaporation of Toluene.

CCDC-number : 1970310

Crystal data and structure refinement for **(NPr_4⊂3-H)BF_4**.

Identification code	jol36	
Empirical formula	$C_{150}H_{184}BF_4N_{13}$	
Formula weight	2255.90	
Temperature	200(2) K	
Wavelength	1.54178 Å	
Crystal system	monoclinic	
Space group	P21/c	
Z	4	
Unit cell dimensions	a = 19.7560(6) Å	α = 90 deg.
	b = 29.7344(12) Å	β =99.806(3) deg.
	c = 22.6749(7) Å	γ = 90 deg.
Volume	13125.4(8) $Å^3$	
Density (calculated)	1.14 g/cm^3	
Absorption coefficient	0.55 mm^{-1}	
Crystal shape	brick	
Crystal size	0.099 x 0.073 x 0.060 mm^3	
Crystal colour	colourless	
Theta range for data collection	2.3 to 55.1 deg.	
Index ranges	$-12 \le h \le 21$, $-31 \le k \le 31$, $-24 \le l \le 24$	
Reflections collected	66503	
Independent reflections	16426 (R(int) = 0.1105)	
Observed reflections	8349 ($I > 2\sigma(I)$)	
Absorption correction	Semi-empirical from equivalents	
Max. and min. transmission	1.30 and 0.74	
Refinement method	Full-matrix least-squares on F^2	
Data/restraints/parameters	6426 / 1683 / 1535	
Goodness-of-fit on F^2	1.01	
Final R indices (I>2sigma(I))	R1 = 0.078, wR2 = 0.165	
Largest diff. peak and hole	0.58 and -0.36 $eÅ^{-3}$	

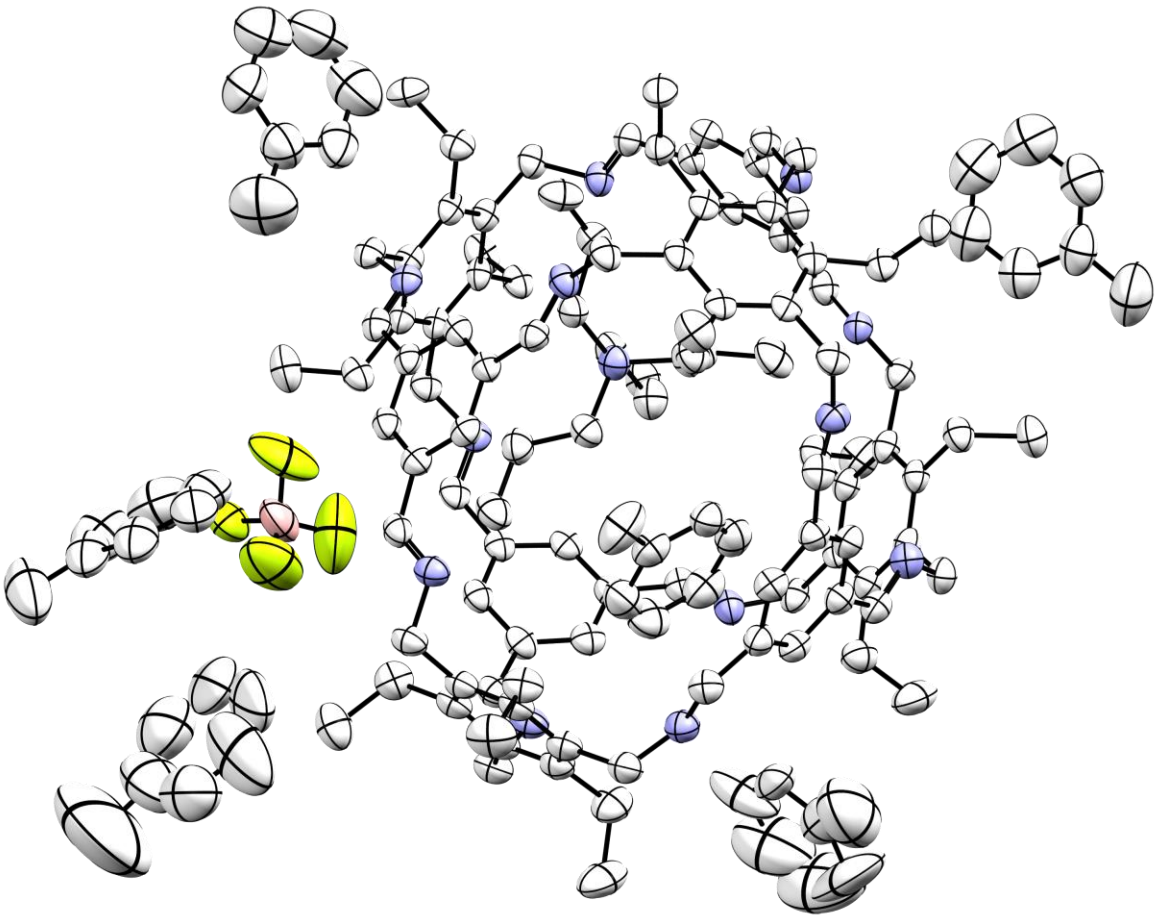

Figure S88: Crystal structure of compound **(NPr_4⊂3-H)BF_4**. Atoms of carbon are depicted in white, nitrogen in blue, fluorine in yellow and boron in pink.

8 Reference

[S1] H. B. Hass, M. L. Bender, *Org Synth* **1950**, *30*, 99-101.

[S2] A. Vacca, C. Nativi, M. Cacciarini, R. Pergoli, S. Roelens, *J. Am. Chem. Soc.* **2004**, *126*, 16456-16465.

[S3] S. Viel, F. Ziarelli, G. Pages, C. Carrara, S. Caldarelli, *J Magn Reson* **2008**, *190*, 113-123.

[S4] Y. H. Zhao, M. H. Abraham, A. M. Zissimos, *J. Org. Chem.* **2003**, *68*, 7368-7373.

[S5] J. C. Lauer, W. S. Zhang, F. Rominger, R. R. Schroder, M. Mastalerz, *Chem. Eur. J.* **2018**, *24*, 1816-1820.

[S6] G. W. T. M. J. Frisch, H. B. Schlegel, G. E. Scuseria, M. A. Robb, J. R. Cheeseman, G. Scalmani, V. Barone, G. A. Petersson, H. Nakatsuji, X. Li, M. Caricato, A. V. Marenich, J. Bloino, B. G. Janesko, R. Gomperts, B. Mennucci, H. P. Hratchian, J. V. Ortiz, A. F. Izmaylov, J. L. Sonnenberg, Williams, F. Ding, F. Lipparini, F. Egidi, J. Goings, B. Peng, A. Petrone, T. Henderson, D. Ranasinghe, V. G. Zakrzewski, J. Gao, N. Rega, G. Zheng, W. Liang, M. Hada, M. Ehara, K. Toyota, R. Fukuda, J. Hasegawa, M. Ishida, T. Nakajima, Y. Honda, O. Kitao, H. Nakai, T. Vreven, K. Throssell, J. A. Montgomery Jr., J. E. Peralta, F. Ogliaro, M. J. Bearpark, J. J. Heyd, E. N. Brothers, K. N. Kudin, V. N. Staroverov, T. A. Keith, R. Kobayashi, J. Normand, K. Raghavachari, A. P. Rendell, J. C. Burant, S. S. Iyengar, J. Tomasi, M. Cossi, J. M. Millam, M. Klene, C. Adamo, R. Cammi, J. W. Ochterski, R. L. Martin, K. Morokuma, O. Farkas, J. B. Foresman, D. J. Fox, *Gaussian 09, Revision D.01* **2016**, *Gaussian Inc., Wallingford, CT*.

[S7] a) P. Hohenberg, W. Kohn, *Phys. Rev. B* **1964**, *136*, B864-+; b) W. Kohn, L. J. Sham, *Phys. Rev.* **1965**, *140*, 1133-&; c) R. G. Parr, S. R. Gadre, L. J. Bartolotti, *Proc. Natl. Acad. Sci. U S A* **1979**, *76*, 2522-2526.

[S8] a) A. D. Becke, *J. Chem. Phys.* **1993**, 5648; b) C. T. Lee, W. T. Yang, R. G. Parr, *Phys. Rev. B* **1988**, *37*, 785-789; c) P. J. Stephens, F. J. Devlin, C. F. Chabalowski, M. J. Frisch, *J. Phys. Chem.-Us* **1994**, *98*, 11623-11627; d) S. H. Vosko, L. Wilk, M. Nusair, *Can. J. Phys.* **1980**, *58*, 1200-1211.

[S9] a) R. Ditchfield, W. J. Hehre, J. A. Pople, *J. Chem. Phys.* **1971**, *54*, 724-+; b) W. J. Hehre, R. Ditchfield, J. A. Pople, *J. Chem. Phys.* **1972**, *56*, 2257-+.

[S10] a) S. Miertus, E. Scrocco, J. Tomasi, *Chem. Phys.* **1981**, *55*, 117-129; b) S. Miertus, J. Tomasi, *Chem. Phys.* **1982**, *65*, 239-245; c) J. L. Pascualahuir, E. Silla, I. Tunon, *J. Comput. Chem.* **1994**, *15*, 1127-1138; d) M. Cossi, V. Barone, R. Cammi, J. Tomasi, *Chem. Phys. Lett.* **1996**, *255*, 327-335; e) V. Barone, M. Cossi, J. Tomasi, *J. Chem. Phys.* **1997**, *107*, 3210-3221; f) E. Cances, B. Mennucci, J. Tomasi, *J. Chem. Phys.* **1997**, *107*, 3032-3041; g) B. Mennucci, E. Cances, J. Tomasi, *J. Phys. Chem. B* **1997**, *101*, 10506-10517; h) B. Mennucci, J. Tomasi, *J. Chem. Phys.* **1997**, *106*, 5151-5158; i) V. Barone, M. Cossi, *J. Phys. Chem. A* **1998**, *102*, 1995-2001; j) V. Barone, M. Cossi, J. Tomasi, *J. Comput. Chem.* **1998**, *19*, 404-417; k) M. Cossi, V. Barone, B. Mennucci, J. Tomasi, *Chem. Phys. Lett.* **1998**, *286*, 253-260; l) R. Cammi, B. Mennucci, J. Tomasi, *J. Phys. Chem. A* **1999**, *103*, 9100-9108; m) M. Cossi, V. Barone, M. A. Robb, *J. Chem. Phys.* **1999**, *111*, 5295-5302; n) J. Tomasi, B. Mennucci, E. Cances, *J Mol Struc-Theochem* **1999**, *464*, 211-226; o) R. Cammi, B. Mennucci, J. Tomasi, *J. Phys. Chem. A* **2000**, *104*, 5631-5637; p) M. Cossi, V. Barone, *J. Chem. Phys.* **2000**, *112*, 2427-2435; q) M. Cossi, V. Barone, *J. Chem. Phys.* **2001**, *115*, 4708-4717; r) M. Cossi, N. Rega, G. Scalmani, V. Barone, *J. Chem. Phys.* **2001**, *114*, 5691-5701; s) R. Cammi, *J. Chem. Phys.* **2009**, *131*; t) F. Lipparini, G. Scalmani, B. Mennucci, E. Cances, M. Caricato, M. J. Frisch, *J. Chem. Phys.* **2010**, *133*; u) G. Scalmani, M. J. Frisch, *J. Chem. Phys.* **2010**, *132*; v) M. Caricato, *J. Chem. Theory Comput.* **2012**, *8*, 4494-4502.

[S11] N. Guex, M. C. Peitsch, *Electrophoresis* **1997**, *18*, 2714-2723.

[S12] P. Thordarson, *Chem. Soc. Rev.* **2011**, *40*, 1305-1323.

[S13] a) S. Akine, M. Miyashita, T. Nabeshima, *J. Am. Chem. Soc.* **2017**, *139*, 4631-4634; b) C. M. Hong, M. Morimoto, E. A. Kapustin, N. Alzakhem, R. G. Bergman, K. N. Raymond, F. D. Toste, *J. Am. Chem. Soc.* **2018**, *140*, 6591-6595; c) A. V. Davis, K. N. Raymond, *J. Am. Chem. Soc.* **2005**, *127*, 7912-7919.

[S14] J. T. B. R. M. Betz, D. A. Case, D. S. Cerutti, T. E. Cheatham, T. A. Darden, R. E. Duke, T. J. Giese, H. Gohlke, A. W. Goetz, N. Homeyer, S. Izadi, P. Janowski, J. Kaus, A. Kovalenko, T. S. Lee, S. LeGrand, P. Li, T. Luchko, R. Luo, B. Madej, K. M. Merz, G. Monard, P. Needham, H. Nguyen, H. T. Nguyen, I. Omelyan, A. Onufriev, D. R. Roe, A. Roitberg, R. Salomon-Ferrer, C. L. Simmerling, W. Smith, J. Swails, R. C. Walker, J. Wang, R. M. Wolf, X. Wu, D. M. York and P. A. Kollman, **2015**, *AMBER*, University of California, San Francisco.

[S15] a) J. M. Wang, R. M. Wolf, J. W. Caldwell, P. A. Kollman, D. A. Case, *J. Comput. Chem.* **2004**, *25*, 1157-1174; b) J. M. Wang, W. Wang, P. A. Kollman, D. A. Case, *Journal of Molecular Graphics & Modelling* **2006**, *25*, 247-260.

[S16] a) G. A. Petersson, A. Bennett, T. G. Tensfeldt, M. A. Allaham, W. A. Shirley, J. Mantzaris, *J. Chem. Phys.* **1988**, *89*, 2193-2218; b) G. A. Petersson, M. A. Allaham, *J. Chem. Phys.* **1991**, *94*, 6081-6090.

[S17] H. J. C. Berendsen, J. P. M. Postma, W. F. Vangunsteren, A. Dinola, J. R. Haak, *J. Chem. Phys.* **1984**, *81*, 3684-3690.

[S18] M. Parrinello, A. Rahman, *J. Appl. Phys.* **1981**, *52*, 7182-7190.

[S19] A. Barducci, G. Bussi, M. Parrinello, *Phys. Rev. Lett.* **2008**, *100*.

[S20] a) D. Van der Spoel, E. Lindahl, B. Hess, G. Groenhof, A. E. Mark, H. J. C. Berendsen, *J. Comput. Chem.* **2005**, *26*, 1701-1718; b) B. Hess, C. Kutzner, D. van der Spoel, E. Lindahl, *J. Chem. Theory Comput.* **2008**, *4*, 435-447; c) T. M. Mark James Abraham, Roland Schulz, Szilárd Páll, Jeremy C. Smith, Berk Hess, Erik Lindahl, *SoftwareX* **2015**, *1–2*, 19-25.

[S21] G. A. Tribello, M. Bonomi, D. Branduardi, C. Camilloni, G. Bussi, *Comput. Phys. Commun.* **2014**, *185*, 604-613.

[S22] W. Humphrey, A. Dalke, K. Schulten, *Journal of Molecular Graphics & Modelling* **1996**, *14*, 33-38.